8-29-2019

Whole Slide Imaging for High-Throughput Monitoring of Microbial Growth and Its Application to Rapid Antimicrobial Susceptibility Testing

Donghui Song
donghui.song@uconn.edu

Whole Slide Imaging for High-Throughput Monitoring of Microbial Growth and Its Application to Rapid Antimicrobial Susceptibility Testing

Donghui Song, Ph.D.

University of Connecticut, 2019

Since conventional culture-based antimicrobial susceptibility testing (AST) methods are too time-consuming (> 24-72 h), rapid AST is urgently needed for preventing the increasing emergence and spread of antimicrobial resistant infections. Although several phenotypic antibiotic resistance sensing modalities are able to reduce the AST time to a few hours or less, concerning the biological heterogeneity, their accuracy or limit of detection are limited by low throughput. Here, we present a rapid AST method based on whole slide imaging (WSI)-enabled high-throughput monitoring microbial growth at single-cell level. The time for determining the minimum inhibitory concentration (MIC) can be sufficiently short to ensure that the growth of each individual cell present in a large population is inhibited. As a demonstration, our technique was able to monitor the growth of several thousand microbes at single-cell level. Reliable MIC for bacteria and fungi was obtained in 1 h and 3 h, respectively. In addition, the application of our method prevails over other imaging-based AST approaches in allowing accurate determination of antibiotic susceptibility for phenotypically heterogeneous samples, in which the number of antimicrobial resistant cells was negligible compared to that of the susceptible cells. Hence, our method shows great

promise for both rapid AST determination and point-of-care testing of complex clinical microorganism isolates.

Whole Slide Imaging for High-Throughput Monitoring of Microbial Growth and Its Application to Rapid Antimicrobial Susceptibility Testing

Donghui Song

B.S. Nankai University, 2010

M.S. University of Connecticut, 2012

A Dissertation

Submitted in Partial Fulfillment of the

Requirements for the Degree of

Doctor of Philosophy

at the

University of Connecticut

2019

APPROVAL PAGE

Doctor of Philosophy Dissertation

Whole Slide Imaging for High-Throughput Monitoring of Microbial Growth and Its Application to Rapid Antimicrobial Susceptibility Testing

Presented by

Donghui Song, M.S.

Major Advisor _____

Dr. Yu Lei

Associate Advisor _____

Dr. Kazunori Hoshino

Associate Advisor _____

Dr. Mu-Ping Nieh

Associate Advisor _____

Dr. Guoan Zheng

University of Connecticut

2019

Acknowledgements

First and foremost, to my Ph.D. major advisor Dr. Yu Lei, thank you for your patience and guidance throughout my graduate studies. I feel so fortunate for having been your student. Words cannot express how grateful I am to your encouragement that helped me get through the backsets and your strong support that motivated me to become a mature researcher.

To my advisory committee members, Drs. Mu-Ping Nieh, Kazunori Hoshino, and Guoan Zheng, thank you for the thoughtful feedback to my dissertation, as well as the advice for my career development.

I would like to thank my past and present labmates, Dr. Xiaoyu Ma, Dr. Jun Chen, Dr. Qiuchen Dong, Yikun Huang, Haomin Liu, Dongwook Kwak, Heejeong Ryu, and James Chapman, for their help in research and daily life. I am particularly grateful to Dr. Qiuchen Dong for helping me quickly adapt to the research transition from science to engineering.

I would like to thank Dr. Yongku Cho for giving me access to use the instruments in his laboratory. I appreciate all the help from Cho's group members, Dr. Dan Li, Shiyao Wang, and Azady Pirhanov.

I also would like to thank Dr. Christopher O'Connell for the trainings for confocal microscopy and valuable advice for my research.

Finally, I would like to express my gratitude to my parents and Yifan. Their endless love has supported me to achieve all the accomplishments in this journey.

Table of Contents

Chapter 1

Introduction

1.1 The crisis of antimicrobial resistance

1.1.1 The emergence of antimicrobial resistance

Since the discovery of penicillin by Sir Alexander Fleming in 1928, antibiotics have saved millions of lives from bacterial infections and extended life spans of human [1]. Despite the remarkable benefits of antibiotics, antimicrobial resistance (AMR) has been noticed as a threat to public health since the emergence of methicillin-resistant *Staphylococcus aureus* (MRSA) in 1960s [2]. Unfortunately, shortly thereafter, AMR has been eventually developed to almost all antibiotics (Figure 1) [3]. Particularly, it had been believed that the resistance against vancomycin was unlikely to occur, but vancomycin resistance was reported only 7 years since the introduction of it to clinical practice in 1972 [2]. Although the pharmaceutical industry has been developing new antibiotics to solve the AMR issue, the pipeline of antimicrobial agents is becoming dry up, which has facilitated the outbreak of multidrug-resistant microbes, which is also referred to as "superbugs" [4].

According to a report published by Centers for Disease Control and Prevention (CDC) in 2013, the top 18 AMR threats, including bacteria and fungi, were outlined [5]. They are categorized as "urgent", "serious", or "concerning" based on the threat level (Table 1). This report sounded an alarm to the danger of AMR infections. In the U.S., over 2 million people are infected by AMR microbes each year, resulting in the death of at least 23,000 people.

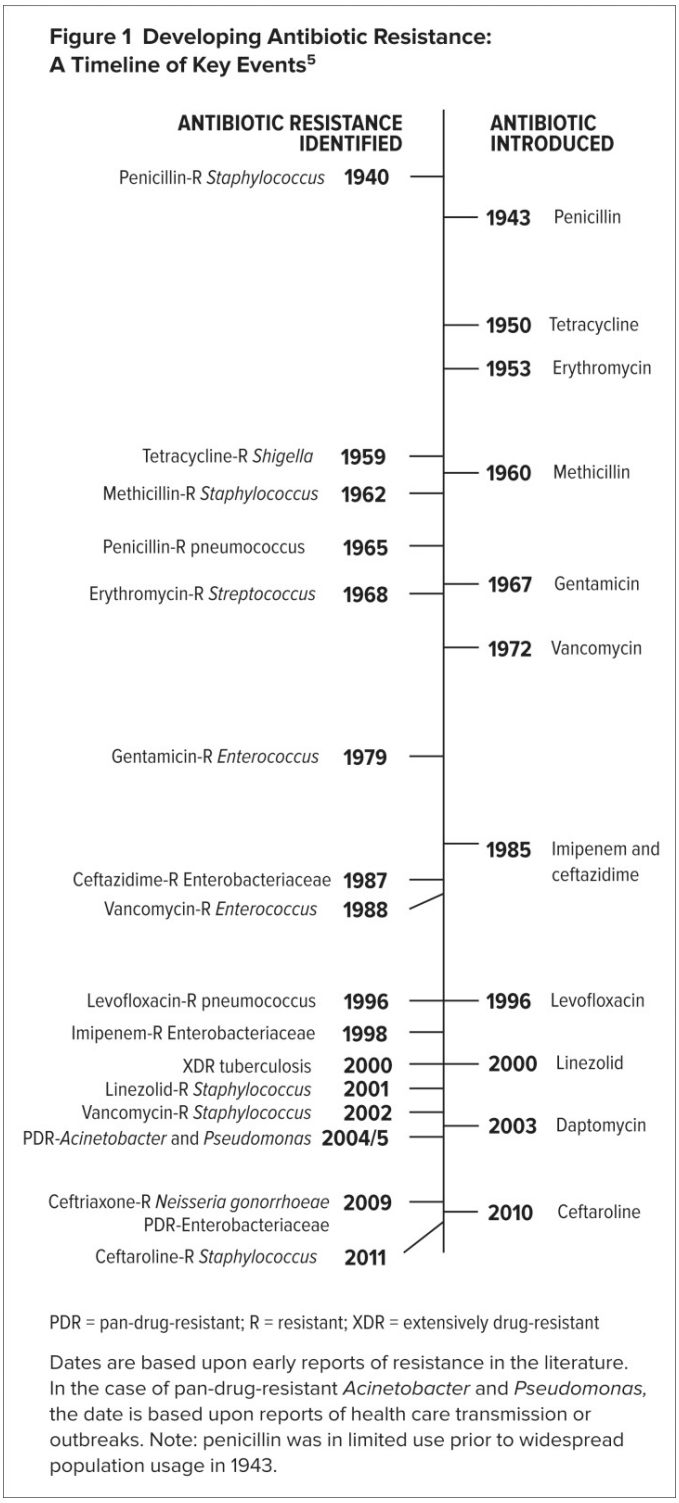

Figure 1. A timeline of AMR development [3].

1.1.2 The causes of the antimicrobial resistance crisis

1.1.2.1 Overuse of antimicrobial agents

Apparently, the overuse of antimicrobial agents is considered as a major driving force for the evolution of AMR. Based on Darwinian theory of evolution, antibiotic stress selects the antibiotic-resistant bacteria to survive by eliminating the antibiotic-sensitive bacteria [6]. Although warnings are posted to reduce the overuse, antibiotics are overprescribed worldwide [7]. Especially in many developing countries, the lacking of regulations allows

Table 1. CDC assessment of AMR threats [5].

Urgent Threats	Serious Threats	Concerning Threats
Clostridioides difficile Carbapenem-resistant *Enterobacteriaceae* (CRE) Drug-resistant *Neisseria gonorrhoeae*	Multidrug-resistant *Acinetobacter* Drug-resistant *Campylobacter* Fluconazole-resistant *Candida* Extended-spectrum Beta-lactamase producing *Enterobacteriaceae* Vancomycin-resistant *Enterococcus* (VRE) Multidrug-resistant *Pseudomonas aeruginosa* Drug-resistant non-typhoidal *Salmonella*	Vancomycin-resistant *Staphylococcus aureus* (VRSA) Erythromycin-resistant Group A *Streptococcus* Clindamycin-resistant Group B *Streptococcus*

	Drug-resistant *Salmonella* Serotype Typhi Drug-resistant *Shigella* Methicillin-resistant *Staphylococcus aureus* (MRSA) Drug-resistant *Streptococcus pneumoniae* Drug-resistant Tuberculosis	

that the antibiotics are available over the counter without a prescription [8]. In addition to prescription to human patients, antibiotics are extensively used in agriculture. According to an estimate, 80% of the antibiotics sold in the U.S. are used in livestock as growth supplements to improve the overall health of the farm animals [9]. As the consequence of overusing antibiotics in livestock, resistant bacteria have been found to infect humans through the food supply [10]. Moreover, as reported in a recent study, triclosan, a non-antibiotic antimicrobial agent commonly seen in toothpaste and hand washing, induces multi-drug resistance through genetic mutation, suggesting that antibacterial products for hygienic purpose may also cause AMR [11].

1.1.2.2 Inappropriate prescribing

Inappropriate prescribing of antimicrobial agents is also considered to be responsible for the rising AMR. Studies have revealed that antibiotic therapy decisions, including the choice of antimicrobial agents or the duration of the treatments, are incorrect in 30-50% cases [5, 6, 12]. Particularly in intensive care units (ICU), 30-60% of the antibiotic

prescriptions have been identified to be unnecessary, inappropriate, or suboptimal [13]. For instance, using broad-spectrum antibiotics, such as quinolones or imipenem, contributes more to the rising resistance than using narrow spectrum-antibiotics, such as amoxicillin, cephalexin, or trimethoprim-sulfamethoxazole [14]. As broad-spectrum antibiotics non-selectively kill bacteria, they cause serious disturbance of gut flora. This disturbance facilitates the thriving emergence of resistance and the transfer of resistance to other species of bacteria [15].

1.1.2.3 Fewer new antimicrobial agents

Although there is an increasing need of new drugs to combat the rising AMR, the pipeline of new antimicrobial agents is continuously shrinking. Unfortunately, as depicted in Figure 2, no new antibiotic launched into the market in 2013-2016, which has aggravated the threat of AMR. As one reason behind it, the pharmaceutical industry no longer considers the development of new antimicrobial drugs as an economically wise investment. In addition to the low cost, physicians typically prescribe the new antibiotics as "last-line" drugs, which leads to the reduced use and diminished return to the investment [1, 16]. As another reason, when the new drugs are eventually introduced into the clinical practices, the microbes adapt to them very fast and the emergence of new resistance is inevitable [16]. Therefore, due to these potential risks, the progress of new drug discoveries has been very slow.

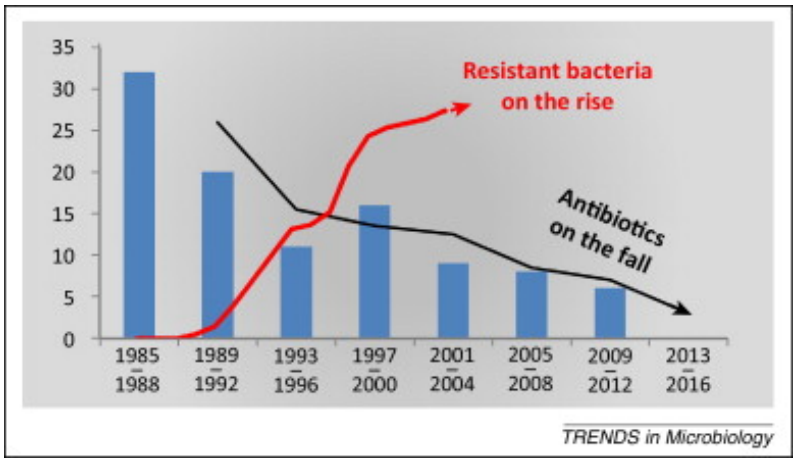

Figure 2. The number of antibiotic-resistant bacteria is increasing while the number of new antibiotics is continuously decreasing [17].

1.1.3 The clinical and economic burden of antimicrobial resistance

As the second leading killer in the world, infectious disease causes 17 million deaths each year. In the U.S., approximately 2 million people are infected with antibiotic-resistant bacteria ("superbugs") and 23,000 of them die [5]. If there is no global action to curb the AMR, the number of deaths would increase to 10 million per year and cost the global economy up to $100 trillion by 2050 [18]. Moreover, 28 million people would be pushed into poverty. As a major example of AMR threat, MRSA causes 19,000 deaths and 360,000 hospitalization each year in the U.S, along with $3-4 billion costs in healthcare [19].

1.2 Tackling the crisis of antimicrobial resistance

1.2.1 Government initiatives

To combat the crisis of AMR, the U.S. government has offered incentives to encourage large pharmaceutical industry to return to antibiotic discovery. Biomedical Advanced R&D

Authority of the U.S. government has supported companies, such as GSK ($200 million) and Cempra ($75 million), to develop new antibiotics [20]. In 2012, the European Innovative Medicines Initiatives started the "New Drugs 4 Bad Bugs" (ND4BB) project. This project contributed $134 million to the development of new antibiotics [21]. In March 2015, the U.S. White House issued a national action plan to combat AMR. The plan aimed to reduce half of the infections caused by some of the most lethal microbes within 5 years [22]. The White House also hopes to fund the discovery of new antimicrobial agents to kill "superbugs" and the innovation of novel diagnostic tools to rapidly detect them.

1.2.2 Preventing transmission of microbial infections

It is known that cross-transmission of resistant microbes, especially those with high potential to spread (e.g. *Clostridium difficile* or carbapenem-resistant *Enterobacteriaceae*), places patients at high-risk [12]. Therefore, it is critical for the healthcare providers to comply with the CDC infection-control guidelines. For example, hand hygiene before and after patient contact is essential to reduce the chance of transmission. In addition, disinfection of healthcare working environment and medical equipment is also required. As another preventative strategy required by CDC, contact tracking is conducted to trace individuals who are infected and their contacts who may have been transmitted [10]. Notably, contact tracking has successfully limited the spread of AMR.

1.2.3 Developing new antimicrobial agents and therapeutic strategies

There is an urgent global need for new antimicrobial agents to combat the crisis. Although only five new antibiotics were approved for clinical use during the decade between 2000 and 2010, the pace of discovering new antibiotics has accelerated (Figure 3) [5].

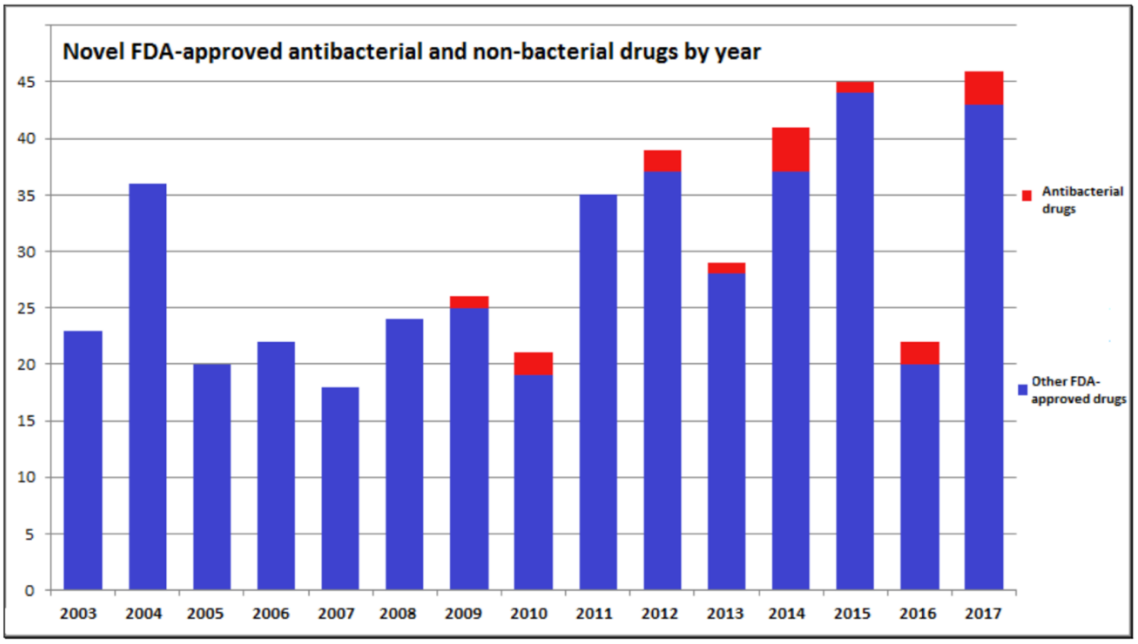

Figure 3. Number of novel FDA-approved antimicrobial drugs each year [23].

Typically, a fixed regimen (e.g. dose, dosage frequency, and length of treatment) is associated with antimicrobial therapy. Such treatment generally last 5-7 days or longer [8]. However, recent studies of clinical trials have discovered that shorter courses of therapy are just as effective as longer ones, indicating that prolonged treatment may be unnecessary [4, 13]. To prevent the enrichment of antibiotic-resistant bacteria, a limited antibiotic dose and a shorter course of treatment is preferred.

As alternative solutions to treat antibiotic-resistant bacteria, more understanding of resistance mechanisms has facilitated the generation of new chemicals that can extend the life of existing antibiotics [24]. For example, a variety of inhibitors of major enzymes that are responsible for the inactivation of antibiotics, such as beta-lactamase and aminoglycoside-resistance enzymes, have been developed to overcome the barriers of

resistance [25-29]. Furthermore, suppressing antibiotic efflux with inhibitors of efflux pump proteins provides another strategy to improve the antimicrobial activities [30-33].

1.2.4 Reducing inappropriate use of antibiotics

Empirical use of antibiotics could be reduced by more rapid and accurate diagnosis [34, 35]. Typically, healthcare providers perform antimicrobial susceptibility testing (AST) to guide the antibiotic prescription. In clinical practice, AST is employed to assess the effectiveness of an antimicrobial agent against certain microbe. The results of AST are reported in the form of minimum inhibitory concentration (MIC), which is the lowest concentration of an antimicrobial agent that inhibits visible growth of a microbe [36]. Since the most routinely used culture-based AST methods generally take 24-72 hours, initial treatment is often empirical, which results in poor outcomes, increased mortality, and prolonged hospitalization [37, 38]. Particularly, for patients with septic shock or bacterial meningitis, empirical antibiotic therapy should be initiated immediately based on the urgency. In an initial empirical therapy, broad-spectrum antibiotics are commonly used. Later, the spectrum of antibiotics is narrowed according to the AST results. Therefore, rapid and accurate AST approaches is urgently needed to reduce the empirical use of broad-spectrum antibiotics and consequent increasing emergence and spread of antibiotic resistance.

1.3 An overview of antimicrobial susceptibility testing (AST) methods

1.3.1 Conventional culture-based AST methods

1.3.1.1 Broth dilution methods

Broth dilution methods, which are used to measure the MICs of antimicrobial agents, are one of the gold standard methods for AST. In broth dilution tests, a known number of microorganisms are inoculated into tubes containing dilutions of antimicrobial agent. As described in Figure 4, the lowest concentration of an antimicrobial agent, at which no visible growth appears within certain period of time, is defined as the MIC [39]. The classic broth dilution requires the broth volume in the testing tube is at least 1 mL. The concentrations of antimicrobial agent are generally 2-fold diluted. The broth dilution methods are typically used to test pure isolates of non-fastidious aerobic microorganisms, which are easily grown by overnight incubation.

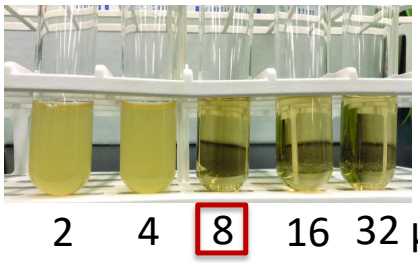

Figure 4. Schematic illustration of classic broth dilution AST method for the determination of MIC.

Since the classic broth dilution methods are laborious, the tests have been miniaturized and standardized by using broth microdilution [40]. The serial dilution of antimicrobial agents is performed in the wells of 96-well plate. Following the inoculation of

microorganisms and incubation, as illustrated in Figure 5, the plates are checked for any visible microbial growth through the colorimetric or turbidity change.

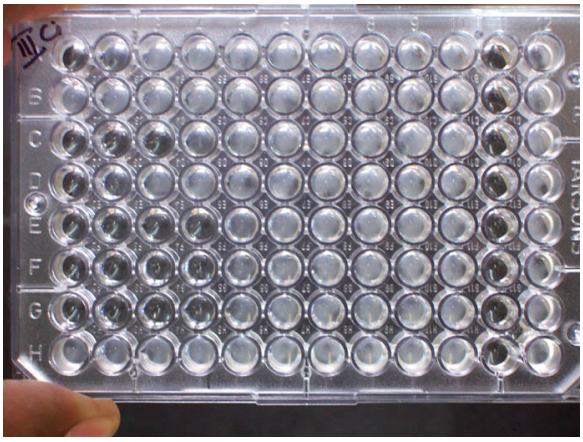

Figure 5. A representative result of broth microdilution AST method. The picture is adapted from the website. https://en.wikipedia.org/wiki/Broth_microdilution

1.3.1.2 Disk diffusion methods

Disk diffusion, or Kirby-Bauer test, is one of the classic AST techniques. Due to its convenience and low cost, the disk diffusion method is very commonly used for determining antimicrobial resistance [40]. In the disk diffusion test, filter paper discs impregnated with various pre-defined concentrations of same or different antimicrobial agents are placed on an agar plate, which has been pre-swabbed uniformly with pure microbial culture. Next, this agar plate is incubated at certain temperature optimal for the growth of a microorganism. The incubation time is dependent on the natural growth rate of the tested microorganism. During the incubation, the antimicrobial agent diffuses from the disc to the agar. The concentration decreases as the distance to the disc increases. If the microorganism is susceptible to an antimicrobial agent in the disc, as shown in Figure 6, there is a clear

inhibition zone around the disc [41]. In general, the larger inhibition zone correlates to higher antimicrobial susceptibility. Therefore, the diameters of the inhibition zones are measured to determine the antimicrobial susceptibility. By comparing the reference table provided by Clinical and Laboratory Standards Institute (CLSI), the size of inhibition zone indicates categorical results (e.g. susceptible, intermediate, resistant) and can be related to MIC [42].

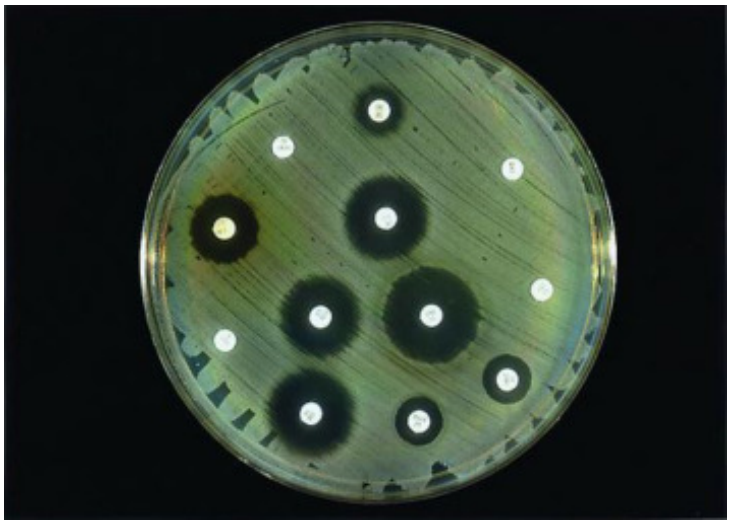

Figure 6. A representative photograph of classic disk diffusion test [41].

As an alternative method derived from disk diffusion test, Etest is used to provide quantitative MIC results. In the Etest, a commercially available thin plastic test strip with continuous gradient of antimicrobial agent is placed on an agar plate, which has been pre-swabbed uniformly with pure microbial culture. Next, this agar plate is incubated. During the incubation, as shown in Figure 7, a continuous gradient of concentrations of antimicrobial agent is created at the intermediate vicinity of the test strip. The concentration gradient remains stable for at least 18-24 hours, which is long enough for most species of fastidious and non-fastidious microorganisms. After overnight incubation, a clear ellipse-

shaped inhibition zone appears along the test strip. The MIC value is read from the scale point where the edge of the ellipse intersects with the strip [43].

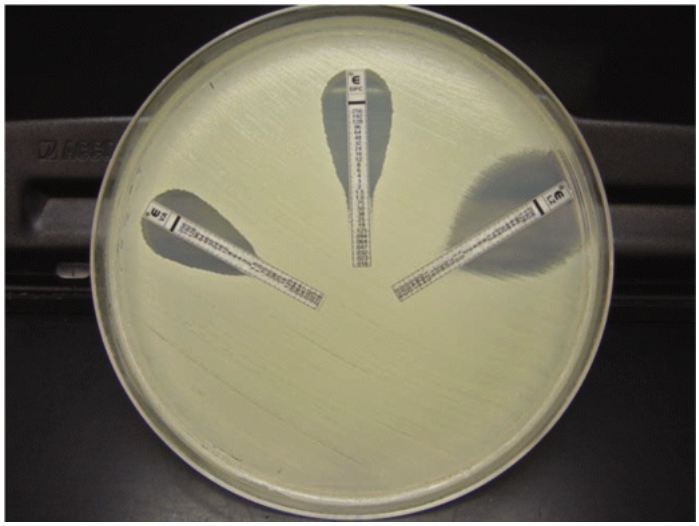

Figure 7. A representative photograph of classic disk diffusion test [43].

As a summary of conventional culture-based AST methods, they are routinely used in clinical microbiology laboratories due to the low cost and simple operation. However, the typical culturing time (at least 16-24 h) is too long for the clinicians to timely decide the most effective antimicrobial therapy. As its consequence, the treatment is generally initiated with broad-spectrum drugs, thus facilitating the emergence of "superbugs". Especially for patients with septic shock, initiation of inappropriate antimicrobial treatment results in a 5-fold decrease in survival [44].

1.3.2 Molecular AST methods

In recent years, more clinical microbiology laboratories are adopting molecular approaches, such as nucleic acid amplification techniques [45, 46] and matrix assisted laser

desorption ionization time of flight mass spectrometry (MALDI-TOF) [47-49], to accelerate the identification of antimicrobial resistance.

Genotypic methods are based on the detection of specific genes responsible for antimicrobial resistance. As the procedures shown in Figure 8, the microorganisms isolated from clinical blood or urine samples are lysed and DNA is extracted. Next, the DNA is fragmented and the fragments are amplified by nucleic acid amplification techniques, such as polymerase chain reaction (PCR) or loop-mediated isothermal amplification (LAMP). Targeted genes subject to antimicrobial resistance are identified from the genomic analysis [50].

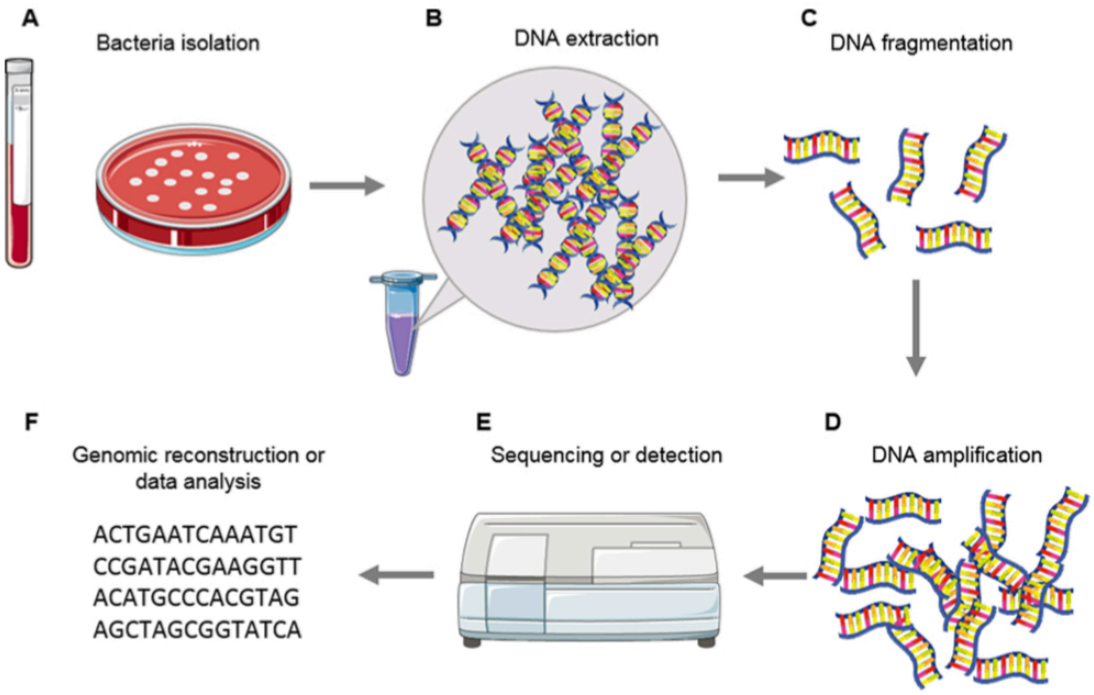

Figure 8. Schematic illustration of general genotypic approach for determining antimicrobial resistance [50].

Mass spectrometry, particularly MALDI-TOF, is also employed for determining antimicrobial susceptibility. The principle is based on the detection of antimicrobial resistance related enzymatic activity. For instance, this method detects mass shift corresponding to the hydrolysis or degradation of antimicrobial agents in the presence of specific enzymes, such as β-lactamase [51, 52] or carbapenemase [53-55].

Although molecular approaches are sensitive and fast, they are unable to distinguish live and dead cells [56], and the exists of genetic biomarkers do not necessarily correlate to cell replication [57]. Furthermore, if new resistance mechanisms arise, they are likely to result in false negatives. Therefore, results from phenotypic AST approaches is considered more reliable.

1.3.3 Commercially available AST instruments

As summarized in Table 1, a variety of commercially available techniques have been suggested as candidates for more rapid AST. To reduce labor-cost and human-prone errors from the conventional phenotypic methods, several automated instruments, such as BD Phoenix, VITEK 2, and MicroScan WalkAway, are used to identify cell growth by tracking the colorimetric, fluorescence, or turbidity changes [58, 59]. These instruments are established on broth microdilution method, and automated robotics are employed to handle standard 96-well microdilution trays. Compared with the manual methods, these instruments are able to save significant time and provide accurate quantitative results. Nonetheless, these

automated techniques still remain slow due to the low sensitivity of the current detection methods.

As one of the latest commercially available AST techniques, the Accelerate PhenoTest BC Kit is able to rapidly identify bacteria within 90 min using fluorescent *in-situ* hybridization (FISH) probes after the cells are isolated from the clinical samples (e.g. blood or urine) through gel filtration and electro-kinetically concentrated on a glass substrate [60]. The cells are cultured in antibiotic-rich media and imaged by dark field microscopy for changes in colony morphology change. The images are analyzed by automated computer algorithms and the MIC can be determined within 7 h.

Another rapid optical imaging-based technique is oCelloScope, which is designed to real-time image growth of bacterial cells in a fluid sample using time-lapse microscopy [61]. The tilted plane of focus enables scanning of volumes and extraction of phase information. Images are then analyzed by an algorithm to render growth curves. MICs can be determined within 1-4 h. However, similar as PhenoTest, oCelloScope is unable to image the growth of bacteria at single-cell level.

Table 1. Summary of commercially available laboratory AST methods.

Method	Measurement	Time of test[a]	Reference
Broth micodilution	Turbidity in liquid medium	>16 h	[62, 63]

Disk diffusion	Diameter of inhibition zone	>16 h	[62, 63]
Etest	Inhibition zone generated by antimicrobial agent gradient strip	>16 h	[62, 63]
Flow cytometry	Fluorescence from live/dead staining	2-4 h	[64]
PCR	DNA amplification of antibiotic resistance related genes	2-4 h	[45, 63]
MALDI-TOF MS	Mass spectra of antibiotic resistance related proteins	1-3 h	[48]
oCelloScope	Time lapse imaging of bacterial growth	2-3 h	[61]
BD Phoenix[b]	Colorimetric and turbidity change	8-10 h	[65]
VITEK 2[b]	Transmittance of light due to turbidity	>7.5 h	[59]
MicroScan WalkAway[b]	Fluorescence due to metabolism or transmittance of light due to turbidity	4.5-18 h	[66]
PhenoTest BC Kit[b]	Real-time imaging of bacterial growth	<7 h	[58, 59]

[a]Time for nonfastidious microorganisms

[b]FDA-approved automated systems

1.3.4 Recent advances in rapid AST approaches

Recently, many innovative modalities have been developed to further shortening the time for phenotypic AST. The following is a brief introduction of those innovative phenotypic AST methods classified by their working mechanisms.

Imaging-based methods

Methods coupling microfluidics with optical imaging have been reported for rapid AST. As depicted in Figure 9, Kwon group demonstrated a microfluidic agarose channel (MAC) system, in which bacterial cells were immobilized in agarose by mixing them in the channels [67]. Antibiotics were then allowed to diffuse into the system to reach desired concentrations. Time-lapse imaging was subsequently conducted on cells in a field of view. The change in the total area occupied by the cells over time was analyzed to determine antibiotic susceptibility. The MICs, defined in this work as the lowest concentration at which such area remains not changed or decreases, were delivered within 3-4 h.

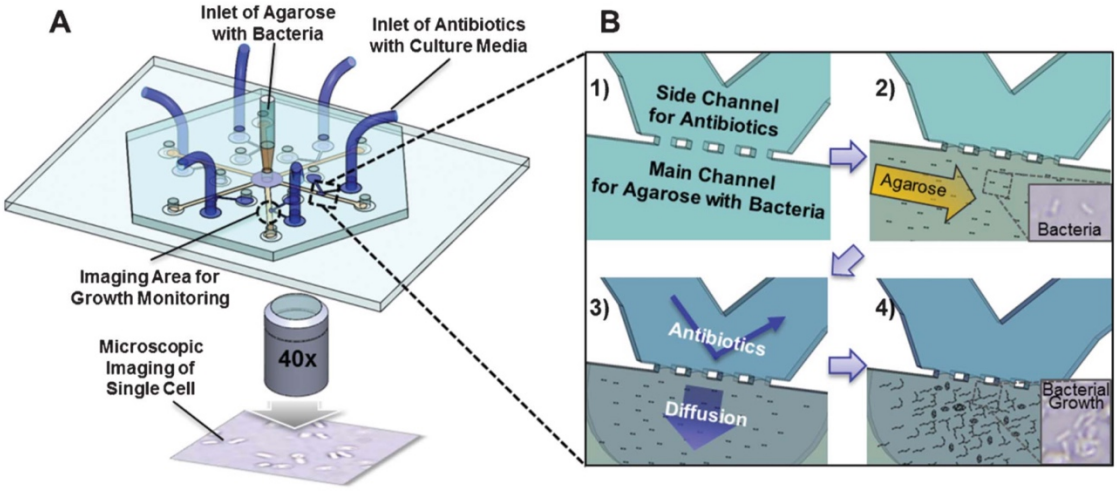

Figure 9. Schematic illustration of microfluidic agarose channel (MAC) system for AST [67]. (A) The setup of the MAC system. It consists of a microfabricated microfluidic chip with inlets of agarose mixed with bacteria, and culture medium containing antibiotics. (B) A mixture of bacteria and agarose was loaded into the chip at the center of the setup. After the agarose is solidified, culture medium

containing antibiotic was loaded through the channels to reach desired concentrations of antibiotic in the agarose gel. Bacterial growth was then monitored under a microscope.

As the derived work of MAC system, imaging-based single-cell morphological analysis (SCMA) was further employed for AST based on the analysis of cell morphology change and the time-to-readout was less than 4 h [68]. In this system, as shown in Figure 10, MAC chip was built in each well of 96-well plate, allowing the system to test multiple concentrations of various antimicrobial agents simultaneously. Moreover, the information from the images, such as the morphology and growth pattern of microorganisms in the presence of antimicrobial agents, can be helpful for the clinicians to identify what would be the specific infections. Nevertheless, in this platform, cells were monitored in only one field-of-view (FOV) (e.g. 0.2mm×0.2mm). Although this approach is able to image bacterial growth at single-cell level, considering that antibiotic resistant and susceptible cells coexist in clinical samples [69, 70], examining only tens of cells would not be sufficient for a convincing conclusion with statistical significance. Furthermore, this method requires a high concentration of cells (> 10^7 cells/mL) to provide enough cell number in such small area. Consequently, if the original cell concentration is low, the actual time for AST was extended by counting the procedure of pre-enrichment cell culture (> 1 h) into the test.

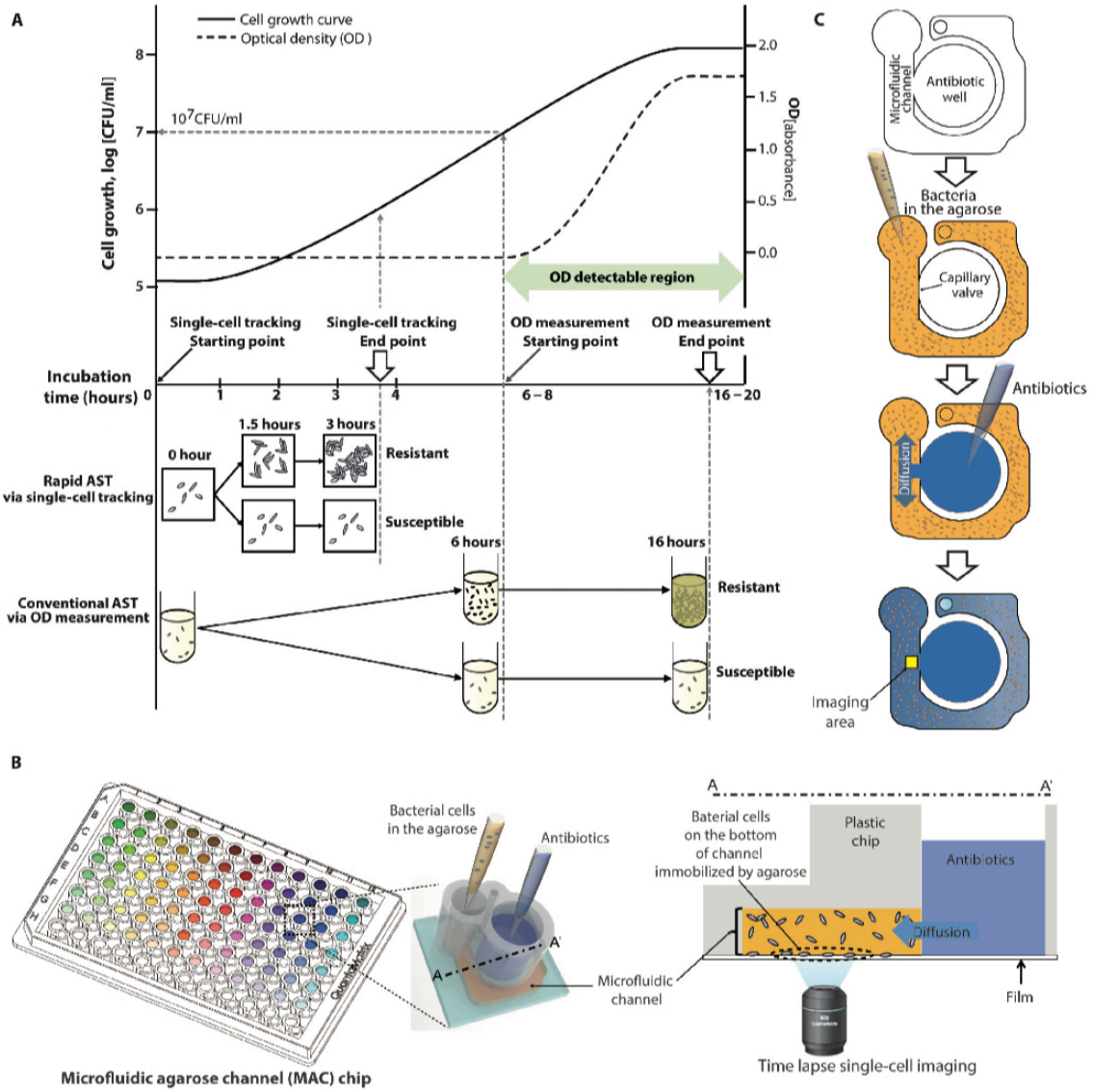

Figure 10. Schematic illustration of imaging-based SCMA system [68].

To facilitate the diagnosis for patients with infections in bloodstream, Kwon group further developed a direct and rapid AST (dRAST) system on the basis of the 96-well plate format MAC chip (Figure 11), which can determine the antimicrobial susceptibility of bacteria in positive blood culture samples in 6 hours [71]. In general, it requires three times of overnight culture, which are blood culture, subculture for bacteria isolation, and AST

culture with the addition of antimicrobial agents. As antibiotic-resistant bacteria grow in the presence of antibiotics while red blood cells do not, these two types of cells can be differentiated using imaging after a few hours of incubation. The advantage of this work lies in saving significant time from bacterial isolation and AST culture. However, it is still associated with the same low-throughput issue shown in the MAC chip-based AST technique.

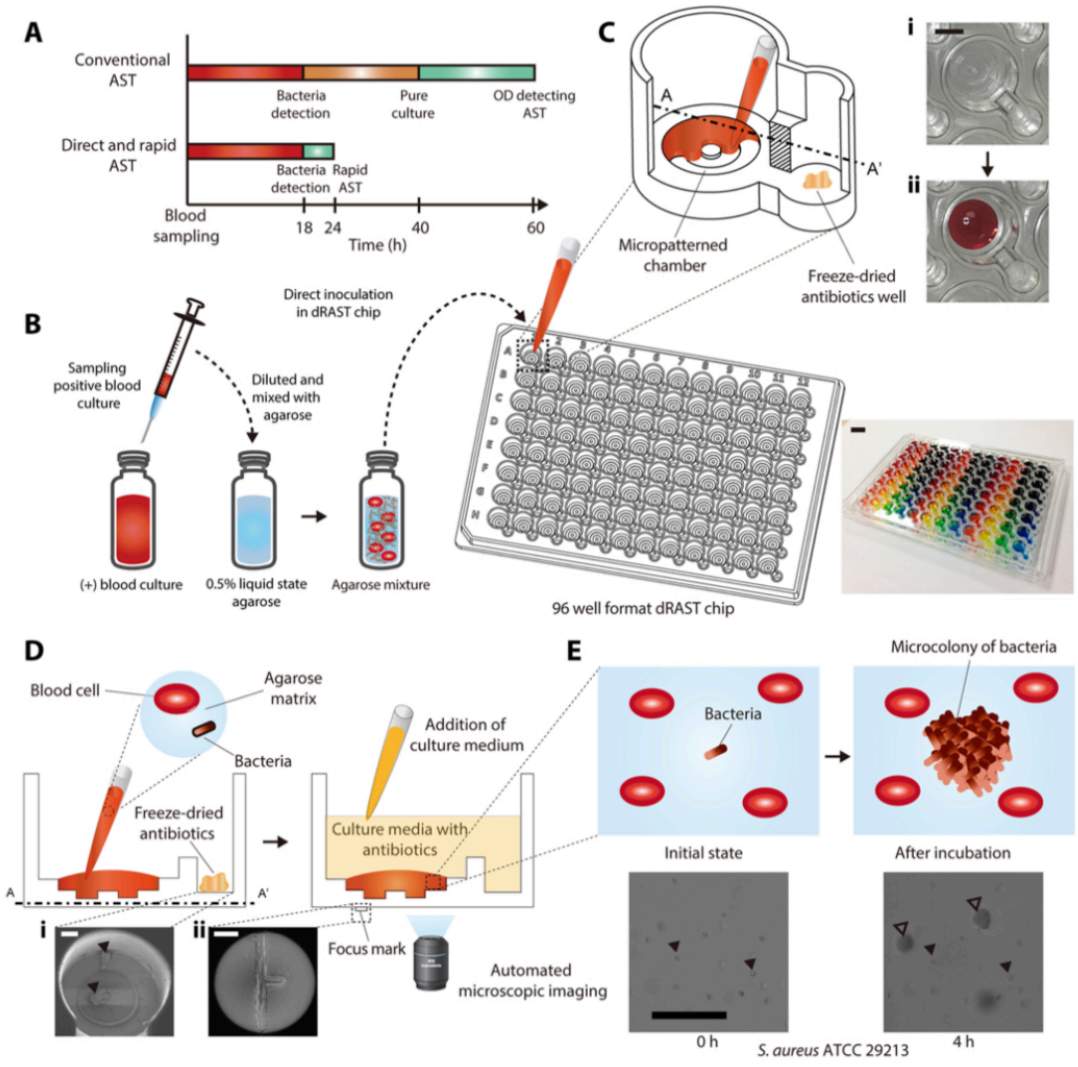

Figure 11. Schematic illustration of dRAST method [71].

Rather than directly imaging bacterial growth, hyperspectral stimulated Raman scattering (SRS) microscopy has been developed to image the metabolic activity of bacteria at single-cell level to predict the cell viability at the presence of antibiotics [72, 73]. In the related studies, as shown in Figure 12, the bacteria were fed with deuterium-labelled glucose or water, and signal from C-D vibration was detected to indicate their metabolic activity. While SRS microscopy benefits the detection due to its high sensitivity and can provide the results within 30 min (typically within a cell cycle), the measured MICs were much larger than the results obtained from the traditional culture-based methods, implying that the toxicity of deuterium to bacteria cannot be ignored. In addition, it is still challenging to enlarge the field-of-view of SRS imaging for improving the throughput.

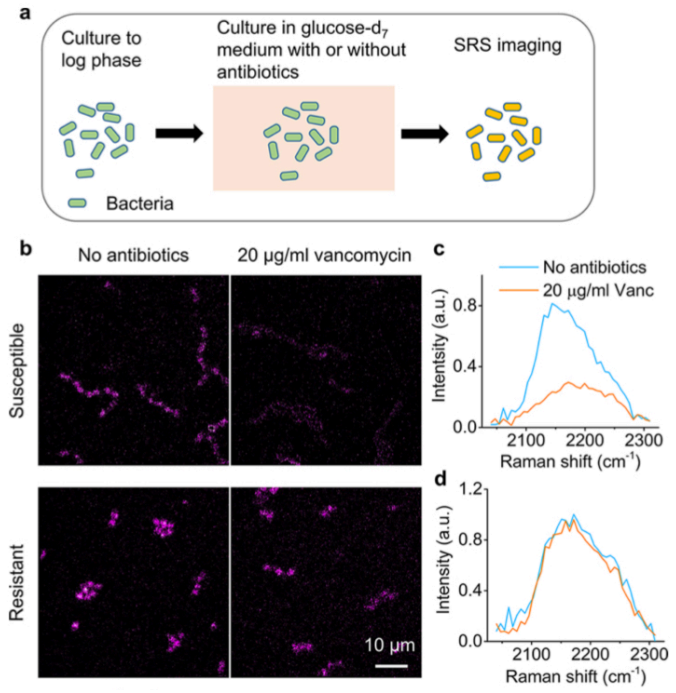

Figure 12. Schematic illustration of AST based on SRS imaging of bacterial metabolic activity [72].

In a study attempting to improve the throughput of tests, a microfluidic platform was developed to encapsulate bacteria in droplets (1-4 bacteria per droplet) and track the growth of bacteria in each droplet through time-lapse imaging (Figure 13) [74]. As the advantages of this platform, the parallelized microfluidic setup can handle multiple tests simultaneously, and time-to-answer can be as fast as 15-30 min. However, due to the partition issue, only about 20 bacteria can be analyzed from the droplet array. Moreover, quantification of bacteria in liquid phase seems to be challenging.

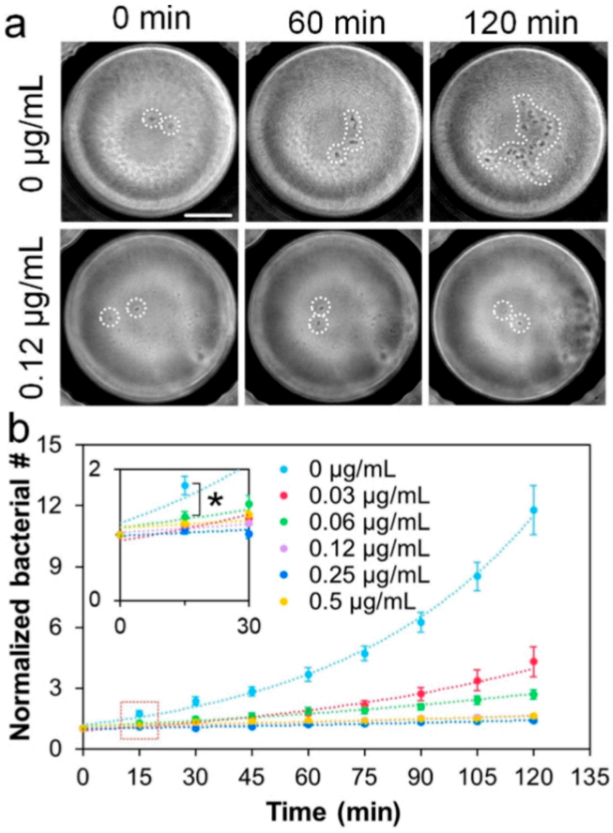

Figure 13. Representative time-lapse images of bacteria in a droplet treated with and without antibiotic (a); and normalized bacterial growth rate over time (b) [74].

In another study attempting to improve the throughput of tests, as illustrated in Figure 15, a microfluidic device containing 2000 channels was designed to trap cells from the fluid sample flowing through into the channels, wherein cell divisions along the line of each channel were imaged by time-lapse microscopy [75]. The length of the lines over time was analyzed to render the growth rate of the cells. Notably, the results can be obtained in less than 30 min. Even though this approach is capable of performing single-cell analysis and works effectively in testing clinical samples, fixed dimensions of the channels would not be able to trap every single cell from those with various size or shape. Moreover, this approach would not work for the bacteria that do not grow in filaments in response to antibiotics treatment.

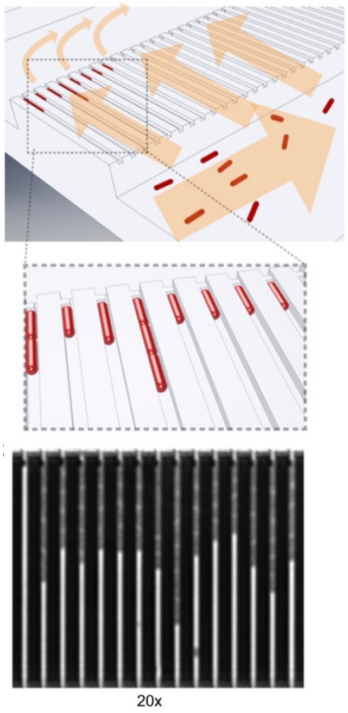

Figure 15. Schematic illustration of the microfluidic-based technique for high-throughput AST [75].

In a recent study attempting to address the limitation of the aforementioned microfluidic-based high-though AST technique, Li *et al* reported an advanced microfluidic system capable of testing polymicrobial samples [76]. In the microfluidic system shown in Figure 16, bacteria with different shape or size can be trapped in different regions according to the applied pressure, which dynamically adjusts the size of channel. Antibiotic susceptibility can be determined in 30 min by using optical imaging to monitor the growth of bacteria at single-cell level. The innovation of this work is based on the automatic separation and classification of bacteria, allowing direct analysis of clinical isolates, blood cultures, urine, and whole blood samples. However, this technique requires highly sophisticated engineering, attenuating its general applicability for clinical use.

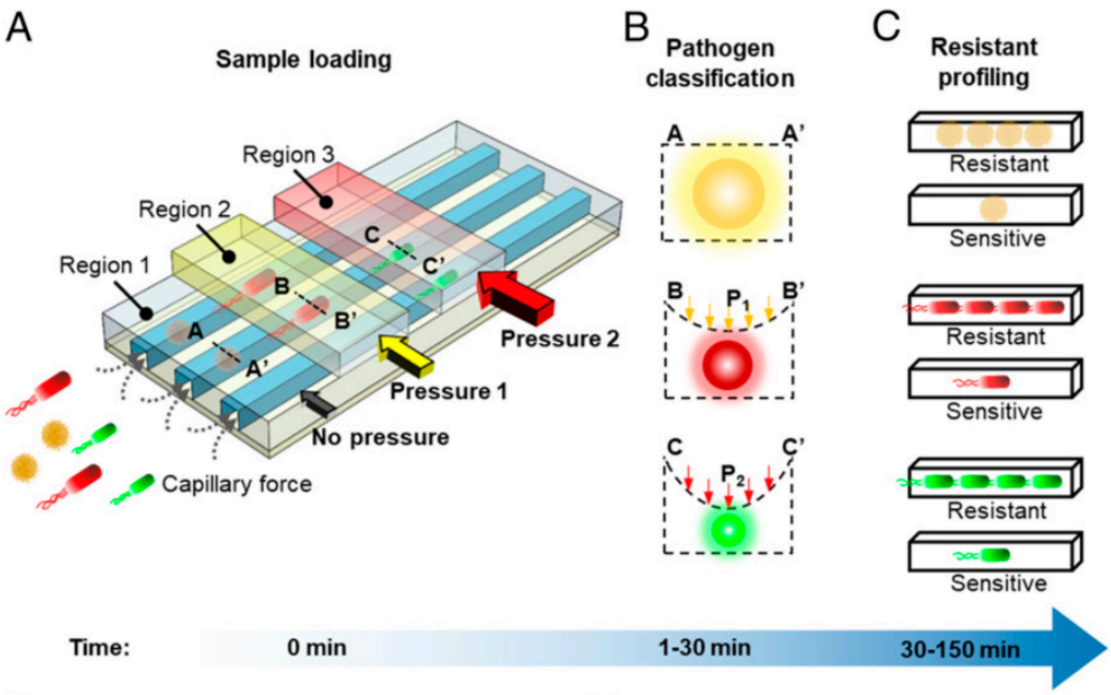

Figure 16. Schematic illustration of adaptable microfluidic device for bacteria classification and AST at single-cell level [76].

Recently, machine learning or deep learning was also employed to detect the increase in the cell number from a video of fluid cell culture medium with the addition of antibiotics (Figure 17) [77]. By training algorithms with large amount of data collected from the experiments, machine learning is able to provide the number of cells freely moving in a liquid sample by defining and quantifying multiple phenotypic features, such as rotation and motion in liquid sample, that traditional 2D image processing algorithms cannot perform [78]. As a powerful method, the results can be obtained within 30 min from an artificial urine sample. However, machine learning for AST is also limited by the programming platforms, as well as the reliance on large sets of clinical data collection. For example, this platform may not be effective on rapidly identifying antimicrobial resistance from an infection caused by a new bacterial species.

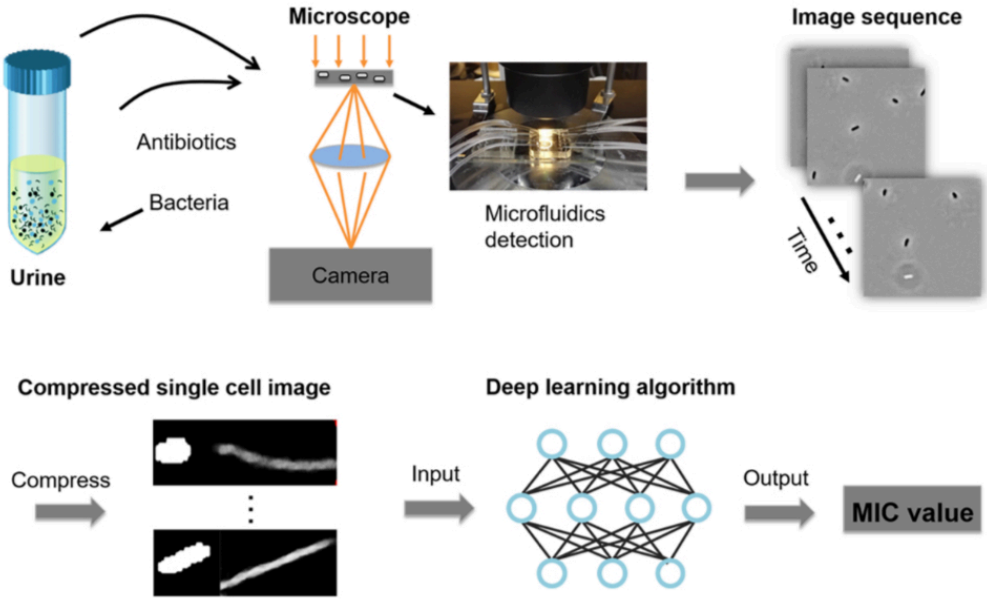

Figure 17. Schematic illustration of deep learning assisted AST technique [77].

Mechanical methods

With the developments in micro- and nanofabrication, several AST platforms have been established using microcantilevers [79-82]. The sensing of bacteria relies on selectively capturing cells by the receptors immobilized on the cantilever surface and translating the binding into mechanical signals as cantilever deflection (static mode) or a shift in resonance frequency (dynamic mode). As recently reported mechanical sensors shown in Figure 18, microcantilevers coupled with microfluidics were used for AST by measuring the single-cell growth rate based on mass change, which corresponded to the resonance frequency [80]. The advantages of this technique are the high sensitivity on detection of nanoscale fluctuations associated with mass change and rapid differentiation of antibiotic resistant and susceptible bacteria in less than 30 min. However, only up to 150 bacterial cells can be monitored per hour, attenuating its applicability for high-throughput detection.

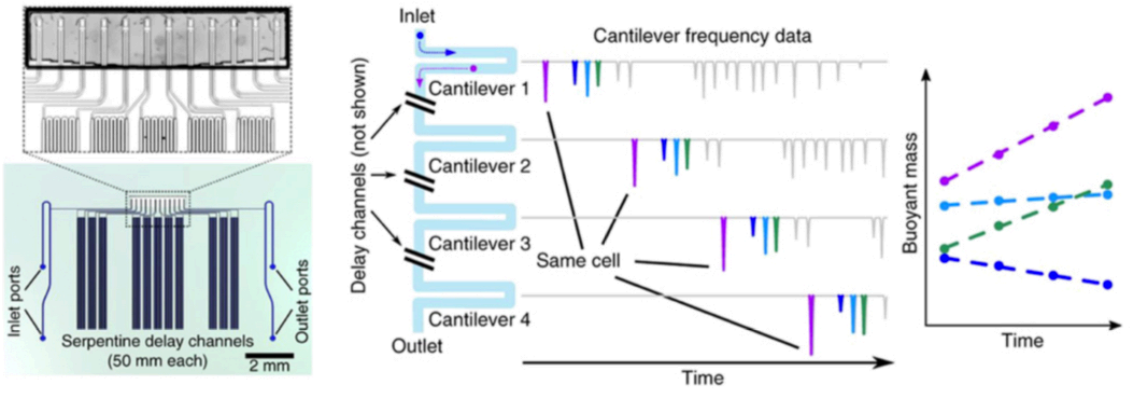

Figure 18. Schematic illustration of microcantilever-based mass sensor array for AST [80].

Electrochemical methods

Despite significant advances in electrochemical biosensors for AST, a majority of available methods were established on the indirect indication of bacterial growth by detecting redox reporters of cell metabolism [83-86]. Metabolically-active bacteria reduce the redox reporter compounds, such as resazurin or methylene blue, and the changes in the redox state of the reporters are detected by electrodes. Since the redox reporters are not pathogen-specific, recent studies have focused more on isolating the bacteria directly from the sample first and performing label-free detection. As an example, Safavieh et al. immobilized bacterial cells on an electrochemical sensing chip with screen-printed electrodes and measured the change of impedance as cells grow for rapid AST [87]. This approach can provide readouts for whole blood samples in 90 min. Although the impedance sensors are advantageous in their simplicity, non-specific binding is considered as a common issue. Furthermore, it is also not clear if the electrical signal is affected by bacterial morphology change or if the bacterial growth is affected by the electrical current.

Summary of recent advances in rapid AST approaches

As summarized in Table 2, based on the working mechanisms, recently emerged platforms for rapid AST can be classified into direct observation of microbial growth through microscopy imaging and indirect sensing microbial growth through the change in physical characteristics, such as mass or impedance. The significant advance is that the time for AST has been shortened to several hours or even less than one hours. In my opinion, since the detection of the subtle changes of physical characteristics is prone to render false positive, microscopically visualizing the microbial cell divisions would be the most straightforward

method to indicate the antimicrobial resistance at single-cell level. However, as the major drawback of microscopy imaging Although coupling the microfluidic techniques with microscopy imaging has allowed high-throughput AST, the incorporation of external circuits and pumps to maintain the flow continuity in the system requires sophisticated engineering, thus increasing the cost. Therefore, rapid and low-cost microscopy imaging-based AST methods are still highly demanded.

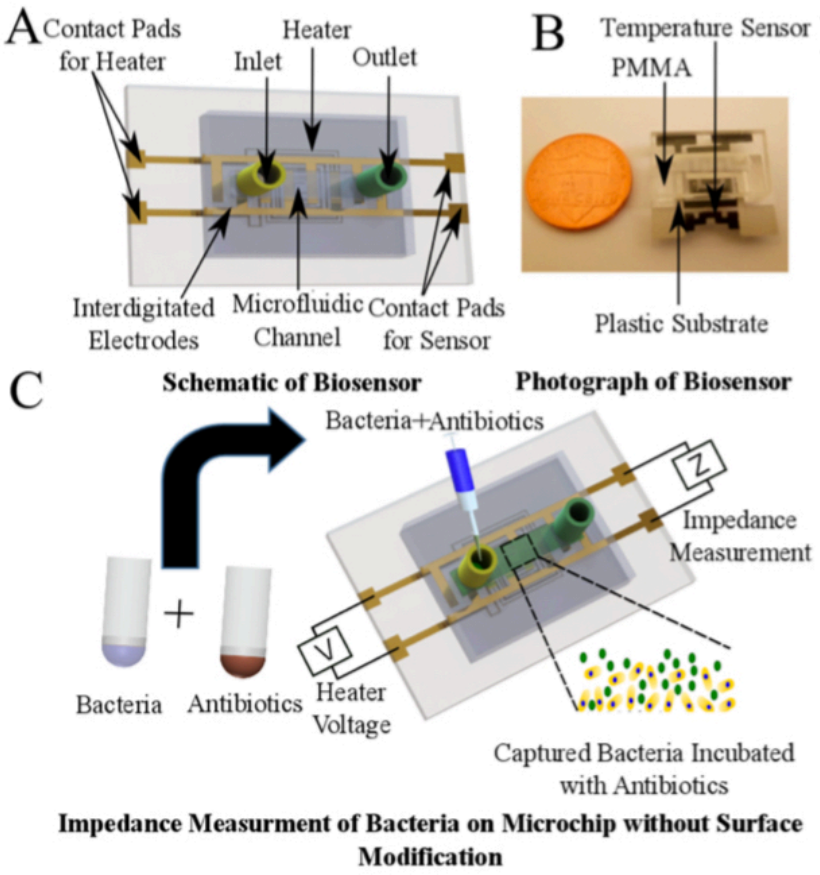

Figure 19. Schematic illustration of an on-chip electrochemical sensor for AST [87].

Table 2. A summary of recent advances in rapid AST approaches.

AST technique	Measurements	Time	Throughput	References
MAC chip	Bacterial growth	3-4 h	Low	[67]
SCMA chip	Bacterial growth and morphological pattern	< 4 h	Low	[68]
dRAST	Proliferating bacteria in blood culture	6 h	Low	[71]
Microfluidic channels cell trappers	Bacterial growth along the channel	< 30 min	High	[75]
Adaptable microfluidic device			High	[76]
Microdroplet array	Bacterial growth	15-30 min	High	[74]
Deep learning assisted video microscopy	Number of cells	< 30 min		[77]
SRS imaging*	Metabolic activity	< 30 min	Low	[72]
Microcantilever mass sensors*	Mass	30 min	Low	[80]

Electrochemical sensors*	Impedance	90 min	[87]

* AST methods that indirectly detect antimicrobial resistance.

1.4 Motivation, research objectives, and organization

1.4.1 Motivation

It is known that the conventional and commercial culture-based AST techniques are established on monitoring the cell growth by the change in their population. As single microbial cells vary widely in their growth rates and the subpopulation that grow faster dominate the overall growth rate, analyzing single-cell growth rate would benefit in facilitating the detection by identifying the rapidly growing subpopulation at the earliest stage. Moreover, antimicrobial-resistant and -susceptible cells generally co-exist in the clinical samples, emphasizing the necessity to respect the biological heterogeneity. As described in the introduction, several microscopy imaging-based techniques are capable of monitoring single-cell growth, but they are limited to low throughput, resulting in no statistical significance in addressing the biological heterogeneity. As the microfluidic-based platform shows high-throughput ability, it is not generalizable to the cells that vary in cell size, shape, and growth pattern. In the dissertation projects, to tackle the challenges that the area of a single FOV of microscopy imaging is so small, we aimed to employing whole slide imaging (WSI) to enlarge the FOV, visualize and track the growth of a large population bacteria. WSI, a technique that composites numerous tiles (each tile is a single microscopic FOV) captured from a specimen on a glass slide into one image, has been exploited in a

variety of biomedical applications, such as whole-slide histopathology analysis. Nonetheless, to our knowledge, few studies have investigated the potentials of WSI in AST. If this concept works, this technique would be able to high-throughput monitor microbial growth at single-cell level, regardless their size, shape, or growth pattern. Furthermore, it can also be employed to evaluate a phenotypically heterogenous sample, in which the antibiotic resistant subpopulation is significantly small. This would be of benefit in monitoring the frequency of rising antibiotic resistance during the treatment and timely adjusting the antibiotic treatment regimen to avoid further aggravation of the drug resistance.

1.4.2 Research objectives

First, we aimed to develop a microbial culture system, which is compatible with whole slide imaging. This system was expected to render images with large FOV, wherein every individual cell is in focus. The previously reported methods for the preparation of microscopy sample slides are suitable for imaging the growth of only one live cell from a single FOV [88-90]. Limited by specific purpose, those methods did not require the gel pad to be very flat. Therefore, our aim was to customize microscope slides, in which the gel pad should be flat enough for imaging a large population of cells.

Second, we aimed to time-lapse image microbial growth at single-cell level using the microbial culture slides customized for whole slide imaging. If necessary, microscope with autofocus function would be applied to ensure every individual cell is in focus.

Third, we aimed to perform antimicrobial susceptibility testing using our microscope culture slides customized for whole slide imaging. To evaluate the performance of our system, bacteria, fungi, and phenotypical heterogeneous samples were to be tested.

1.4.3 Organization

In Chapter 2, we describe the development of microbial culture slides compatible with whole slide imaging. To identify if the surface of agarose gel pad is flat enough, we first evaluated the performance of our microscope culture slides through the enumeration of the bacterial micro-colonies.

In Chapter 3 and 4, we introduce a WSI-based AST approach, which is capable of determining antimicrobial susceptibility of bacteria, fungi, and phenotypical heterogeneous samples by monitoring the growth of a large population of single cells.

In Chapter 5, the projects present in this dissertation is summarized. Based on the advantages and limitations of our AST technique, the potential applicability of this technique for point-of-care purpose is described.

Chapter 2

Development of Custom-Built On-Glass-Slide Microbial Culturing System for Whole Slide Imaging

2.1 Introduction

In microbiological research, it is essential to accurately enumerate microbial cells. For example, as a key step in developing new antimicrobial agents, the determination of minimum inhibitory concentration (MIC) requires inoculation of precise number of viable microorganisms [39, 42]. To date, colony-forming unit (CFU) has been used as a gold standard method for estimating the number of viable microbial cells [91]. In this conventional method, liquid microbial suspension is uniformly spread on the surface of semi-solid nutrient agar plate by an inoculation loop. Next, the plate is incubated at an optimal temperature until the cells grow to visible colonies [92, 93]. The number of colonies is referred to as CFU.

As major advantages of agar plate method, the materials are inexpensive and the procedures are simple enough for trainees to follow. However, long cell culture time (up to a few days) and laborious manual counting result in poor time and cost efficiency [91]. To reduce manual work and its related human error, commercial automated colony-counters, such as ProtoCOL (Synbiosis, UK), have been established through applications of imaging processing algorithms. Nonetheless, the counting results are accurate only when the number

of colonies per plate is between 10 and 200 [94]. Thus, serial dilutions of microbial samples are necessary to ensure a countable range. As a major concern of serial dilutions, errors become larger as dilution times increase or total counts per plate decrease [95].

To address the shortcomings of the conventional method, counting invisible growing micro-colonies (average radius <100 microns) at the very early stage of culturing provides a potentially alternative tool [96-99]. On one hand, it enables much faster detection of viable microbial cells by significantly shortening cell culture time. On the other hand, considering the large difference in size, same culture area can accommodate a lot more micro-colonies and thereby reduce dilution-induced errors. These previous attempts can be classified into using lensless techniques and conventional light microscopy. Recently, Jung *et al.* employed a complementary metal-oxide-semiconductor (CMOS) sensor chip to real-time image the microbial cells growing into micro-colonies and demonstrated that micro-colony-based enumeration results were comparable to conventional method [97]. However, the non-movable small imaging area (5.7 mm × 4.3 mm) and limited sample loading volume (1 μL) failed to exceed the cell capacity of agar plate. Moreover, limited nutrition and air in their isolated cell culture setup resulted in delayed growth of aerobic bacteria, which would not significantly shorten the detection time. Hence, this on-chip imaging technique seemed not to overcome the limitations faced by the conventional counting method. Compared to the lensless imaging systems, conventional light microscopy can deliver higher resolution of images with clear morphology and contrast of the micro-colonies [90]. Although field-of-view (FOV) of each image captured by microscope is very small, microscope is capable of producing a large image in any desired size by stitching numerous images taken from the

culture area of interest [100]. In previous studies, wide-field fluorescence microscopy was employed to rapidly enumerate micro-colonies stained by fluorescent probes, which served as viable cell indicators [96]. However, the counts from microscope could be 50 times larger than those from conventional method [96]. In addition to the interference caused by light scattering, lacking of solid data of accuracy validation restrained microscopy-based counting techniques from broader applications.

In this study, we demonstrated a novel microscopy-based viable bacteria enumeration technique that employed large-area microscopic scanning to achieve rapid, accurate, and label-free enumeration. Specifically, we first developed a bacteria culturing device for microscopic scanning. This device enabled rapid formation of micro-colonies on a 0.38 mm-thick gel film without suffering from nutrient and oxygen deprivation. Next, an imaging setup was customized for rapid automated scanning of the micro-colonies. As a demonstration, EGFP-expressing *E. coli* was used to evaluate the performance of the bacteria culturing device and the imaging setup. Herein, a modified confocal microscope with a motorized x-y sample holder plane was employed to scan the sample area and create phase contrast and fluorescence images side by side. Using fluorescence as a reference, automatically counting the micro-colonies in the phase contrast image was able to accurately provide the number of them. More importantly, this technique not only shortened the culturing time to within 5 hours, but also allowed the labor-intensive plate counting work to be automatically conducted on a glass slide, thoroughly overcoming the limitations of the conventional method.

2.2 Materials and Methods

2.2.1. Materials and Instruments

Luria-Bertani (LB) broth for growing bacteria was purchased from Sigma-Aldrich. Agarose was from Promega. Silicon wafer was obtained from University Wafer (Boston, MA). Agar, polystyrene petri dishes (diameter 100 mm), glass microscope slides and coverslips were purchased from Thermo Fisher Scientific. Escherichia coli (E. coli) K-12 expressing enhanced green fluorescent protein (EGFP) was received as gift from Dr. Yongku Cho's laboratory (University of Connecticut). The fluorescence from E. coli expressed EGFP was used only for validation purpose. Images were captured by Nikon A1R confocal microscope (Nikon, Japan) and processed using Nikon NIS Elements AR 4.40 software.

2.2.2. Preparation of On-Glass-Slide Bacteria Culturing Device

A microscope glass slide with two pieces of spacers (0.38 mm-thick silicon wafer) on the top of it was placed in a petri dish. Another piece of cover glass slide was then mounted on the silicon wafers to form an empty chamber between the two glass slides. Next, 2% (w/v) LB culture media and 0.6% (w/v) agarose were suspended in deionized water. This mixture was sterilized by autoclaving at 121 °C for 15 minutes. When the media cooled down below 60 °C, kanamycin was added to a final concentration of 50 μg/mL for the selection of EGFP expression. This molten medium was poured into the petri dish and filled the empty chamber. After the media was kept at room temperature for 20 minutes and became solidified, the cover glass slide was gently removed to present a thin film of nutrient gel with flat surface.

2.2.3. Preparation of Bacterial Samples

The cell culture media, 2% (w/v) LB broth was prepared by dissolving 2 g of LB powder (a mixture of 1 g tryptone, 0.5 g yeast extract, and 0.5 g sodium chloride) in 100 mL deionized water. Since *E. coli* cells carried antibiotic resistant gene as a reporter of the production of EGFP, kanamycin was added to a final concentration of 50 μg/mL for the selection of EGFP expression. *E. coli* cells from the stock were inoculated into LB broth and pre-enriched at 200 rpm in a 37 °C shaker for 4 hours to ensure the bacterial growth was at log phase. Then, the cells were diluted into various concentrations of interest with phosphate buffered saline (PBS). Bacterial suspension (5 μL) was dropped onto the aforementioned thin film of LB-agarose gel. After the drop completely evaporated, the petri dishes were transferred into a 37 °C incubator. The surface of culture area was placed upside down to prevent the loss of water content.

2.2.4. Imaging Bacterial Micro-colonies using Microscopic Scanning

After a 5-hour incubation, the glass slide with the thin film was taken out by cutting off the surrounding bulk of LB-agarose gel. Then, the silicon wafer spacers were removed and a glass coverslip was gently mounted on the cell culture area that carries micro-colonies. To ensure the distance between the micro-colonies and the lens constant, the coverslip side of the gel was mounted on a supporting glass slide. This setup was next placed on the motorized x-y sample holder stage of confocal microscope, where the supporting glass slide was at the bottom (Figure 2A). After the horizontal plane of micro-colonies was focused by the objective lens, images were continuously captured as the sample holder stage moved along a sequential path programmed by the control panel of Nikon software until the entire sample area was scanned (Figure 2C). Herein, tiles of phase contrast and fluorescence images (0.665

mm × 0.665 mm for each tile) were acquired simultaneously by an S Plan Fluor ELWD Ph1 20× objective lens (NA 0.45, Nikon, Japan). Finally, the Nikon NIS Elements software automatically created a large image by stitching all the tiles together.

2.2.5. Image Processing and Micro-colony Enumeration

The large image obtained from the confocal microscopic scanning was analyzed by using ImageJ software (NIH, USA). First, the threshold was adjusted to enhance the contrast of the objects of interest. Second, the image was binarized to remove the noise by rendering micro-colony regions with clear boundaries as black and surrounding background as white. After the binarization, filling-holes processing was conducted to ensure each closed region represents one intact micro-colony. Finally, micro-colony regions above desired size were outlined and the number of these regions was automatically counted by ImageJ software. An example of image processing is described in detail in Figure 5.

2.2.6. Bacteria Enumeration using Conventional Agar Plate

A sterile molten liquid mixture of 2% (w/v) LB culture media and 1.5% (w/v) agar supplemented with 50 μg/mL kanamycin was poured into petri dishes. As a gelling reagent, the agar can be replaced by agarose and the concentration of it can be adjusted according to specific need. After the media was solidified in 20 minutes, 100 μL of *E. coli* suspension was inoculated onto the surface of the gel by uniformly spreading it using a metal loop. The petri dishes were then incubated at 37 °C. After the bacterial colonies were detectable by naked eyes, the number of colonies was manually counted.

2.3 Results and Discussion

2.3.1 Preparation and Evaluation of On-Glass-Slide Bacteria Culturing Device

In previous studies, micro-colonies were grown and imaged on a film of nutrient gel, which had to be thin enough to deliver good transparency and thereby generate high-quality images. To prevent the thin gel film from drying out, it was sealed in a closed chamber during cell culture and imaging [90, 97]. However, limited nutrition and isolating oxygen supplies resulted in slow cell growth. To address this issue, we invented a special on-glass-slide bacteria culturing device (details of preparation is described in Experimental Section). As illustrated in Figure 1A, a glass slide was embedded in LB-agarose gel. On the top of the glass slide was a flat thin gel film, whose thickness (0.38 mm) was determined by that of the spacer. The cross-section of this device (Figure 1B) shows that the thin film is like a "bridge" connected the bulk gel. This unique design ensures that the film can continuously receive water and nutrition from the bulk gel, as well as oxygen from the ambient air, allowing long time incubation without gel drying and rapid formation of micro-colonies without suffering from any restriction on cell growth.

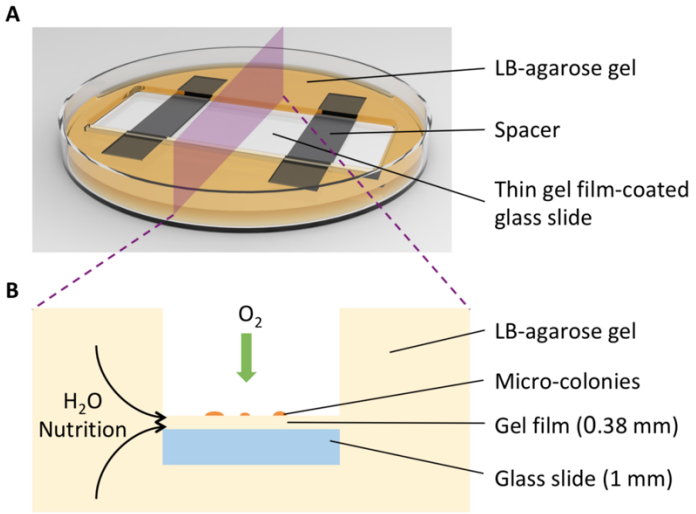

Figure 1. Schematics of the reported custom-built on-glass-slide microbial culturing device. (A) A thin LB-agarose gel film with flat surface created on a glass slide in a petri dish. The components of the device are described. (B) A cross-section of the device showing its capability of culturing microorganisms on the thin gel film without any growth limitation.

Regarding the composition of the semi-solid culture media, there was only one difference between our system and the conventional method. Here, we used agarose instead of agar to prepare the nutrient gel. Typically, agar is added to aqueous nutrition to form gel matrix, which helps immobilize microbial cells and support them to multiply to colonies. However, the opaque appearance of agar gel determines that it is not a good choice for imaging application [101]. As an alternative, agarose gel has been extensively employed for imaging due to better optical clarity [67, 72, 90, 97, 102-105]. Notably, the flatness of the gel surface is critical for acquirement of high quality scanning image and the accuracy of micro-colonies counting. Hence, we prepared the gel matrix using 0.6% (w/v) agarose rather than widely used 1.5%, since it was difficult to generate flat thin gel film when the agarose concentration was above 0.6%. Even though the gel becomes softer as agarose content decreases, as previously reported, 0.6% agarose or agar gel still possessed good ability to immobilize microbial cells and support their growth without any issue [103, 106].

To evaluate the cell-cultivability of this device, we inoculated same amount of bacterial suspension on LB-agarose thin film, conventional LB agar (1.5%) plate, and LB agarose (0.6% and 1.5%) plate respectively and monitored the growth of bacteria. Since inoculation, pictures of these LB agar/agarose plates were captured at 0, 8, 11, 13, 15, and 17 hours. It

was observed that the bacterial colonies became visible to naked eye and manually countable at 13 hours. The average size of the colonies from these methods showed no remarkable difference (Figure 2), suggesting that the cells on our custom-designed thin gel film grew as fast as on conventional agar plates. Therefore, microscopically analyzing the invisible micro-colonies would significantly shorten the detection time.

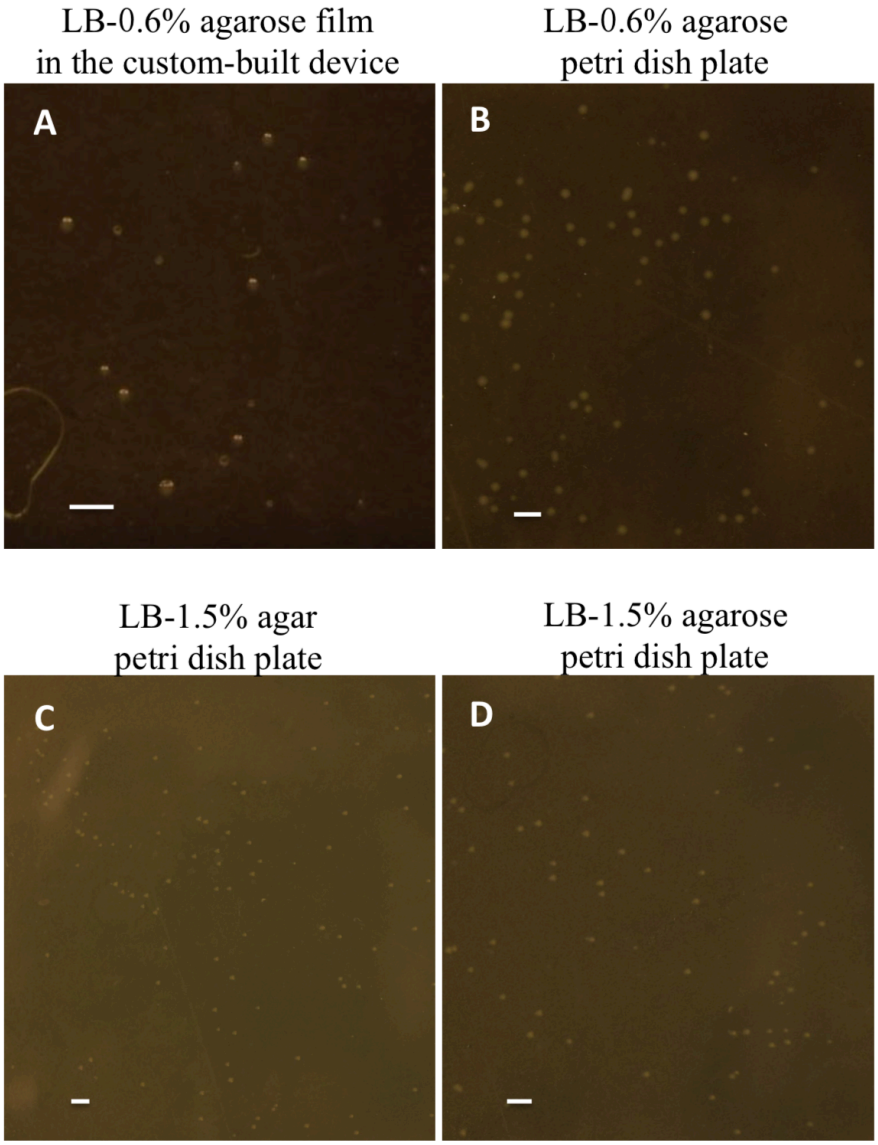

Figure 2. Representative images of bacterial colonies on LB-0.6% agarose thin film in the custom-built device (A), LB-0.6% agarose petri dish plate (B), LB-1.5% agar petri dish plate (C), and LB-1.5% agarose petri dish plate (D). The images were captured after 13 hours incubation at 37 °C. Scale bars: 2 mm.

2.3.2 Microscopic Scanning Micro-colonies on a Large Sample Area

Since bacteria cells are transparent in reality and do not affect the amplitude of visible light waves passing through them, high-contrast images are needed for recognizing them. Presented in Figure 3 are images of *E. coli* micro-colonies captured in phase contrast and DIC, respectively. Obviously, compared to DIC, it is much easier to utilize phase contrast to distinguish the micro-colonies from the background. Moreover, a halo surrounding each micro-colony indicates the boundary and further benefits the identification. Therefore, it is more suitable to utilize phase contrast for digitally recognizing the micro-colonies by using image-processing software.

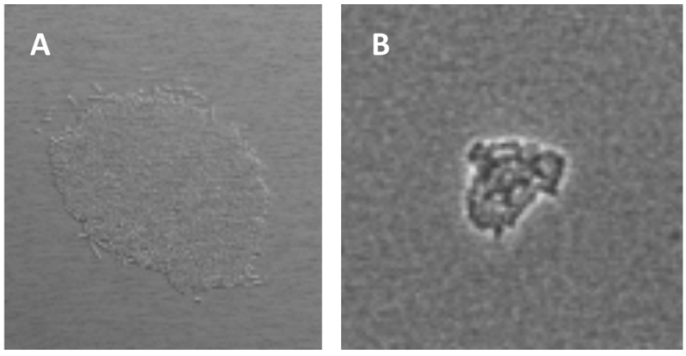

Figure 3. Representative images of bacterial micro-colonies in DIC (A) and phase contrast (B).

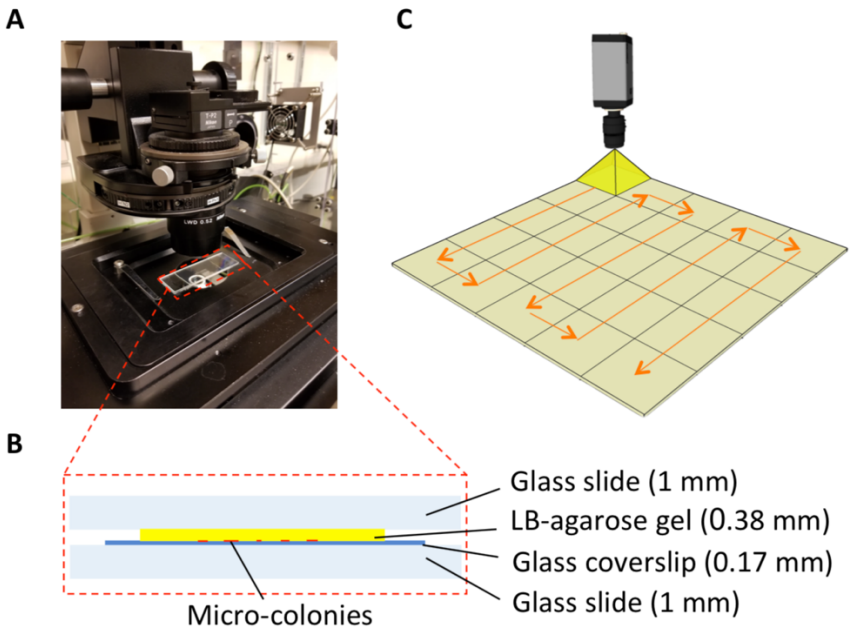

Figure 4. Schematic illustration of the reported micro-colony imaging system. (A) a photograph of the experimental setup. (B) The components of a sample setup. The thickness of each component is described. (C) The scanning of the entire cell culture area on thin LB-agarose gel film is conducted by sequentially capturing images in field-of-views. Each square on the plane represents a field-of-view. The arrows indicate the path of the movement of the camera.

Aiming at recording all the micro-colonies in one image, we employed microscopic scanning technique to generate an image encompassing the entire sample area. Such scanning was conducted by continuously capturing tiles of images on certain focal plane and stitching the tiles together into a large image. Considering bacterial micro-colonies growing on gel matrix actually expand in three dimensions [107] and their thickness may not be uniform, significantly more time would be consumed on locating each object through continuously focusing at different depths in the z-direction. To enable fast imaging, we

customized the sample setup to ensure that all the micro-colonies could be scanned without conducting any z-scanning. As illustrated in Figure 4B, the setup consisted of a glass slide on the top, a gel film in the middle, a coverslip and a supporting glass slide on the bottom. The micro-colonies at the bottom side of the gel film were compressed on the coverslip by the gravity of the glass slide on the top. The robust flat surface of the supporting glass slide rendered a horizontal coverslip-gel interface, which could be considered as a perfect target plane for the scanning. Moreover, the thickness of the coverslip and supporting glass was fixed, assuring that the distance between the target plane and the lens remained constant. Hence, no concern about any out-of-focus issue was expected.

To test the performance of this system, we used EGFP-expressing E. coli as a model bacterium and conducted scanning of the micro-colonies grown from them. Although bacteria cells in reality are seldom fluorescent, the green fluorescence from micro-colonies was merely used as a reference to corroborate the accuracy of the result obtained from phase contrast images. Herein, we chose confocal microscopy to meet the specific need of both phase contrast and high-quality fluorescence images in this study. As the LB-agarose gel is a thick specimen with considerable autofluorescence, the confocal microscope can block the out-of-focus light above and below the focal plane by the spatial pinhole and therefore provides higher resolution and enhanced contrast by increasing signal-to-noise ratio [108-110]. Additionally, since the transmitted light mode of confocal microscopy can also view specimen through phase contrast [111], confocal microscopy is capable of simultaneously generating high-quality fluorescence and phase contrast images and viewing them side by side, whereas this cannot be achieved by other microscopy. However, it is worth noting that

confocal microscopy is not required for real applications if only phase contrast is employed in enumeration of viable microorganisms. After the bacteria cells on thin gel film were incubated at 37 °C for 5 hours, the culture area was scanned at a speed of approximately 17.7 mm^2/min by a 20× objective lens. Figure 5 displays a large image (1.16 cm × 1.81 cm) created by stitching tiles of images together. The area was large enough to accommodate all the micro-colonies. Zooming in the large image enabled us to identify each micro-colony by phase contrast or fluorescence. It was clear that the micro-colonies presented on the boundaries between the tiles were in their normal shape, suggesting that there was no stitching artifact, such as duplication or disappearance. Therefore, the large image acquisition function presented here was able to accurately deliver the number of the micro-colonies.

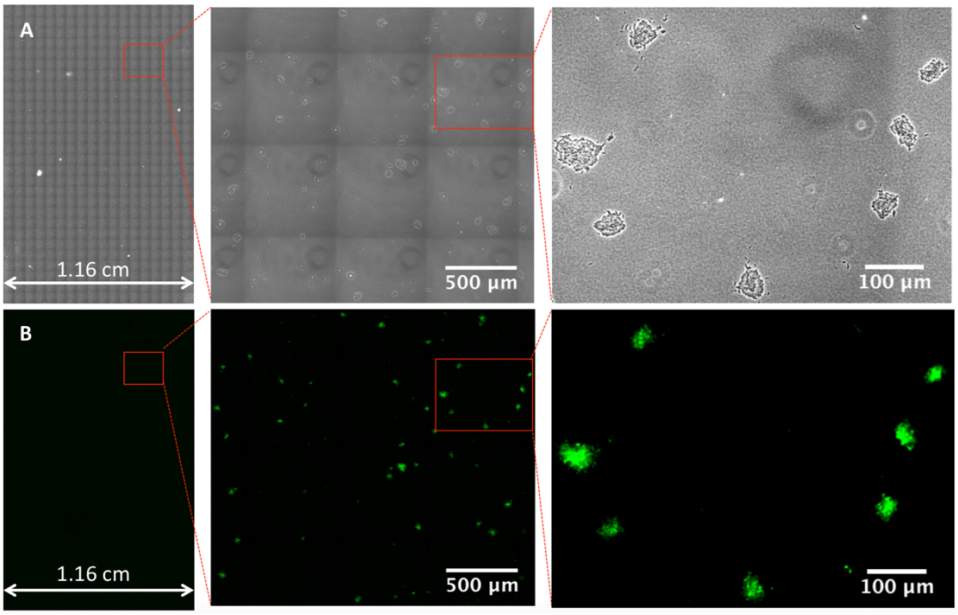

Figure 5. Representative images captured by using the reported platform. Transmitted light (A) and fluorescence (B) images of bacterial micro-colonies presented on an area of 1.16 cm × 1.81 cm. Fluorescence image was only used for confirmation purpose.

2.3.3 Micro-colony Enumeration

After the images were acquired by confocal microscopy scanning, the micro-colonies appeared there were enumerated by using image-processing software. Figure 6A presents a selected area containing micro-colonies grown from the cells in 5 μL bacterial suspension. In addition to micro-colonies, empty regions that could be produced by artifacts or tiny air bubbles were also shown in the image. Nonetheless, these objects do not cause any interference in recognizing the micro-colonies. It is known that phase contrast is generated by the difference in density. Since no other elements, such as the empty regions, throughout the imaged area were as dense as the micro-colonies, micro-colonies can be easily distinguished by filtering the objects with low contrast. Figure 6B shows the corresponding processed image, in which the total number of micro-colonies (dark regions) was counted as 155 (details of the algorithms applied in automated enumeration are described in Figure 7). The locations of the micro-colonies and the number of them were consistent with those obtained from the fluorescence image (Figure 6C), indicating that the result obtained from phase contrast image was trustworthy. To validate if this result represented actively growing micro-colonies, the imaged sample was placed back into the agar plate and further cultured *in situ* for 20 hours at room temperature until visible colonies appeared. The image of these

visible colonies (Figure 6D), which was captured by a Nikon D5300 DSLR camera (Nikon, Japan), was used to compare with that of micro-colonies side by side.

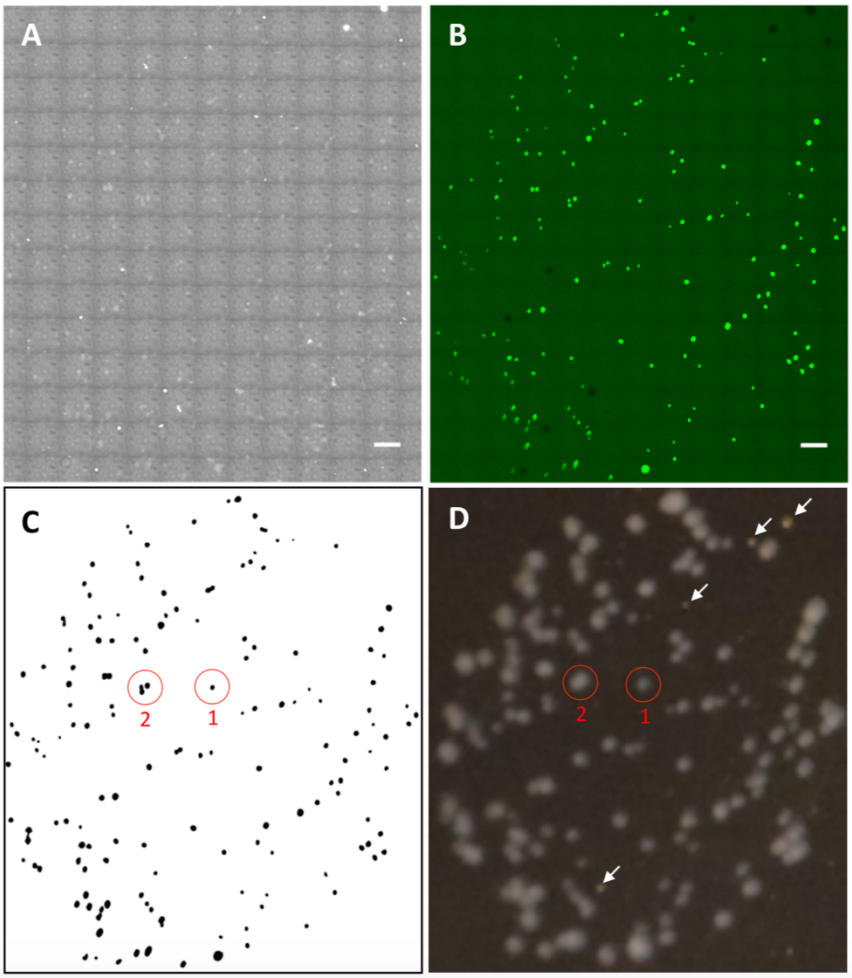

Figure 6. Phase contrast (A) and fluorescence (B) images of an area (7.9 mm × 9.0 mm) containing micro-colonies grown from the inoculated cells in 5 µL bacterial suspension. Scale bars: 500 µm. Fluorescence image was only used for confirmation purpose. (C) An image processed from the raw image in (A). The black spots indicate micro-colonies. (D) A photograph of visible colonies in situ developed from the micro-colonies shown in (A) and (B). The whitish dots were

bacterial colonies. The objects pointed by the white arrows were debris, which can be distinguished from the bacterial colonies by the colors. The difference in color can be more easily identified from the high-resolution photograph shown in Figure 8.

Apparently, all the micro-colonies were capable of actively growing, indicating that the number of micro-colonies certainly represents that of viable microbial microorganisms. Furthermore, we found that, multiple micro-colonies in close proximity to each other, which could eventually develop to one single visible colony under the conventional agar plate enumerating method, can be identified and differentiated microscopically using our method. For instance, colony 1 was derived from one micro-colony, whereas colony 2 was developed from three neighboring micro-colonies. This finding suggests that, especially when the density of cells inoculated on an agar plate is high, the counts obtained from the conventional method are much likely to be underestimated. By contrast, our digital enumeration technique can differentiate the neighboring micro-colonies at the earliest stage and be more accurate than counting large visible colonies used in conventional methods. According to specific needs, the upper counting limit can be increased by simply expanding the scanning area. This feature allow that fewer or even no dilutions are needed using our enumerating method, which could reduce the serial dilution-induced error. Furthermore, enumerating around 200 micro-colonies within an area of 60 mm^2, which is the maximum limit of a 100 mm agar plate, took only around 3 minutes, freeing up more space and workload on sample preparation through miniaturizing the work on a piece of glass slide. It is worthy of noting that the scanning time was limited by the function of confocal microscopy. In this study,

confocal microscopy was only used to evaluate the performance of our custom-designed bacteria culturing and imaging system in the compatibility with the microscopic scanning function. In practice, since the technique reported here can accurately deliver the counts of micro-colonies only from phase contrast images (fluorescence imaging is not necessary), some recently emerged ultrafast high-resolution microscopic scanning techniques [112-114], which can conduct whole glass slide scanning in a few minutes, would be able to further reduce the scanning time per unit area and thereby provide counting result in a timely and high-throughput manner.

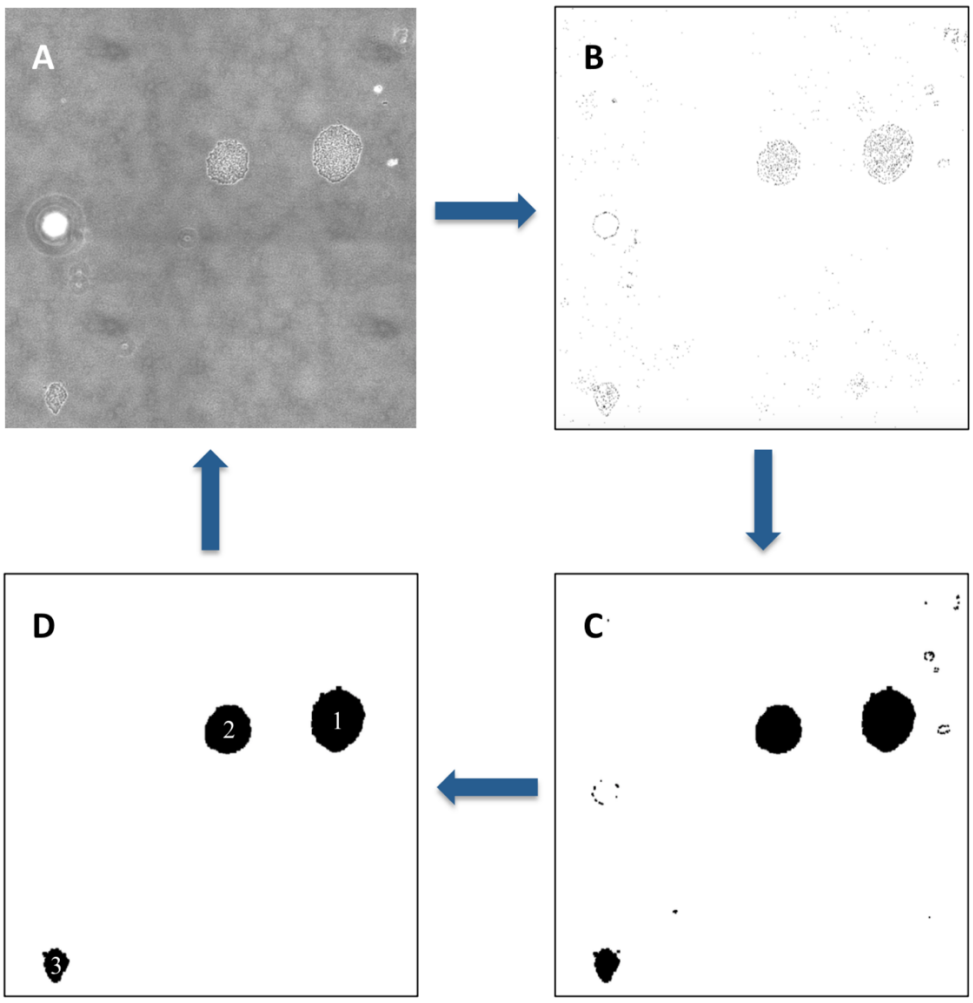

Figure 7. An example of automated enumeration of micro-colonies. The original transmitted light image (A) was processed through adjusting threshold (B), finding edges, binarization, and filling the holes (C), and the black regions above certain size were counted by using ImageJ (D).

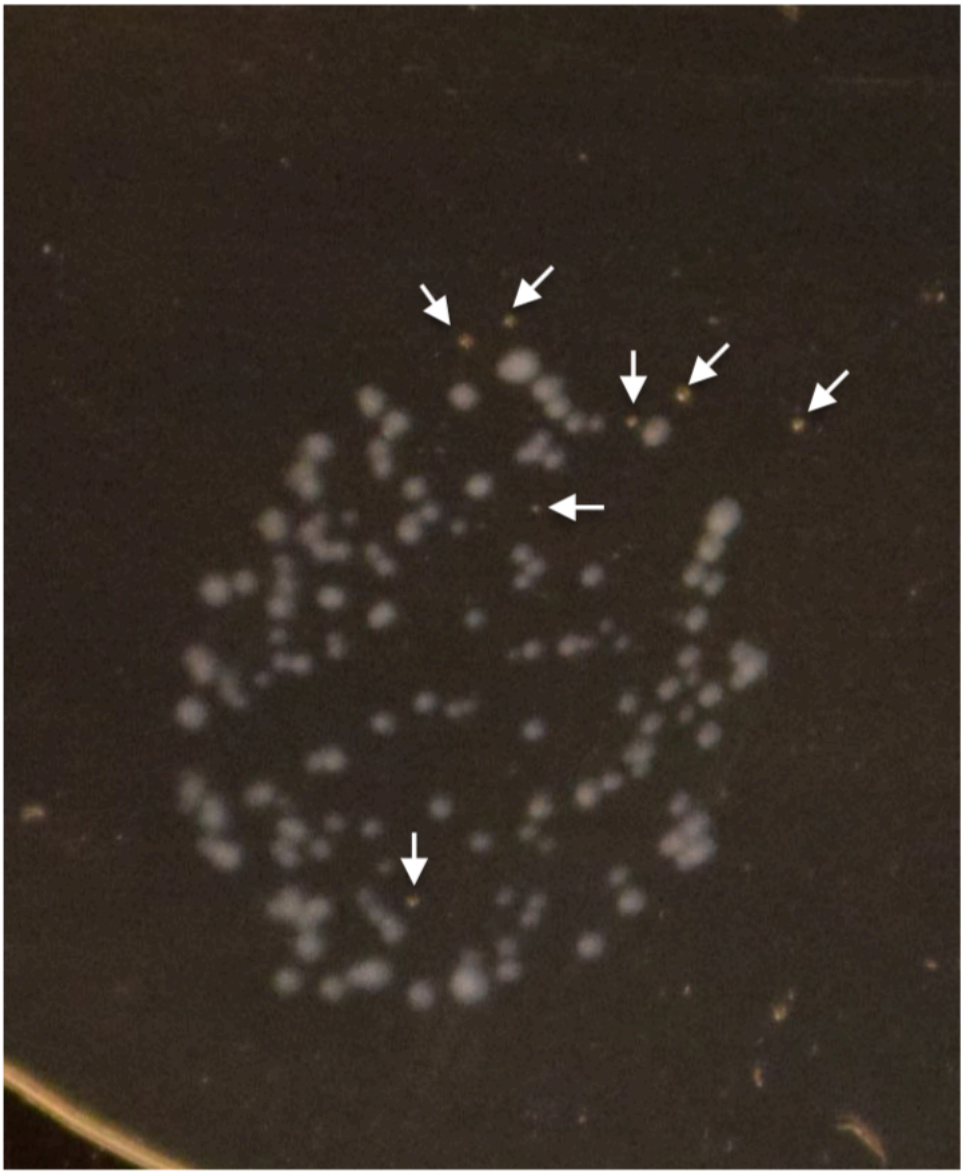

Figure 8. The original photograph of visible colonies shown in Figure 4D. The whitish dots were bacterial colonies. The objects pointed by white arrows were debris, which can be distinguished from the bacterial colonies by the colors.

2.4 Conclusions

We demonstrated a unique technique that enabled digital, rapid, accurate, label-free enumeration of viable microorganisms using optical scanning microscopy. A custom-built bacteria culturing and imaging system was applied to ensure that all the micro-colonies on the large sample area could be displayed on an image generated by microscopic scanning. Since the micro-colonies can be counted based on their phase contrast rather than fluorescent staining, the procedures are much simplified, rendering this technique applicable to a wide range of microorganisms that can form micro-colonies with clear edges. Employing *E. coli* as a model bacterium, our method reduced the cell culture time from at least 13 hours required for the conventional method to within 5 hours. Compared to conventional enumerating methods requiring an overnight (18-24 hours) incubation, such improvement would benefit the analytical methods that require rapid and accurate quantitative determination of bacteria. Moreover, since the employment of confocal microscopy proved that this enumeration system was compatible with the microscopic scanning function, the application of cost-effective ultrafast microscopic scanning techniques in the future would significantly enhance the performance of our system by miniaturizing the bacteria enumeration work with hundreds of agar plates into a piece of microscope glass slide. Notably, regarding the quantification of viable bacteria, this method is more accurate than the conventional agar plate method due to the fact that neighboring bacteria before merging

into one large visible colony can be differentiated using our method. Therefore, this microscopic scanning-based micro-colony enumeration system has great potential for being adopted as a standard tool for quantifying viable microorganisms.

Chapter 3

Whole Slide Imaging for High-throughput Monitoring Bacterial Growth at Single-Cell Level and Its Application to Rapid Antibiotic Susceptibility Testing

3.1 Introduction

Due to the overuse and misuse of antibiotics, the increasing emergence and spread of antibiotic-resistant bacteria in human infections, such as MRSA,VRE, ESBL- and carbapenemase-producers, has become a global threat to public health [8, 115-119]. Unfortunately, the lacking of newly developed antimicrobial agents has been worsening the crisis [120, 121]. To reduce inappropriate use of antibiotics, antibiotic susceptibility testing (AST) is employed by healthcare providers to guide the prescription of antibiotics. The most widely accepted AST methods, such as broth/agar dilution and Kirby-Bauer disk diffusion, are based on the observation of visible bacterial growth in the presence of antibiotics [40]. These conventional methods are routinely used and cost-effective, but they typically require at least 24-72 h for reliable readout [122]. Such delay leads to empirical use of antibiotics and consequent increase in mortality [123, 124]. Especially for patients with septic shock, initiation of inappropriate antimicrobial treatment results in a 5-fold decrease in survival [44]. An alternative AST approach relies on the detection of specific genes or proteins responsible for antibiotic resistance by molecular techniques, such as polymerase chain

reaction (PCR) and mass spectrometry [46, 47, 125-129]. Although molecular methods are sensitive and fast, the existence of biomarkers do not always correlate to phenotypic antibiotic resistance [130]. Furthermore, if new resistance mechanisms arise, they are likely to result in false negatives [131]. Thus, rapid AST techniques without compromising accuracy are urgently needed.

To date, a plethora of innovative approaches have been developed to shorten the time for AST to a few hours or less [50, 132]. Particularly, several platforms employed microfluidics, optical imaging techniques, or mass sensor arrays to determine antibiotic susceptibility by monitoring single-cell growth [67, 68, 71, 74, 75, 80]. Considering that antibiotic resistant and susceptible cells coexist in clinical samples [69, 70], apparently, detecting the rapidly multiplying individuals in a background of dying cells would take much less time than assays monitoring population growth. Thus, single-cell AST techniques would be more applicable for point-of-care tests. Nevertheless, since bacterial cells vary largely in their growth rates, the ability of available single-cell AST methods in providing precise results with statistical significance is hindered by low throughput. In a recent study, the throughput was significantly improved by analyzing the growth rates of thousands of single cells confined in microfluidic channels [75]. Although the concept introduced in this work is elegant, as clinical samples are typically polymicrobial and even genetically identical cells vary in size and shape [133-135], fixed dimensions of the channels would not be able to trap every single cell with various size and shape, thus losing potentially useful data concerning biological heterogeneity. In addition, since cells were confined to proliferate in only one direction, and the ability of each cell to overcome the external restriction may vary, detection

of growth rate using this method might not be as accurate as the results obtained from free-growing cells.

Here, we report a novel single-cell AST technique based on whole slide imaging (WSI) technique. Capable of digitizing a specimen on a glass slide into a single image, WSI has been extensively exploited to image histopathology slides for diagnostic use [136-138]. However, to our knowledge, the applications of WSI in AST have not been reported yet. In this study, WSI was employed to expand the imaging area, thereby allowing the visualization of a large population of cells regardless of their biological heterogeneity. As a demonstration, we conducted time-lapse imaging of thousands of *E. cloacae* cells in a WSI-compatible bacterial culturing glass slides that we previously reported [139] to track single-cell growth. Antibiotic susceptibility profiles of *E. cloacae* against gentamicin was determined by high-throughput analyzing single-cell growth rate. Moreover, to address the advantage of the significant improvement in throughput, our technique was applied to determining antibiotic susceptibility of an artificial phenotypically heterogeneous sample, in which the number of antibiotic resistant cells was negligible compared to that of the susceptible cells. For validation purposes, results obtained from our method were compared with the gold standard broth dilution method.

3.2 Results and Discussion

3.2.1 WSI-based monitoring bacterial growth at single-cell level

To obtain an image encompassing a large population of single cells, "sandwich" slides with great bacterial cultivability that we previously customized for WSI was employed

[139]. As illustrated in Scheme 1, this system consists of a cover glass on the top, a supporting glass at bottom, and a 0.38 mm-thick gel pad with good optical transparency in between. Bacterial cells are immobilized on the interface between the gel and the supporting glass. Notably, owing to the "sandwich" structure and refined composition of the gel, the gel pad is robust enough and tightly adhered to the supporting glass to avoid any deformation or sliding during WSI. Next, phase contrast images of the entire sample area were acquired as the sample stage moves and seamlessly stitched together into one image.

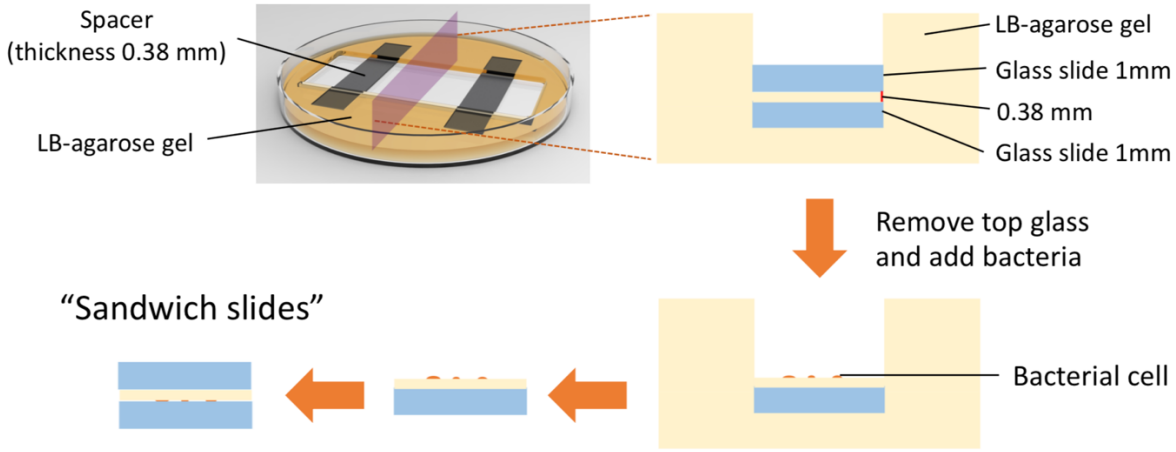

Scheme 1. Schematic illustration of the preparation of the "sandwich slides" for bacterial culturing and whole slide imaging.

To test the performance of this system, we conducted WSI to image *E. cloacae* cells deposited into the "sandwich" slides. Considering that the bacteria cells are small and might not sit on the same focal plane, rapid autofocus technology was applied to minimize out-of-focus issue. As a demonstration, Figure 1 displays a composite image of a sample area (8.48 mm × 7.69 mm). Zooming in the image enabled the visualization of individual cells, which

were all in-focus. Herein, using a 40× objective lens, the imaging took only 3.5 min. Considering that the natural doubling time of bacteria is ~20 min and even longer during antibiotic treatment, it was assumed that there was no significant change in cell size during such fast imaging.

To employ this system to monitor single-cell growth, the "sandwich" slides were incubated at 37 °C and a humidity of 90%, under which condition the dimensions of the gel pad were not changed. Subsequently, time-lapse imaging was conducted on the same sample area at 15, 30, 45, and 60 min. After the composite images were collected, they were processed by ImageJ software and converted into binary format images, in which the cells were black and background was white. Since each composite image was in gigabytes, we selected a small subarea containing 9 cells as a demonstration of analyzing single-cell growth (Figure 2). To quantify the bacterial size, the area occupied by a single cell or the corresponding microcolony developed from it was measured from the processed images. Since there was no significant drifting of the x-y coordinates while the bacterial cells were growing, the areas with matched coordinates represented a group of bacteria originated from the same cell. For each individual cell, the normalized growth rate at time t was calculated using equation (1), where A_t and A_0 are the areas originated from the same cells at time t and time 0, respectively. Depicted in Figure 3 are the growth rate curves of 9 cells. Apparently, at each time point, the variation of the growth rates was large, emphasizing the necessities of analyzing a large population of cells for accurate determination of antibiotic susceptibility at single-cell level.

$$Normalized\ growth\ rate = \frac{A_t}{A_0} \qquad (1)$$

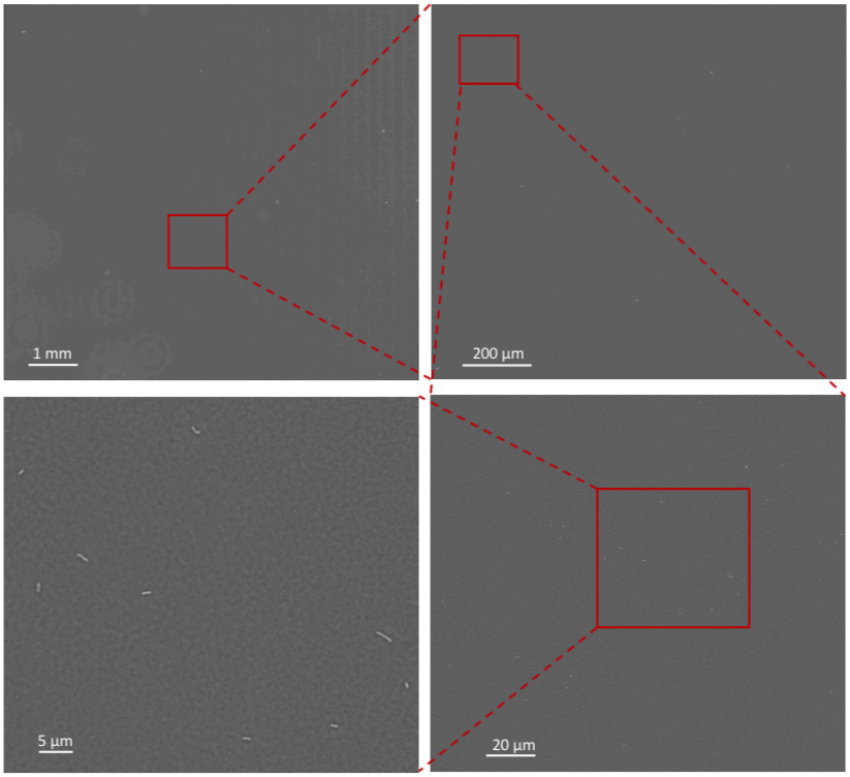

Figure 1. A representative composite image captured by the reported platform. Zooming in the image allows the visualization of single bacterial cells.

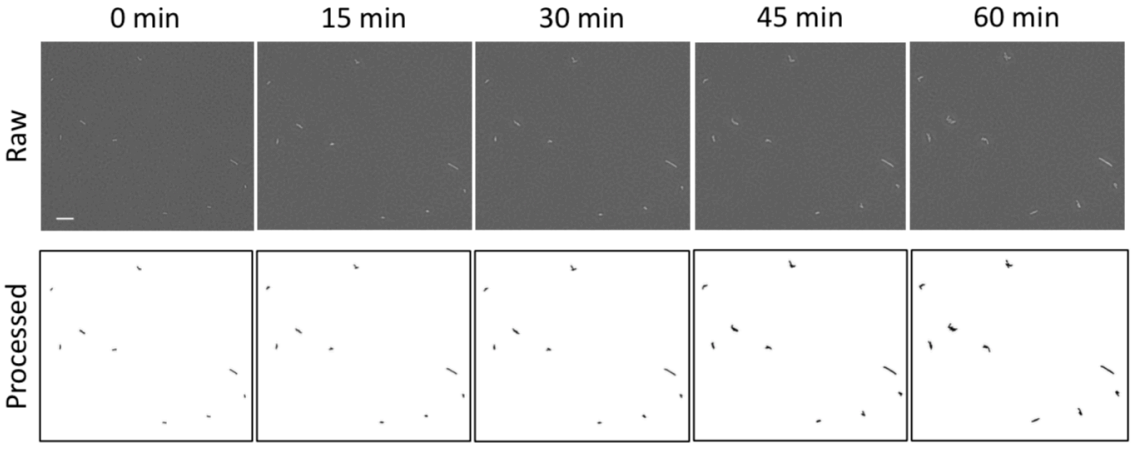

Figure 2. Time-lapse images of one representative area selected from the composite image in Figure 1 and corresponding post-processing binary images. Scale bar, 5 μm.

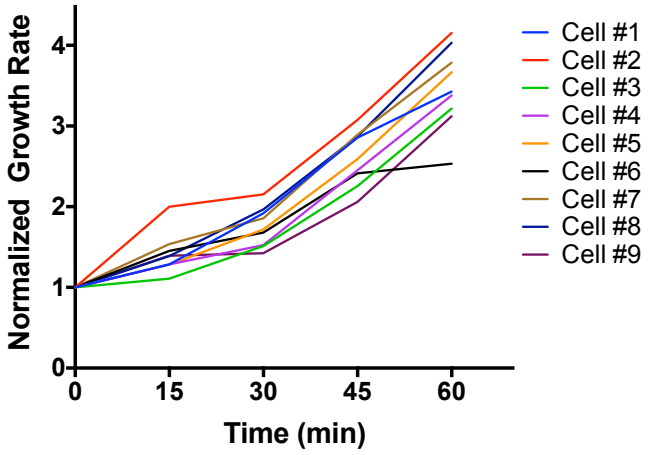

Figure 3. Single-cell growth rate of bacterial cells presented in Figure 2.

3.2.2 Determination of minimal inhibitory concentration (MIC) by WSI-based AST

To investigate the ability our method to determine antibiotic susceptibility, we performed tests through tracking single-cell growth of *E. cloacae* in response to gentamicin treatments, which is illustrated in Scheme 2. Herein, the tested concentrations of gentamicin in gel pad were 2, 4, 8, and 16 μg/mL and the number of cells treated at each antibiotic concentration were 3964, 4387, 5199, and 5778, respectively. The populations were sufficiently large to show statistically significance in addressing the biological heterogeneity. Based on the analysis results obtained from time-lapse images of the sample area captured at 0, 15, 30, 45, and 60 min, we found that the growth rates of the cells at each time point were highly diverse and displayed broad distributions (Figure 4). To simplify the

analysis, we set integral bins for the growth rates and obtained cell count-based distributions shown in Figure 5. Assuming that the fraction of cells beyond the threshold of 2 were those had been replicated, obviously, such fractions treated with 2 and 4 μg/mL gentamicin increased over time, suggesting that a majority of cells were continuously growing. In the groups treated with 8 and 16 μg/mL gentamicin, even though the replication of most of cells were arrested, a tiny portion of cells still survived and completed one replication. By specifically examining the growth rates of these cells, we learned that all of them were in a trend to stop growing by 60 min. Regarding the effectiveness of eventually inhibiting cell growth, as depicted in Figure 6, MIC could be determined as 8 μg/mL, which agreed with the result from conventional broth dilution method (Figure 7).

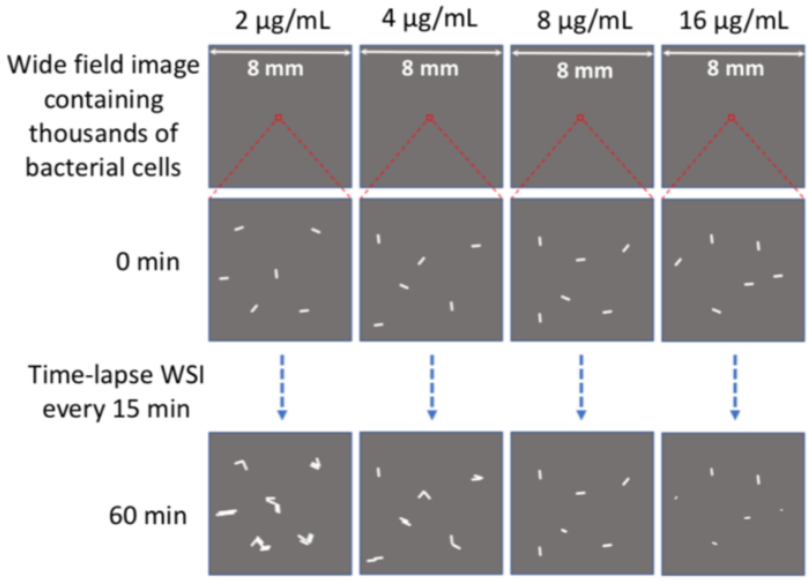

Scheme 2. Schematic illustration of WSI-based approach for rapid AST.

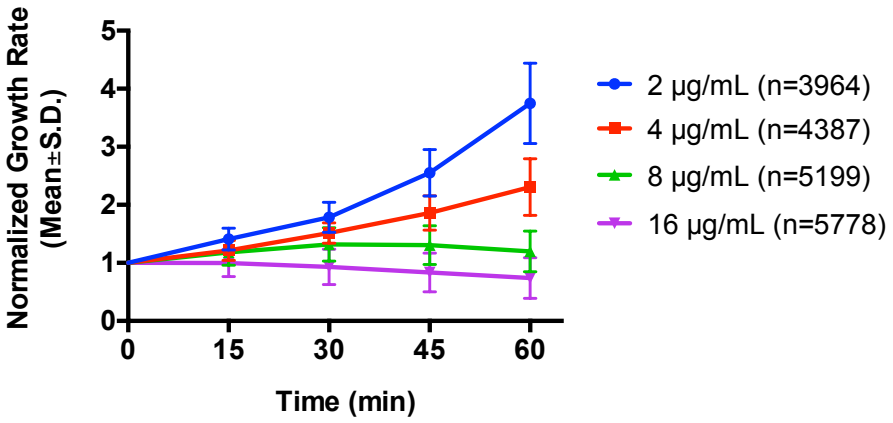

Figure 4. Normalized growth rate (Mean ± S.D.) versus incubation time.

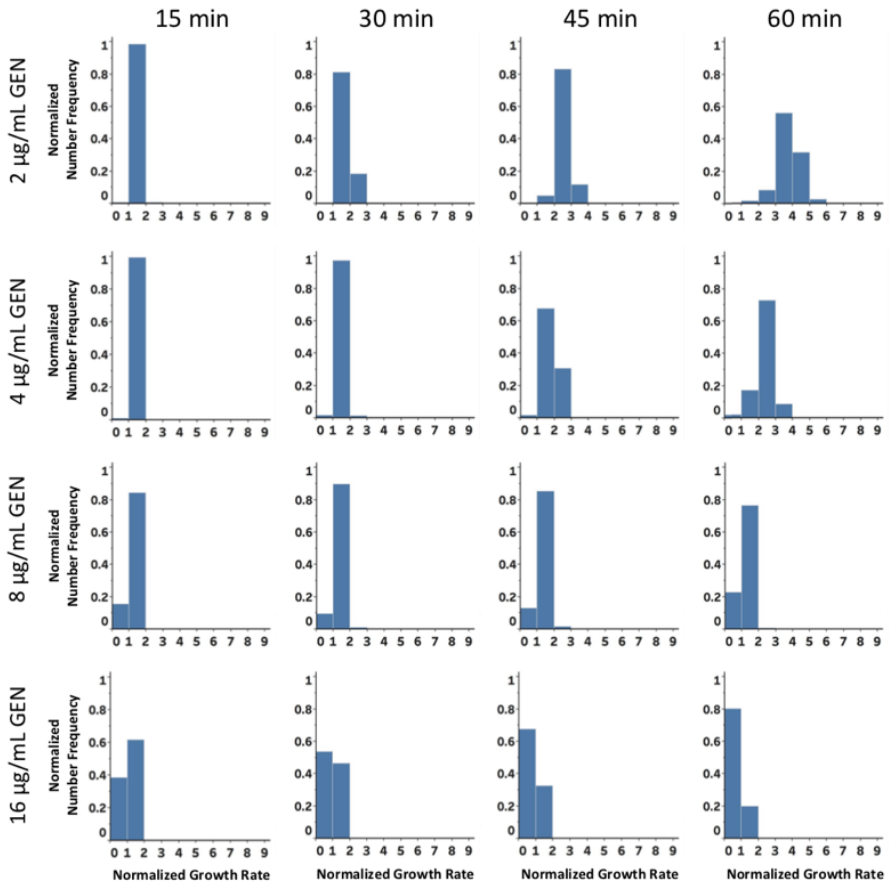

Figure 5. Number-based distribution of normalized single-cell growth rate for several thousand *E. cloacae* cells treated with 2, 4, 8, and 16 µg/mL of gentamicin.

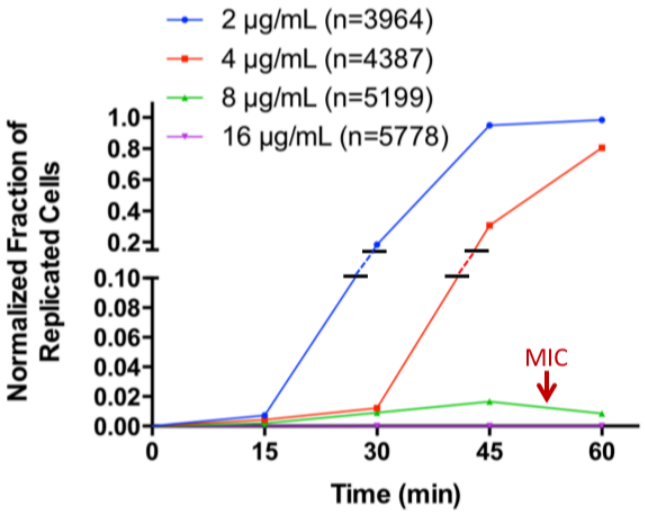

Figure 6. MIC determination by reported AST approach. The curves were plotted by normalized fraction of replicated cells from each treated group versus time.

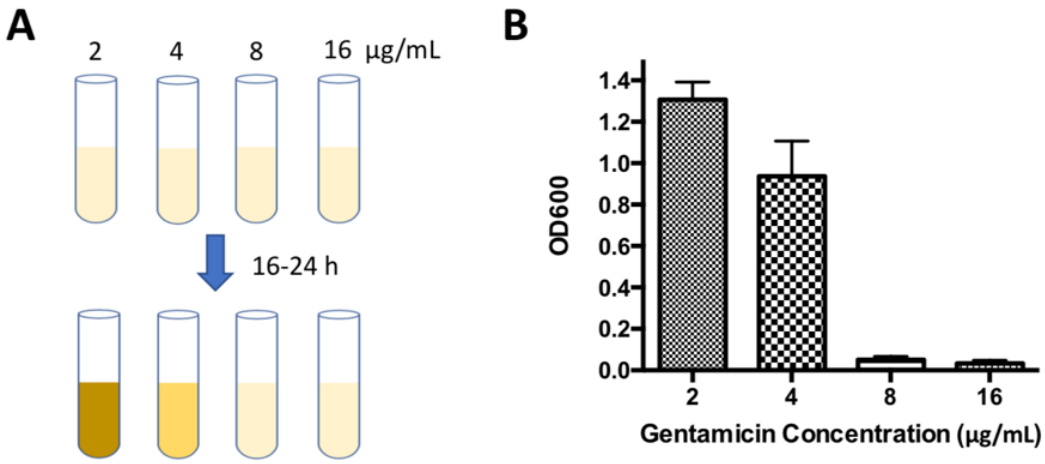

Figure 7. (A) Graphic description of MIC determination by broth dilution method. (B) OD600 obtained after the bacteria were incubated for 16 h.

3.2.3 Rapid antibiotic susceptibility determination of phenotypically heterogeneous samples

In practice, clinical bacteria isolates are complex because antibiotic resistant and susceptible bacteria coexist. Especially if the portion of the resistant phenotype is extremely small, accurately assessing the antibiotic susceptibility of such sample still remains challenging. Herein, our AST platform was further employed to analyze an artificial sample containing a mixture of kanamycin resistant *E. coli* and kanamycin susceptible *E. cloacae*, where the number of resistant cells was extremely low. Cells were treated with 50 μg/mL kanamycin, which was effective enough to selectively allow *E. coli* proliferate, while kill *E. cloacae*. Figure 8 and 9 show a representative field of view selected from an area of 7.46 mm × 7.12 mm and the corresponding plot of normalized growth rate versus time. Apparently, only one out of five bacteria was actively growing. Depicted in Figure 10 are single-cell growth rate distributions for a total 2189 cells in the sample area at different time points. If a value of 2 is set as the threshold to separate replicated and non-replicated populations, as illustrated in Figure 11, the fractions of replicated cells at 15, 30, 45, and 60 min are 0, 0.05%, 0.82%, and 1.15%, respectively. In contrast, the majority remained non-replication and their size shrank over time, indicating that they were sensitive to kanamycin. Further examining each cell growth rate curve confirmed that 25 cells (1.15% of total count) continuously multiplied while the others did not. Therefore, our method was able to distinguish antibiotic resistant phenotype from susceptible phenotype within 1 h, especially the portion of resistant subpopulation was as small as only about 1%. For comparison, conventional broth dilution was performed with sample volume of tested sample. The liquid medium turned to turbid after 20 h incubation, suggesting that our approach was powerful in saving significant time without compromising the accuracy.

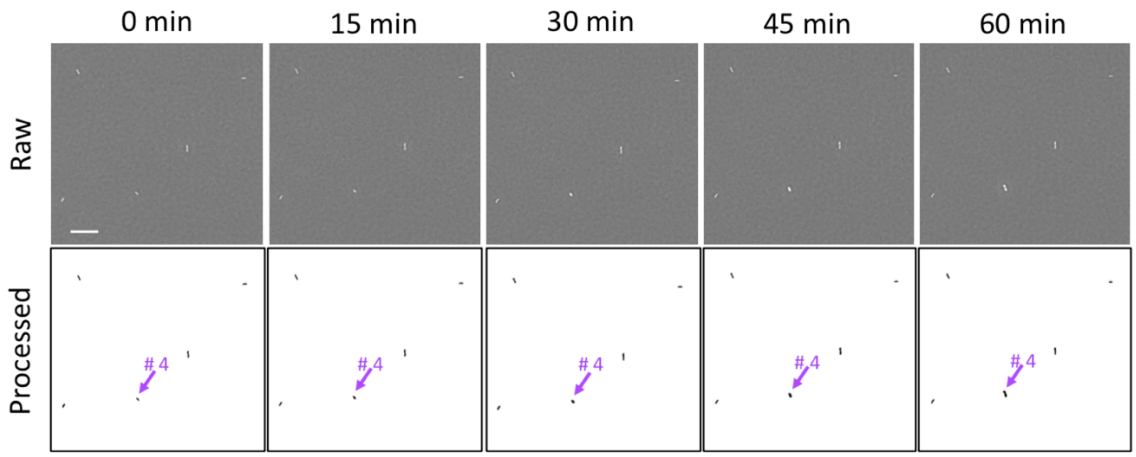

Figure 8. Time-lapse images of one representative area, where kanamycin resistant *E. coli* and susceptible *E. cloacae* cells coexist in the presence of 50 μg/mL of kanamycin, and corresponding post-processing binary images. Scale bar, 10 μm. Actively growing cells are marked with purple arrows.

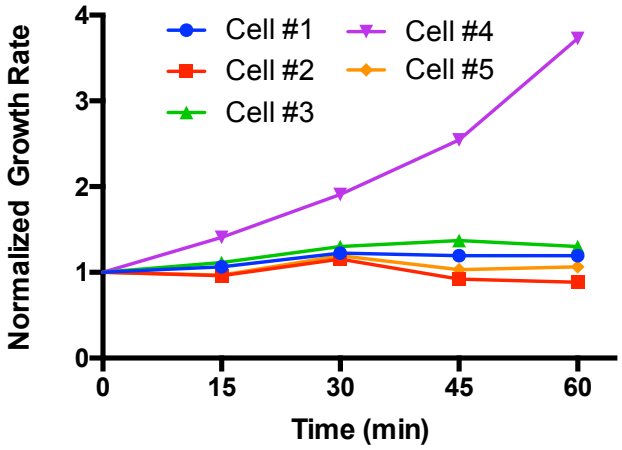

Figure 9. Single-cell growth rate of bacterial cells shown in Figure 5.

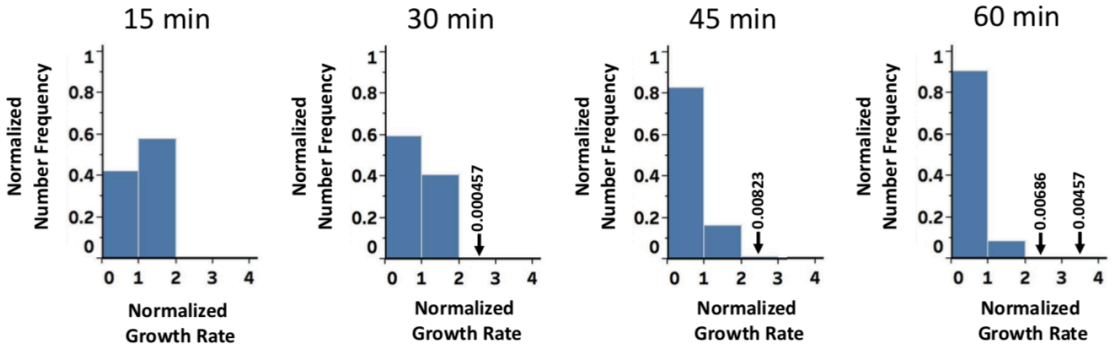

Figure 10. Number-based distribution of normalized single-cell growth rate for several thousand mixed bacterial cells treated with 50 μg/mL of kanamycin.

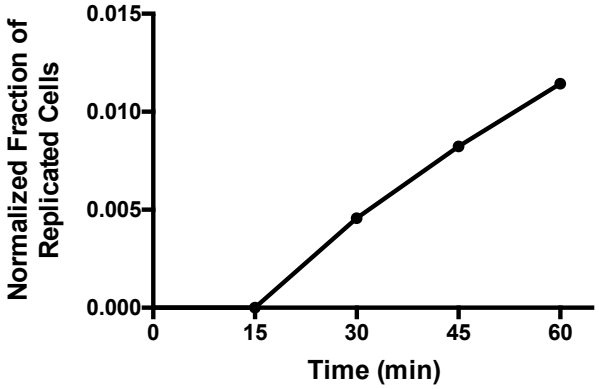

Figure 11. Normalized fraction of replicated cells versus time.

Despite the great performance in accurately determining the antibiotic susceptibility profiles for complicated bacterial samples, as the acquisition of a wide-field image containing several thousand cells takes about 4 minutes, testing multiple antibiotic concentrations simultaneously is still challenging. However, recently emerged ultrafast high-resolution WSI techniques [113, 114, 140]would raise the promise in solving this issue by completing the acquisitions of multiple wide-field images in one minute.

3.3 Materials and Methods

3.3.1 *Materials and instruments*

Mueller-Hinton (MH) broth, Luria-Bertani (LB) broth, ampicillin sodium salt, and gentamicin sulfate were purchased from Sigma-Aldrich (St. Louis, MO, USA). Agarose was obtained from Promega (Madison, WI, USA). Silicon wafer was purchased from University Wafer (Boston, MA, USA). Kanamycin sulfate, polystyrene petri dishes (diameter 100 mm), and glass microscope slides were purchased from Thermo Fisher Scientific (Waltham, MA, USA). *Enterobacter cloacae* (*E. cloacae*) (ATCC 13047) was purchased from the American Type Culture Collection (Manassas, VA, USA). A genetically engineered kanamycin resistant *Escherichia coli* (*E. coli*) strain was used as a model bacterium. Image acquisition was conducted using BZ-X800 All-in-One fluorescence microscope (Keyence Corporation, Japan).

3.3.2 Bacterial cell culture

As the bacteria used in this study are resistant to certain antibiotics, corresponding antibiotics were added into the culture medium for the selection purpose. *E. cloacae* and kanamycin resistant *E. coli* were cultured in LB medium supplemented with 50 μg/mL ampicillin and 50 μg/mL kanamycin, respectively. All the antibiotics solutions were sterilized by being filtered through 0.2 μm PVDF membrane (EMD Millipore, Burlington, MA, USA) prior to the addition to LB medium. After the stocked bacteria were inoculated in LB medium and pre-enriched in a 37 °C shaker for 3 hours, the cells were diluted with phosphate buffered saline (PBS) to desired concentrations for the testing.

3.3. Sample preparation

First, two parallel microscope glass slides with two pieces of spacers (0.38 mm-thick silicon wafer) in between were placed in a petri dish. Next, MH medium with 0.6% (w/v) agarose suspended in it was sterilized by autoclaving at 121 °C for 15 min. After the media cooled down below 50 °C, antibiotic was added, and this molten medium was subsequently poured into a petri dish and filled the empty chamber between the glass slides. This petri dish was placed on a horizontal benchtop at room temperature. After the medium was sufficiently solidified, the cover glass slide was gently removed to present a thin gel pad with flat surface. Then, 2.5 μL bacterial suspension was carefully loaded onto the gel pad without disrupting the surface. After the drop completely evaporated, the glass slide and the thin gel pad together was taken out by cutting off the surrounding bulk gel and mounted the side of gel pad with bacteria on another glass slide for WSI.

3.3.4 Whole slide imaging

The aforementioned sandwiched glass slides were placed on the imaging stage of microscopy cell incubator, wherein the bacteria side of the gel was in contact with the supporting glass slide. After the horizontal plane of bacterial cells was focused by the objective lens, the boundary of sample area was determined by the auto-searching function of the Keyence microscope. Next, cells in 10 different FOVs throughout the sample area were focused one by one to ensure the autofocusing during the scanning. Subsequently, tiles of phase contrast images were continuously captured as the sample holder stage moved along a sequential path programmed by the imager software until the entire sample area was scanned. Herein, tiles (0.362 mm × 0.272 mm for each tile) were acquired by a 40× objective

lens (NA=0.60, S Plan Fluor ELWD Ph2, Nikon). Then, the BZ-X800 analyzer software automatically created a composite image by seamlessly stitching all the tiles together. After the first scanning, the temperature of the incubator was set to 37 °C. The scanning was repeated at 15, 30, 45, and 60 min after the temperature reached 37 °C.

3.3.5 Image processing and data analysis

The images obtained from WSI were processed by ImageJ software version 1.52i (NIH, Bethesda, MD, USA). First, the threshold was adjusted to enhance the contrast of the bacterial cells and render cells as black and background as white. Next, the area of each cell or microcolony developed from it was measured in pixels. Those below 15 pixels were filtered as they were considered as noise from the background. Then, these values of area were grouped according to the x-y coordinates on the image to deliver the change in size as each single cell grew over time. Finally, the normalized single-cell growth rate was calculated from the normalized change in size.

3.3.6 WSI-based AST

To evaluate the accuracy of our WSI-based AST method in the determination of MIC, *E. cloacae* and gentamicin were used as model bacterium and antibiotic, respectively. *E. cloacae* were treated with a series of concentrations (2, 4, 8, and 16 μg/mL) of gentamicin generated in the gel pad of bacterial culturing slides. The testing for each concentration was performed once using the aforementioned time-lapse WSI-based method to monitor the growth of each individual bacterial cell.

In addition, to assess the ability of our method in testing a polymicrobial and phenotypically heterogenous bacterial sample, we mixed kanamycin-sensitive *E. cloacae* and kanamycin-resistant *E. coli* together to stimulate the expected sample. Next, a WSI-based test was performed by treating the cells from this sample with 50 μg/mL kanamycin.

3.3.7 AST using broth dilution method

For comparison, AST was also performed by the gold standard broth dilution method [39]. In this work, antibiotic was added to MH medium and serially diluted to desired concentrations. Subsequently, same number of bacteria used for WSI-based test were inoculated into test tubes containing 5 mL MH medium with antibiotics and one tube of antibiotic-free medium as a control. After incubation at 37 °C for 16-24 h, the MIC was determined as the lowest concentration at which no visible bacterial growth was observed. Here, bacterial growth was quantified by measurement of OD600 using UV-Vis spectrophotometer (Nanodrop 1000, Thermo Fisher Scientific). This test was conducted in triplicate.

3.4 Conclusions

In this study, we demonstrated a novel rapid and accurate AST method established on WSI, which enabled high-throughput analysis of single-cell growth rates regardless of the variations in bacteria size and shape. As a demonstration of employing this new method to perform AST, the MIC of *E. cloacae* against gentamicin was determined within the theoretically shortest time that ensures the growth of each individual bacterium is inhibited. Notably, our technique was able to rapidly identify antibiotic resistant cells from a large

population of antibiotic susceptible cells, in which the portion of resistant subpopulation was about 1%. In addition, microscopy imaging shows no limitation in analyzing cells in diverse size or shape, suggesting that this method can be generalized to most bacteria species. Therefore, our AST approach would show great potential in determining antibiotic susceptibility of complex clinical bacteria isolates. Moreover, owing to the feature of high-throughput quantitative analysis, our approach can be applied to timely identifying the rising antibiotic resistance adapted to the treatment and guiding the adjustment of treatment strategy to prevent the aggravation of antibiotic resistance.

Chapter 4

Whole Slide Imaging for High-throughput Monitoring Fungal Growth at Single-Cell Level and Its Application to Rapid Antifungal Susceptibility Testing

4.1 Introduction

Invasive fungal infections, especially those caused by *Candida* species, are associated with high morbidity and mortality to the immunocompromised population [141-144]. In the past a few decades, empirical use of antifungal agents has promoted the emergence and spread of drug resistance in fungi which are normally susceptible to the treatment [145, 146]. As recently reported, *Candida auris* have become multidrug resistant and thus life-threatening [147-150]. Typically, healthcare providers employ antifungal susceptibility testing (AFST) to guide the prescription of antifungal drugs. The gold standard AFST methods, such as broth microdilution and disk diffusion, are based on the observation of visible fungal growth in the presence of antifungal drugs [151-153]. To facilitate standardized AFST, commercial automated instruments, such as Sensititre YeastOne (Thermo Fisher Scientific, MA, USA) and VITEK-2 (bioMérieux, France), have been developed [154]. However, the culture-based methods typically take up to several days [155], resulting in urgent need of rapid AFST to accelerate the initiation of appropriate antifungal treatment. Novel AFST approaches relying on the detection of specific genetic

mutations or changes of proteome corresponding to antifungal resistance by molecular techniques, such as DNA sequencing, real-time polymerase chain reaction (PCR), and matrix-assisted laser desorption-ionization time-of-flight mass spectrometry (MALDI-TOF MS), could be promising alternatives [49, 156-163]. Although molecular methods are sensitive and fast, a full understanding of the mechanisms of antifungal resistance to certain drugs is essential for reliable results [156]. Thus, rapid AFST techniques without compromising accuracy are urgently needed.

Herein, we report a novel AFST technique based on whole slide imaging (WSI) technique. As previously reported, we developed a WSI-based antibiotic susceptibility testing (AST) approach to determine the antibacterial susceptibility by high-throughput monitoring single-bacterium growth [164]. In this study, we used this approach for AFST. As a demonstration, we conducted time-lapse imaging of thousands of *C. albicans* cells and monitored single-cell growth. Antifungal susceptibility profiles of *C. albicans* against fluconazole was determined within 3 h, whereas the same results obtained from conventional broth dilution method took 72 h.

4.2 Results and Discussion

4.2.1. WSI-based monitoring fungal cell growth

In this study, we adapted the same microbial culturing "sandwich slides" as depicted in Scheme 1 (Chapter 3) for WSI. *C. albicans* cells are immobilized on the interface between the gel and the supporting glass. Next, bright-field images of the entire sample area were acquired as the sample stage moves and seamlessly stitched together into one image. As a

demonstration, Figure 1 displays a composite image of a sample area (5.689 mm × 5.408 mm). Zooming in the image enabled the visualization of individual cells, which were all in-focus. Herein, using a 40× objective lens, the imaging process took only 2 min. Considering that the doubling time of *C. albicans* is 1h in pure medium and it may be even longer during antifungal treatment, it was assumed that there was no observable cell growth during the 2 min imaging time under microscope.

To employ this system to monitor single-cell growth, the "sandwich" slides with *C. albicans* cell deposited in it were incubated at 37 °C and a humidity of 90%, under which condition the dimensions of the gel pad were not changed over the course of experiments. Subsequently, time-lapse imaging was conducted on the same sample area at 0.5, 1, 1.5, 2, 2.5, and 3 h. After the time-lapse composite images were collected, the numbers of cells developed from the same cell at different time points were read from the images. Since each composite image was in gigabytes, we selected a small subarea containing 5 cells as a demonstration of monitoring cell growth (Figure 2). As a yeast, *C. albicans* proliferate through budding. That is, a small bud emerges on the mother cell and its size keeps growing until reaching a certain level. Then the budding recurred on the daughter cell. To address this special cell growth pattern, we used cell number to determine the cell growth rates, which was more accurate to indicate cell replication than using cell area change. For each individual cell, the normalized growth rate at time t was calculated using equation (1), where N_t and N_0 are the numbers of cells with same location in the images captured at time t and time 0, respectively. Depicted in Figure 3 are the growth rate curves of 5 cells. Apparently,

at each time point, the growth rates varied, emphasizing the necessities of analyzing a large population of cells for accurate determination of antifungal susceptibility at single-cell level.

$$Normalized\ growth\ rate = \frac{N_t}{N_0} \qquad (1)$$

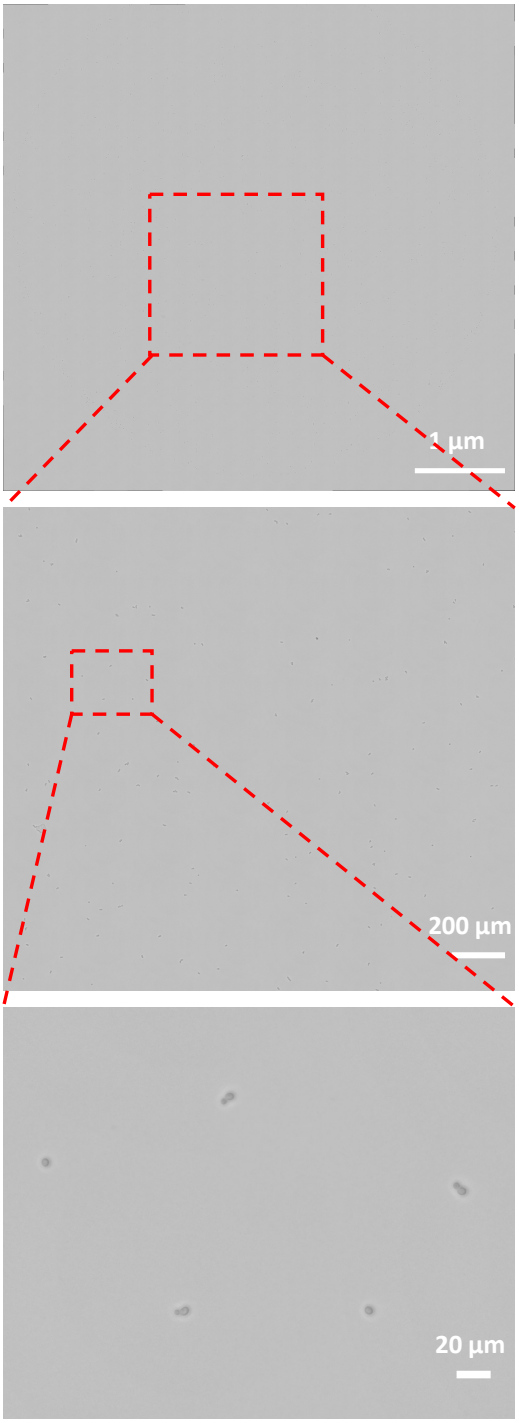

Figure 1. A representative composite image captured by the reported platform. Zooming in the image allows the visualization of single fungal cells.

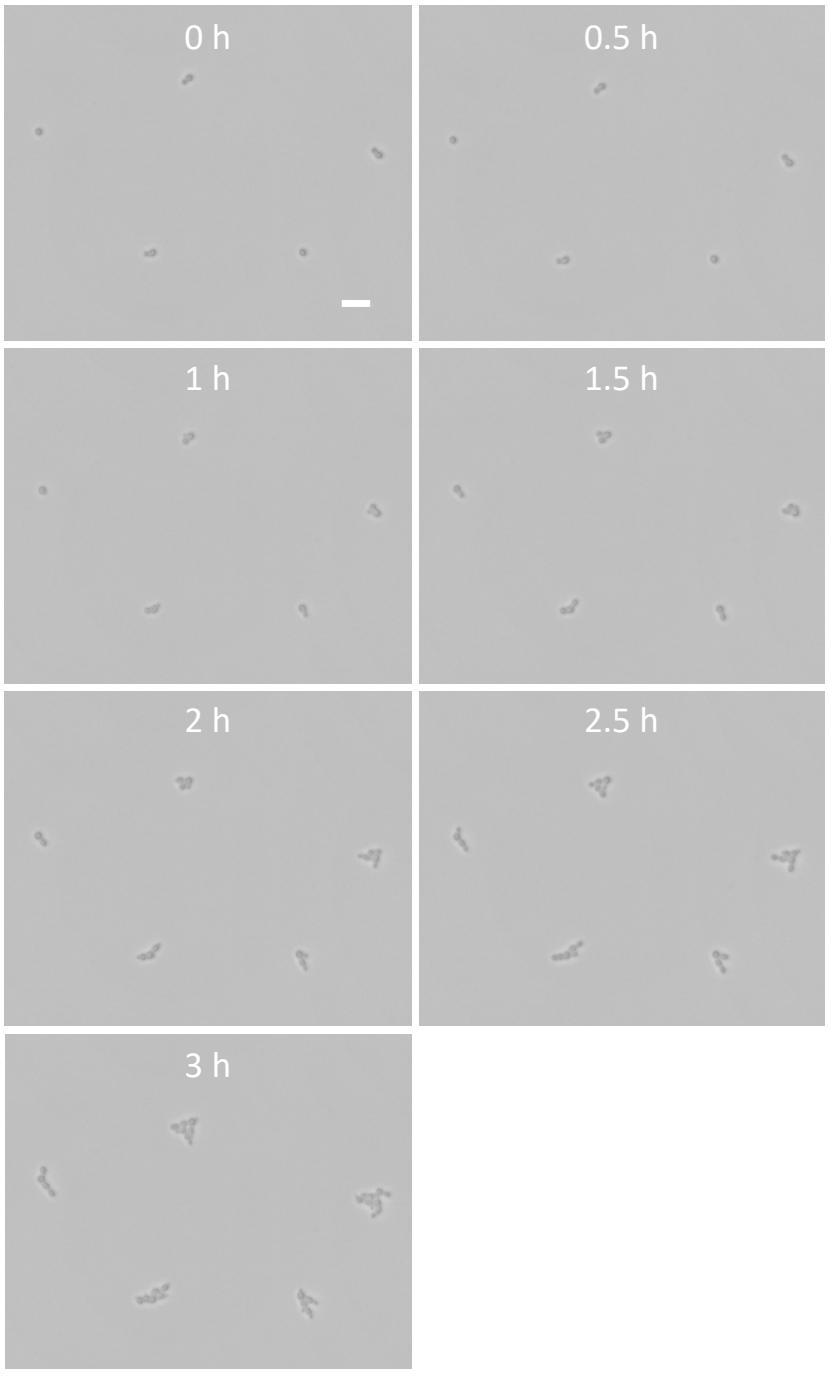

Figure 2. Time-lapse images of one representative area selected from the composite image in Figure 1. Scale bar, 20 µm.

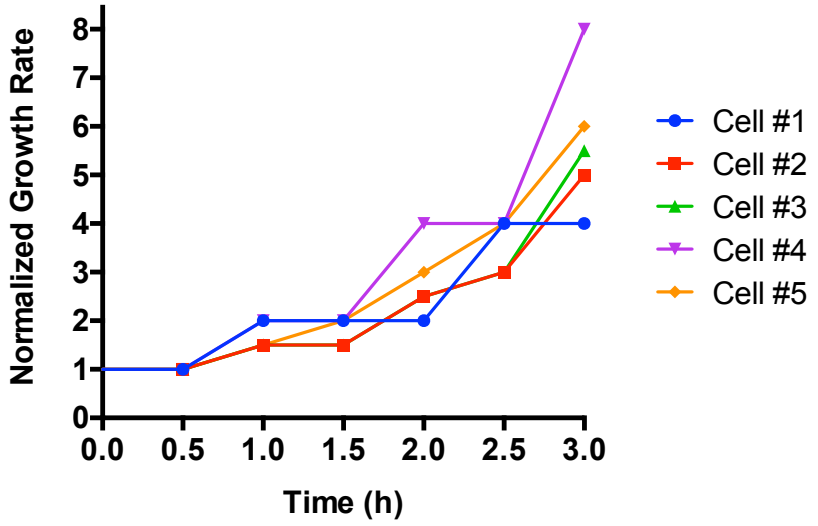

Figure 3. A representative single-cell growth rate of bacterial cells presented in Figure 2.

4.2.2. Determination of minimal inhibitory concentration (MIC) by WSI-based AFST

To investigate the ability of our method to determine antibiotic susceptibility, we performed tests through tracking cell growth of *C. albicans* in response to fluconazole treatments. Herein, the tested concentrations of fluconazole in gel pad were 0, 4, 8, 16, 32, 64, and 128 μg/mL and the number of cells treated at each antibiotic concentration were 675, 638, 644, 564, 644, 578, and 611, respectively. The populations were sufficiently large to show statistically significance in addressing the biological heterogeneity with respect to the growth rate. Based on the analysis results obtained from time-lapse images of the sample area captured at 0.5, 1, 1.5, 2, 2.5, and 3 h (Figure 4), we found that the growth rates of the cells at each time point were highly diverse and displayed broad distributions. To simplify the analysis, we set integral bins for the growth rates and obtained cell count-based

distributions shown in Figure 5. Setting threshold of 2 to indicate those had been replicated, obviously, such fractions treated with 0, 4, 8, 16, and 32 μg/mL fluconazole increased over time, suggesting that a majority of cells were continuously growing. In the groups treated with 64 and 128 μg/mL fluconazole, the growth of every individual cell was inhibited. By plotting the fraction of replicated cells versus time, as depicted in Figure 6, MIC was determined as 64 μg/mL, which agreed with the result from conventional broth dilution method (Figure 7).

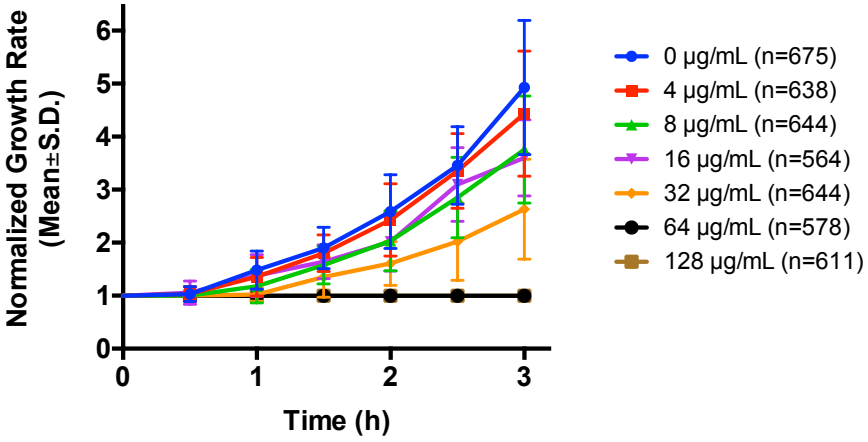

Figure 4. Normalized growth rate (Mean ± S.D.) versus incubation time.

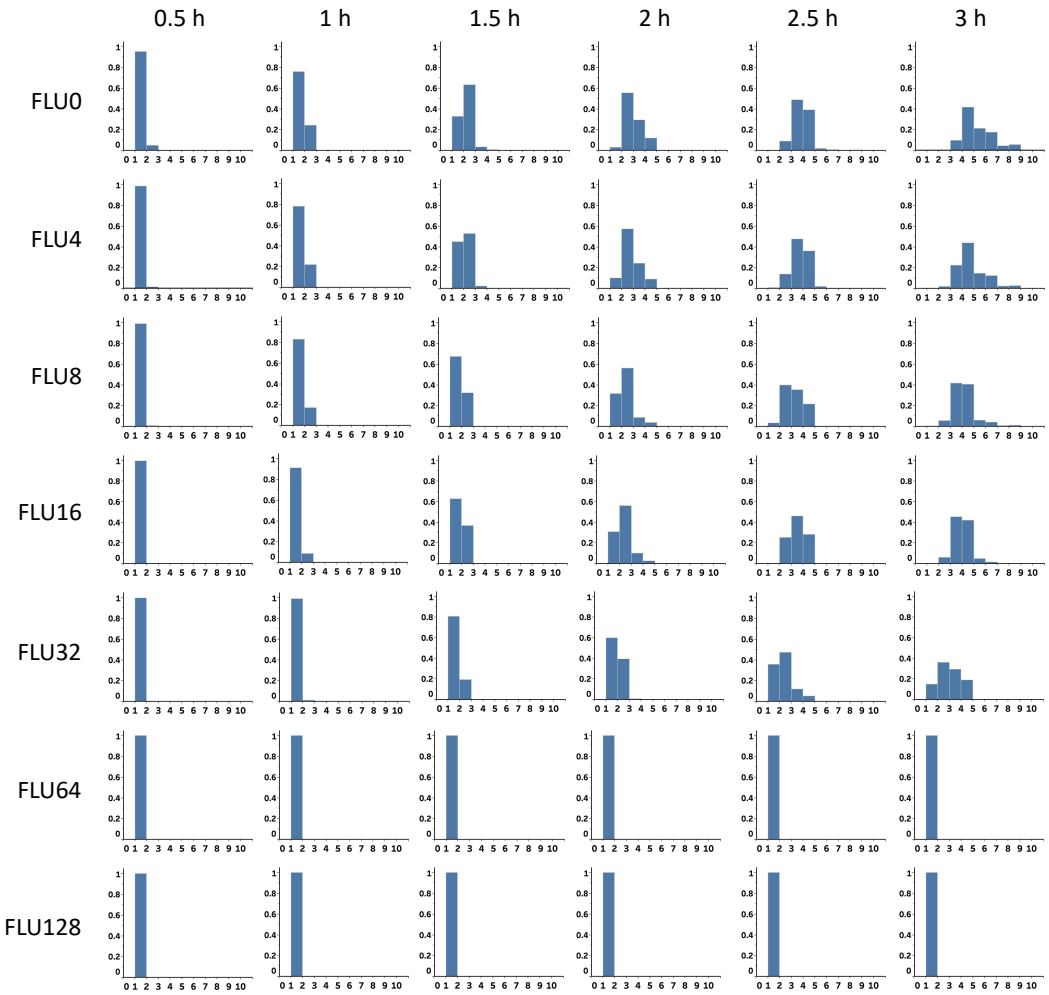

Figure 5. Number-based distribution of normalized single-cell growth rate for several thousand *C. albicans* cells treated with 0, 4, 8, 16, 32, 64, and 128 μg/mL fluconazole. In each histogram diagram, x-axis indicates normalized growth rates and y-axis indicates number-based fraction of cells.

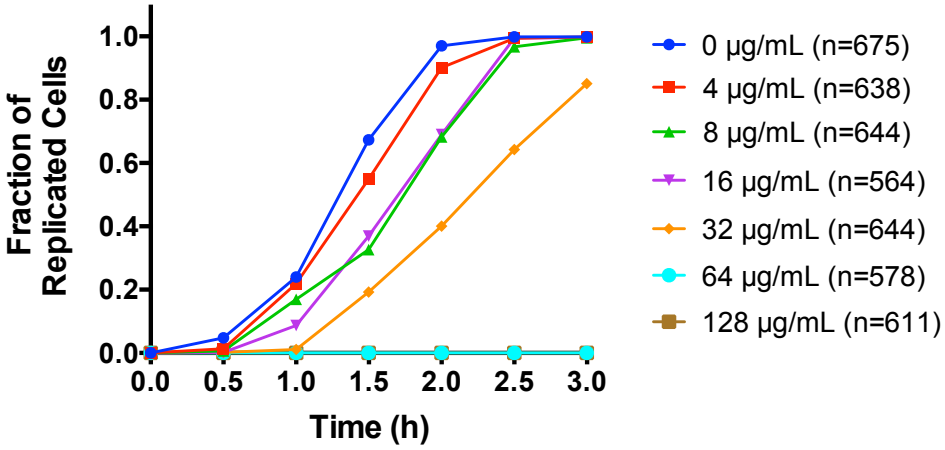

Figure 6. MIC determination by reported AFST approach. The curves were plotted by fraction of replicated cells from each treated group versus time.

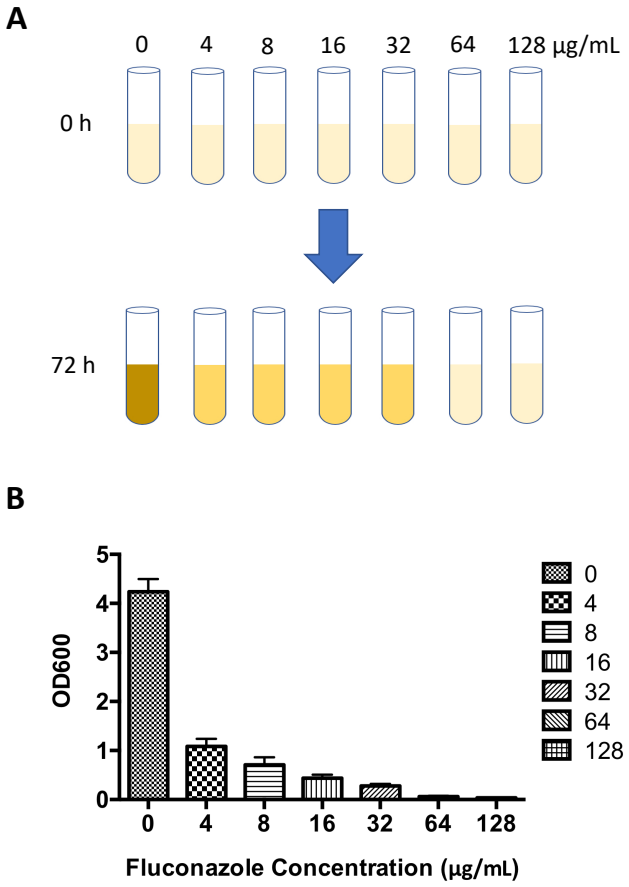

Figure 7. (A) Graphic description of MIC determination by broth dilution method. (B) OD600 obtained experimentally after the bacteria were incubated for 72 h.

4.3 Materials and Methods

4.3.1 Materials and instruments

As the composition of Sabouraud dextrose broth (SDB), dextrose and peptone were purchased from Sigma-Aldrich (St. Louis, MO, USA). Agarose was obtained from Promega (Madison, WI, USA). Silicon wafer was purchased from University Wafer (Boston, MA, USA). Chloramphenicol, fluconazole, polystyrene petri dishes (diameter 100 mm), and glass

microscope slides were purchased from Thermo Fisher Scientific (Waltham, MA, USA). *Candida albicans* (*C. albicans*) (strain SC5314) was received as a gift from Professor Anna Dongari-Bagtzoglou. Image acquisition was conducted using BZ-X800 All-in-One fluorescence microscope (Keyence Corporation, Japan).

4.3.2 Fungal cell culture

As the culture medium for *C. albicans*, SDB medium was prepared with 40 g/L dextrose, 10 g/L peptone, and 0.05 g/L chloramphenicol. The pH of medium was adjusted to 5.6 and filtration sterilized through 0.2 μm PVDF membrane (EMD Millipore, Burlington, MA, USA). After overnight culturing of stocked *C. albicans* in a 37 °C shaker, the cells were diluted with phosphate buffered saline (PBS) to desired concentrations for the testing.

4.3.3 Sample preparation

First, two parallel microscope glass slides with two pieces of spacers (0.38 mm-thick silicon wafer) in between were placed in a petri dish. Next, SDB medium with 0.6% (w/v) agarose suspended in it was sterilized by autoclaving at 121 °C for 15 min. After the media cooled down below 50 °C, antibiotic was added, and this molten medium was subsequently poured into a petri dish and filled the empty chamber between the glass slides. This petri dish was placed on a horizontal benchtop at room temperature. After the medium was sufficiently solidified, the cover glass slide was gently removed to present a thin gel pad with flat surface. Then, 2.5 μL bacterial suspension was carefully loaded onto the gel pad without disrupting the surface. After the drop completely evaporated, the glass slide and the

thin gel pad together was taken out by cutting off the surrounding bulk gel and mounted the side of gel pad with bacteria on another glass slide for WSI.

4.3.4 Whole slide imaging

The aforementioned sandwiched glass slides were placed on the imaging stage of microscopy cell incubator, wherein the bacteria side of the gel was in contact with the supporting glass slide. After the horizontal plane of bacterial cells was focused by the objective lens, the boundary of sample area was determined by the auto-searching function of the Keyence microscope. Next, cells in 10 different FOVs throughout the sample area were focused one by one to ensure the autofocusing during the scanning. Subsequently, tiles of bright-field images were continuously captured as the sample holder stage moved along a sequential path programmed by the imager software until the entire sample area was scanned. Herein, tiles (0.362 mm × 0.272 mm for each tile) were acquired by a 40× objective lens (NA=0.60, S Plan Fluor ELWD Ph2, Nikon). Then, the BZ-X800 analyzer software automatically created a composite image by seamlessly stitching all the tiles together. After the first scanning, the temperature of the incubator was set to 37 °C. The scanning was repeated at 0.5, 1, 1.5, 2, 2.5, and 3 h after the temperature reached 37 °C.

4.3.5 Image analysis

The number of cells was read from the image. The group of numbers originated from the same cell were plotted over time to quantify the cell growth rate.

4.3.6 WSI-based AFST

To evaluate the accuracy of our WSI-based AFST method in the determination of MIC, *C. albicans* and fluconazole were used as model fungus and antifungal agent, respectively. *C. albican* was treated with a series of concentrations (0, 4, 8, 16, 32, 64 and 128 μg/mL) of fluconazole generated in the gel pad of bacterial culturing slides. The testing for each concentration was performed once using the aforementioned time-lapse WSI-based method to monitor the growth of each individual fungal cell.

4.3.7 AFST using broth dilution method

For comparison, AFST was also performed by the gold standard broth dilution method [39]. In this work, fluconazole was added to SDB medium and diluted to a series of concentrations (0, 4, 8, 16, 32, 64 and 128 μg/mL). Subsequently, similar number of *C. albicans* cells used for WSI-based test were inoculated into test tubes containing 5 mL SDB medium with fluconazole and one tube of pure medium as a control. After incubation at 37 °C for 72 h, the MIC was determined as the lowest concentration at which no visible cell growth was observed. Fungal cell growth was quantified by measurement of OD600 using UV-Vis spectrophotometer (Nanodrop 1000, Thermo Fisher Scientific). This test was conducted in triplicate.

4.4 Conclusions

In this study, we demonstrated a novel rapid and accurate AFST method based on WSI, which enabled high-throughput analysis of fungal growth rates. For the first time, the cell growth rate was calculated directly from the change in cell number, significantly improving the accuracy. As a demonstration of employing this new method for rapid AFST, the MIC

of *C. albicans* against fluconazole was determined within 3 h, whereas the conventional broth dilution method took 72 h. The developed AFST method shows significant improvement in term of rapidness compared to conventional method, which could play a significant role in protecting public health.

Chapter 5

Summary and Outlook

5.1 Summary

Accurately measuring the number of viable microorganisms plays an essential role in microbiological studies. Since the conventional agar method of enumerating visible colonies is time-consuming and not accurate, efforts have been made towards overcoming these limitations by counting the invisible micro-colonies. However, none of studies on micro-colony counting was able to save significant time or provide accurate results. Herein, we developed an on-glass-slide cell culture device that enables rapid formation of micro-colonies on a 0.38 mm-thick gel film without suffering from nutrient and oxygen deprivation during bacteria culturing. Employing a phase contrast imaging setup, we achieved rapid microscopic scanning of micro-colonies within a large sample area on the thin film without the need of fluorescent staining. Using *Escherichia coli* (*E. coli*) as a demonstration, our technique was able to shorten the culturing time to within 5 h and automatically enumerate the micro-colonies from the phase contrast images. Moreover, this method delivered more accurate counts than the conventional visible colony counting methods. Due to these advantages, this imaging-based micro-colony enumeration technique provides a new platform for the quantification of viable microorganisms.

Since conventional culture-based antibiotic susceptibility testing (AST) methods are too time-consuming (typically 24–72 h), rapid AST is urgently needed for preventing the

increasing emergence and spread of antibiotic resistant infections. Although several phenotypic antibiotic resistance sensing modalities are able to reduce the AST time to a few hours or less, concerning the biological heterogeneity, their accuracy or limit of detection are limited by low throughput. Here, we present a rapid AST method based on whole slide imaging (WSI)-enabled high-throughput sensing antibiotic resistance at single-bacterium level. The time for determining the minimum inhibitory concentration (MIC) was theoretically shortest, which ensures that the growth of each individual cell present in a large population is inhibited. As a demonstration, our technique was able to sense the growth of at least several thousand bacteria at single-cell level. Reliable MIC of *Enterobacter cloacae* against gentamicin was obtained within 1 h, while the gold standard broth dilution method required at least 16 h for the same result. In addition, the application of our method prevails over other imaging-based AST approaches in allowing rapid and accurate determination of antibiotic susceptibility for phenotypically heterogeneous samples, in which the number of antibiotic resistant cells was negligible compared to that of the susceptible cells. Hence, our method shows great promise for both rapid AST determination and point-of-care testing of complex clinical bacteria isolates.

Since fungi have become multi-drug resistant and lethal, we utilized the WSI-based AST methods for rapidly and accurately determining antifungal susceptibility. For the first time, the cell growth rate was calculated directly from the change in cell number, rendering precise high-throughput analysis of fungal growth rates. As a demonstration of employing this new method for rapid antifungal susceptibility testing (AFST), the MIC of *C. albicans* against

fluconazole was shortened to within 3 h, whereas the conventional broth dilution method took 72 h.

5.2 Outlook

Although our WSI-based AST technique enables rapid and accurate testing for bacteria, fungi, and phenotypically heterogeneous samples, the single concentration of antimicrobial agent presents in one microscopy "sandwich" slides, which restrains this technique from being used for testing multiple concentrations simultaneously. Furthermore, the "sandwich" microbial culture slides developed in our laboratory is very cost-effective, especially compared to those sophisticated microfluidic devices. Although conventional optical microscopes are commonly equipped in every clinical or biomedical laboratory, microscopes with autofocus function are expensive and only available for specific purposes, such as digital pathology. Hence, our AST technique still has not met the needs for point-of-care diagnosis.

To eventually apply our WSI-based AST techniques to point-of-care diagnosis, there are a few ways to improve the performance of this technique, in the meanwhile decrease its cost.

First, the microscopy scanning speed can be significantly increased to enable testing multiple concentrations of antimicrobial agent simultaneously for the same microbial sample. As the general principle of whole slide imaging employed in our work, a large composite image was generated by stitching numerous images of single FOV together. Thus, the exposure time for each capture of single FOV determines the total time for the microscopy

scanning. Besides, employing larger magnification of objective lens results in higher resolution, but it takes longer time for microscopy scanning. Since it is feasible to engineer "sandwich" slides, in which the gel pad is split into multiple pieces containing various concentrations, the only technical barrier is the lacking of advanced optical sensors to capture images of microorganisms immobilized in the multiple pieces of gel pad simultaneously. As a recently emerged imaging technology, wide-field lens-free on-chip imaging seems to be a promising modality to overcome the technical barrier [165]. The imaging FOV can reach up to 18.15 cm^2 and the image acquisition time is less than 1 s, which would be sufficient for the purpose of rapid multiple testing.

Second, conventional optical microscopy-based diagnosis requires well-trained technician and eligible laboratory infrastructure, which are limited in developing countries, especially in infection-endemic regions. Thus, it is essential to further reduce the cost and improve the portability of the reported AST setup. As a future direction, smartphone camera can be used to replace the lens of conventional optical microscope. In a recent study, a smartphone-based microscope was designed for wide-field imaging parasite eggs and diagnosis of schistosomiasis [166]. By incorporating a battery-powered X-Y stage, this handheld smartphone-based microscope is able to produce high-resolution images of about 1 cm^2 FOV, which shows great promise in being used for high-throughput AST. Furthermore, as a significant improvement, although the smartphone camera is generally equipped with low numerical aperture, the application of advanced deep learning algorithms can render high-resolution images, matching the performance of conventional optical microscope with high-end objective lens [167, 168].

Third, since microorganism samples are typically from blood, urine, or stool, and isolating the microorganisms is time-consuming, it is critical to develop novel AST methods to directly test original clinical samples. As machine learning or deep learning has been applied to the differentiation of different microbial species [169, 170], it is believed that advanced algorithms can be developed for the differentiation of microorganisms from non-microbial substance in the future. Therefore, the total time for AST would be significantly shortened.

Fourth, although 2-fold dilution is generally accepted for AST, accurately identification of real MIC is essential. To test numerous concentrations of antimicrobial agent in one test, it would be great to limit the size of each gel pad to as small as possible. Therefore, as the future work, the minimum number of microorganisms for providing results as accurate as those from several thousand cells is to be determined using statistic tools.

References

1. Piddock, L. J., The crisis of no new antibiotics--what is the way forward? *Lancet Infect Dis* **2012,** 12, (3), 249-53.
2. Sengupta, S.; Chattopadhyay, M. K.; Grossart, H. P., The multifaceted roles of antibiotics and antibiotic resistance in nature. *Front Microbiol* **2013,** 4, 47.
3. Ventola, C. L., The antibiotic resistance crisis: part 1: causes and threats. *P T* **2015,** 40, (4), 277-83.
4. Spellberg, B.; Gilbert, D. N., The future of antibiotics and resistance: a tribute to a career of leadership by John Bartlett. *Clin Infect Dis* **2014,** 59 Suppl 2, S71-5.
5. Frieden, T., Antibiotic resistance threats in the United States, 2013. *Centers for Disease Control and Prevention, US Department of Health and Human Services* **2013**.
6. Read, A. F.; Woods, R. J., Antibiotic resistance management. *Evol Med Public Health* **2014,** 2014, (1), 147.
7. Van Boeckel, T. P.; Gandra, S.; Ashok, A.; Caudron, Q.; Grenfell, B. T.; Levin, S. A.; Laxminarayan, R., Global antibiotic consumption 2000 to 2010: an analysis of national pharmaceutical sales data. *Lancet Infect Dis* **2014,** 14, (8), 742-750.
8. Michael, C. A.; Dominey-Howes, D.; Labbate, M., The antimicrobial resistance crisis: causes, consequences, and management. *Front Public Health* **2014,** 2, 145.
9. Gross, M., Antibiotics in crisis. *Curr Biol* **2013,** 23, (24), R1063-5.
10. Bartlett, J. G.; Gilbert, D. N.; Spellberg, B., Seven ways to preserve the miracle of antibiotics. *Clin Infect Dis* **2013,** 56, (10), 1445-50.
11. Lu, J.; Jin, M.; Nguyen, S. H.; Mao, L.; Li, J.; Coin, L. J. M.; Yuan, Z.; Guo, J., Non-antibiotic antimicrobial triclosan induces multiple antibiotic resistance through genetic mutation. *Environ Int* **2018,** 118, 257-265.
12. Lushniak, B. D., Antibiotic resistance: a public health crisis. *Public Health Rep* **2014,** 129, (4), 314-6.
13. Luyt, C. E.; Brechot, N.; Trouillet, J. L.; Chastre, J., Antibiotic stewardship in the intensive care unit. *Crit Care* **2014,** 18, (5), 480.
14. Harris, A. M.; Hicks, L. A.; Qaseem, A., Appropriate Antibiotic Use for Acute Respiratory Tract Infection in Adults. *Ann Intern Med* **2016,** 165, (9), 674.
15. Jernberg, C.; Lofmark, S.; Edlund, C.; Jansson, J. K., Long-term impacts of antibiotic exposure on the human intestinal microbiota. *Microbiology* **2010,** 156, (Pt 11), 3216-23.
16. Gould, I. M.; Bal, A. M., New antibiotic agents in the pipeline and how they can help overcome microbial resistance. *Virulence* **2013,** 4, (2), 185-91.
17. Schaberle, T. F.; Hack, I. M., Overcoming the current deadlock in antibiotic research. *Trends Microbiol* **2014,** 22, (4), 165-7.
18. Luepke, K. H.; Suda, K. J.; Boucher, H.; Russo, R. L.; Bonney, M. W.; Hunt, T. D.; Mohr, J. F., 3rd, Past, Present, and Future of Antibacterial Economics: Increasing Bacterial Resistance, Limited Antibiotic Pipeline, and Societal Implications. *Pharmacotherapy* **2017,** 37, (1), 71-84.

19. Walsh, C. T.; Fischbach, M. A., New ways to squash superbugs. *Sci Am* **2009,** 301, (1), 44-51.
20. Butler, M. S.; Blaskovich, M. A.; Cooper, M. A., Antibiotics in the clinical pipeline in 2013. *J Antibiot (Tokyo)* **2013,** 66, (10), 571-91.
21. Roberts, J. P., Incentives aim to boost antibiotic development. *Nat Biotechnol* **2012,** 30, (8), 735.
22. House Clears Chemicals Bill. *Chemical & Engineering News Archive* **2015,** 93, (26), 6.
23. Andrei, S.; Valeanu, L.; Chirvasuta, R.; Stefan, M. G., New FDA approved antibacterial drugs: 2015-2017. *Discoveries* **2018,** 6, e81.
24. Wright, G. D.; Sutherland, A. D., New strategies for combating multidrug-resistant bacteria. *Trends Mol Med* **2007,** 13, (6), 260-7.
25. Neu, H. C.; Fu, K. P., Clavulanic acid, a novel inhibitor of beta-lactamases. *Antimicrob Agents Chemother* **1978,** 14, (5), 650-5.
26. Buynak, J. D., The discovery and development of modified penicillin- and cephalosporin-derived beta-lactamase inhibitors. *Curr Med Chem* **2004,** 11, (14), 1951-64.
27. Weiss, W. J.; Petersen, P. J.; Murphy, T. M.; Tardio, L.; Yang, Y.; Bradford, P. A.; Venkatesan, A. M.; Abe, T.; Isoda, T.; Mihira, A.; Ushirogochi, H.; Takasake, T.; Projan, S.; O'Connell, J.; Mansour, T. S., In vitro and in vivo activities of novel 6-methylidene penems as beta-lactamase inhibitors. *Antimicrob Agents Chemother* **2004,** 48, (12), 4589-96.
28. Toney, J. H.; Fitzgerald, P. M.; Grover-Sharma, N.; Olson, S. H.; May, W. J.; Sundelof, J. G.; Vanderwall, D. E.; Cleary, K. A.; Grant, S. K.; Wu, J. K.; Kozarich, J. W.; Pompliano, D. L.; Hammond, G. G., Antibiotic sensitization using biphenyl tetrazoles as potent inhibitors of Bacteroides fragilis metallo-beta-lactamase. *Chem Biol* **1998,** 5, (4), 185-96.
29. Simm, A. M.; Loveridge, E. J.; Crosby, J.; Avison, M. B.; Walsh, T. R.; Bennett, P. M., Bulgecin A: a novel inhibitor of binuclear metallo-beta-lactamases. *Biochem J* **2005,** 387, (Pt 3), 585-90.
30. Michalet, S.; Cartier, G.; David, B.; Mariotte, A. M.; Dijoux-franca, M. G.; Kaatz, G. W.; Stavri, M.; Gibbons, S., N-caffeoylphenalkylamide derivatives as bacterial efflux pump inhibitors. *Bioorg Med Chem Lett* **2007,** 17, (6), 1755-8.
31. Stavri, M.; Piddock, L. J.; Gibbons, S., Bacterial efflux pump inhibitors from natural sources. *J Antimicrob Chemother* **2007,** 59, (6), 1247-60.
32. Stermitz, F. R.; Lorenz, P.; Tawara, J. N.; Zenewicz, L. A.; Lewis, K., Synergy in a medicinal plant: antimicrobial action of berberine potentiated by 5'-methoxyhydnocarpin, a multidrug pump inhibitor. *Proc Natl Acad Sci U S A* **2000,** 97, (4), 1433-7.
33. Ball, A. R.; Casadei, G.; Samosorn, S.; Bremner, J. B.; Ausubel, F. M.; Moy, T. I.; Lewis, K., Conjugating berberine to a multidrug efflux pump inhibitor creates an effective antimicrobial. *ACS Chem Biol* **2006,** 1, (9), 594-600.
34. Rice, L. B., Rapid diagnostics and appropriate antibiotic use. *Clin Infect Dis* **2011,** 52 Suppl 4, S357-60.

35. Leekha, S.; Terrell, C. L.; Edson, R. S., General principles of antimicrobial therapy. *Mayo Clin Proc* **2011,** 86, (2), 156-67.
36. Andrews, J. M., Determination of minimum inhibitory concentrations. *J Antimicrob Chemother* **2001,** 48 Suppl 1, 5-16.
37. Ibrahim, E. H.; Sherman, G.; Ward, S.; Fraser, V. J.; Kollef, M. H., The influence of inadequate antimicrobial treatment of bloodstream infections on patient outcomes in the ICU setting. *Chest* **2000,** 118, (1), 146-55.
38. Kollef, M. H.; Sherman, G.; Ward, S.; Fraser, V. J., Inadequate antimicrobial treatment of infections: a risk factor for hospital mortality among critically ill patients. *Chest* **1999,** 115, (2), 462-74.
39. Wiegand, I.; Hilpert, K.; Hancock, R. E., Agar and broth dilution methods to determine the minimal inhibitory concentration (MIC) of antimicrobial substances. *Nat Protoc* **2008,** 3, (2), 163-75.
40. Jorgensen, J. H.; Ferraro, M. J., Antimicrobial susceptibility testing: a review of general principles and contemporary practices. *Clin Infect Dis* **2009,** 49, (11), 1749-55.
41. Sandle, T., 14 - Antibiotics and preservatives. In *Pharmaceutical Microbiology*, Sandle, T., Ed. Woodhead Publishing: Oxford, 2016; pp 171-183.
42. Balouiri, M.; Sadiki, M.; Ibnsouda, S. K., Methods for in vitro evaluating antimicrobial activity: A review. *J Pharm Anal* **2016,** 6, (2), 71-79.
43. Reller, L. B.; Weinstein, M.; Jorgensen, J. H.; Ferraro, M. J., Antimicrobial Susceptibility Testing: A Review of General Principles and Contemporary Practices. *Clinical Infectious Diseases* **2009,** 49, (11), 1749-1755.
44. Kumar, A.; Ellis, P.; Arabi, Y.; Roberts, D.; Light, B.; Parrillo, J. E.; Dodek, P.; Wood, G.; Kumar, A.; Simon, D. J. C., Initiation of inappropriate antimicrobial therapy results in a fivefold reduction of survival in human septic shock. **2009,** 136, (5), 1237-1248.
45. Brennan, R. E.; Samuel, J. E., Evaluation of Coxiella burnetii antibiotic susceptibilities by real-time PCR assay. *J Clin Microbiol* **2003,** 41, (5), 1869-74.
46. Rolain, J. M.; Mallet, M. N.; Fournier, P. E.; Raoult, D., Real-time PCR for universal antibiotic susceptibility testing. *J Antimicrob Chemother* **2004,** 54, (2), 538-41.
47. Sparbier, K.; Schubert, S.; Weller, U.; Boogen, C.; Kostrzewa, M., Matrix-assisted laser desorption ionization-time of flight mass spectrometry-based functional assay for rapid detection of resistance against beta-lactam antibiotics. *J Clin Microbiol* **2012,** 50, (3), 927-37.
48. Angeletti, S., Matrix assisted laser desorption time of flight mass spectrometry (MALDI-TOF MS) in clinical microbiology. *J Microbiol Methods* **2017,** 138, 20-29.
49. Vella, A.; De Carolis, E.; Mello, E.; Perlin, D. S.; Sanglard, D.; Sanguinetti, M.; Posteraro, B., Potential Use of MALDI-ToF Mass Spectrometry for Rapid Detection of Antifungal Resistance in the Human Pathogen Candida glabrata. *Sci Rep* **2017,** 7, (1), 9099.
50. Leonard, H.; Colodner, R.; Halachmi, S.; Segal, E., Recent Advances in the Race to Design a Rapid Diagnostic Test for Antimicrobial Resistance. *ACS Sens* **2018,** 3, (11), 2202-2217.

51. Sparbier, K.; Schubert, S.; Weller, U.; Boogen, C.; Kostrzewa, M., Matrix-Assisted Laser Desorption Ionization–Time of Flight Mass Spectrometry-Based Functional Assay for Rapid Detection of Resistance against β-Lactam Antibiotics. *Journal of Clinical Microbiology* **2012,** 50, (3), 927-937.
52. De Carolis, E.; Paoletti, S.; Nagel, D.; Vella, A.; Mello, E.; Palucci, I.; De Angelis, G.; D'Inzeo, T.; Sanguinetti, M.; Posteraro, B.; Spanu, T., A rapid diagnostic workflow for cefotaxime-resistant Escherichia coli and Klebsiella pneumoniae detection from blood cultures by MALDI-TOF mass spectrometry. *PLoS One* **2017,** 12, (10), e0185935.
53. Burckhardt, I.; Zimmermann, S., Using matrix-assisted laser desorption ionization-time of flight mass spectrometry to detect carbapenem resistance within 1 to 2.5 hours. *J Clin Microbiol* **2011,** 49, (9), 3321-4.
54. Oviano, M.; Bou, G., Imipenem-avibactam: a novel combination for the rapid detection of carbapenemase activity in Enterobacteriaceae and Acinetobacter baumannii by matrix-assisted laser desorption ionization-time of flight mass spectrometry. *Diagn Microbiol Infect Dis* **2017,** 87, (2), 129-132.
55. Oviano, M.; Ramirez, C. L.; Barbeyto, L. P.; Bou, G., Rapid direct detection of carbapenemase-producing Enterobacteriaceae in clinical urine samples by MALDI-TOF MS analysis. *J Antimicrob Chemother* **2017,** 72, (5), 1350-1354.
56. Rogers, G. B.; Marsh, P.; Stressmann, A. F.; Allen, C. E.; Daniels, T. V.; Carroll, M. P.; Bruce, K. D., The exclusion of dead bacterial cells is essential for accurate molecular analysis of clinical samples. *Clin Microbiol Infect* **2010,** 16, (11), 1656-8.
57. Martineau, F.; Picard, F. J.; Lansac, N.; Menard, C.; Roy, P. H.; Ouellette, M.; Bergeron, M. G., Correlation between the resistance genotype determined by multiplex PCR assays and the antibiotic susceptibility patterns of Staphylococcus aureus and Staphylococcus epidermidis. *Antimicrob Agents Chemother* **2000,** 44, (2), 231-8.
58. Horstkotte, M. A.; Knobloch, J. K.; Rohde, H.; Dobinsky, S.; Mack, D., Evaluation of the BD PHOENIX automated microbiology system for detection of methicillin resistance in coagulase-negative staphylococci. *J Clin Microbiol* **2004,** 42, (11), 5041-6.
59. Eigner, U.; Schmid, A.; Wild, U.; Bertsch, D.; Fahr, A. M., Analysis of the comparative workflow and performance characteristics of the VITEK 2 and Phoenix systems. *J Clin Microbiol* **2005,** 43, (8), 3829-34.
60. Pancholi, P.; Carroll, K. C.; Buchan, B. W.; Chan, R. C.; Dhiman, N.; Ford, B.; Granato, P. A.; Harrington, A. T.; Hernandez, D. R.; Humphries, R. M.; Jindra, M. R.; Ledeboer, N. A.; Miller, S. A.; Mochon, A. B.; Morgan, M. A.; Patel, R.; Schreckenberger, P. C.; Stamper, P. D.; Simner, P. J.; Tucci, N. E.; Zimmerman, C.; Wolk, D. M., Multicenter Evaluation of the Accelerate PhenoTest BC Kit for Rapid Identification and Phenotypic Antimicrobial Susceptibility Testing Using Morphokinetic Cellular Analysis. *J Clin Microbiol* **2018,** 56, (4).
61. Fredborg, M.; Andersen, K. R.; Jorgensen, E.; Droce, A.; Olesen, T.; Jensen, B. B.; Rosenvinge, F. S.; Sondergaard, T. E., Real-time optical antimicrobial susceptibility testing. *J Clin Microbiol* **2013,** 51, (7), 2047-53.

62. Wheat, P. F., History and development of antimicrobial susceptibility testing methodology. *J Antimicrob Chemother* **2001,** 48 Suppl 1, 1-4.
63. van Belkum, A.; Dunne, W. M., Jr., Next-generation antimicrobial susceptibility testing. *J Clin Microbiol* **2013,** 51, (7), 2018-24.
64. Braga, P. C.; Bovio, C.; Culici, M.; Dal Sasso, M., Flow cytometric assessment of susceptibilities of Streptococcus pyogenes to erythromycin and rokitamycin. *Antimicrob Agents Chemother* **2003,** 47, (1), 408-12.
65. Donay, J. L.; Mathieu, D.; Fernandes, P.; Pregermain, C.; Bruel, P.; Wargnier, A.; Casin, I.; Weill, F. X.; Lagrange, P. H.; Herrmann, J. L., Evaluation of the automated phoenix system for potential routine use in the clinical microbiology laboratory. *J Clin Microbiol* **2004,** 42, (4), 1542-6.
66. McGregor, A.; Schio, F.; Beaton, S.; Boulton, V.; Perman, M.; Gilbert, G., The MicroScan WalkAway diagnostic microbiology system--an evaluation. *Pathology* **1995,** 27, (2), 172-6.
67. Choi, J.; Jung, Y. G.; Kim, J.; Kim, S.; Jung, Y.; Na, H.; Kwon, S., Rapid antibiotic susceptibility testing by tracking single cell growth in a microfluidic agarose channel system. *Lab Chip* **2013,** 13, (2), 280-7.
68. Choi, J.; Yoo, J.; Lee, M.; Kim, E. G.; Lee, J. S.; Lee, S.; Joo, S.; Song, S. H.; Kim, E. C.; Lee, J. C.; Kim, H. C.; Jung, Y. G.; Kwon, S., A rapid antimicrobial susceptibility test based on single-cell morphological analysis. *Sci Transl Med* **2014,** 6, (267), 267ra174.
69. Davies, N. G.; Flasche, S.; Jit, M.; Atkins, K. E., Within-host dynamics shape antibiotic resistance in commensal bacteria. *Nat Ecol Evol* **2019,** 3, (3), 440-449.
70. Colijn, C.; Cohen, T.; Fraser, C.; Hanage, W.; Goldstein, E.; Givon-Lavi, N.; Dagan, R.; Lipsitch, M., What is the mechanism for persistent coexistence of drug-susceptible and drug-resistant strains of Streptococcus pneumoniae? *J R Soc Interface* **2010,** 7, (47), 905-19.
71. Choi, J.; Jeong, H. Y.; Lee, G. Y.; Han, S.; Han, S.; Jin, B.; Lim, T.; Kim, S.; Kim, D. Y.; Kim, H. C.; Kim, E. C.; Song, S. H.; Kim, T. S.; Kwon, S., Direct, rapid antimicrobial susceptibility test from positive blood cultures based on microscopic imaging analysis. *Sci Rep* **2017,** 7, (1), 1148.
72. Hong, W.; Karanja, C. W.; Abutaleb, N. S.; Younis, W.; Zhang, X.; Seleem, M. N.; Cheng, J. X., Antibiotic Susceptibility Determination within One Cell Cycle at Single-Bacterium Level by Stimulated Raman Metabolic Imaging. *Anal Chem* **2018,** 90, (6), 3737-3743.
73. Hong, W.; Cheng, J.-X., Rapid Determination of Antibiotic Susceptibility by Stimulated Raman Scattering Imaging of D_2O Metabolism. *bioRxiv* **2018**, 496778.
74. Kang, W.; Sarkar, S.; Lin, Z. S.; McKenney, S.; Konry, T., Ultrafast Parallelized Microfluidic Platform for Antimicrobial Susceptibility Testing of Gram Positive and Negative Bacteria. *Anal Chem* **2019,** 91, (9), 6242-6249.
75. Baltekin, O.; Boucharin, A.; Tano, E.; Andersson, D. I.; Elf, J., Antibiotic susceptibility testing in less than 30 min using direct single-cell imaging. *Proc Natl Acad Sci U S A* **2017,** 114, (34), 9170-9175.

76. Li, H.; Torab, P.; Mach, K. E.; Surrette, C.; England, M. R.; Craft, D. W.; Thomas, N. J.; Liao, J. C.; Puleo, C.; Wong, P. K., Adaptable microfluidic system for single-cell pathogen classification and antimicrobial susceptibility testing. *Proc Natl Acad Sci U S A* **2019,** 116, (21), 10270-10279.
77. Yu, H.; Jing, W.; Iriya, R.; Yang, Y.; Syal, K.; Mo, M.; Grys, T. E.; Haydel, S. E.; Wang, S.; Tao, N., Phenotypic Antimicrobial Susceptibility Testing with Deep Learning Video Microscopy. *Anal Chem* **2018,** 90, (10), 6314-6322.
78. Frymier, P. D.; Ford, R. M.; Berg, H. C.; Cummings, P. T., Three-dimensional tracking of motile bacteria near a solid planar surface. *Proc Natl Acad Sci U S A* **1995,** 92, (13), 6195-9.
79. Longo, G.; Alonso-Sarduy, L.; Rio, L. M.; Bizzini, A.; Trampuz, A.; Notz, J.; Dietler, G.; Kasas, S., Rapid detection of bacterial resistance to antibiotics using AFM cantilevers as nanomechanical sensors. *Nat Nanotechnol* **2013,** 8, (7), 522-6.
80. Cermak, N.; Olcum, S.; Delgado, F. F.; Wasserman, S. C.; Payer, K. R.; M, A. M.; Knudsen, S. M.; Kimmerling, R. J.; Stevens, M. M.; Kikuchi, Y.; Sandikci, A.; Ogawa, M.; Agache, V.; Baleras, F.; Weinstock, D. M.; Manalis, S. R., High-throughput measurement of single-cell growth rates using serial microfluidic mass sensor arrays. *Nat Biotechnol* **2016,** 34, (10), 1052-1059.
81. Etayash, H.; Khan, M. F.; Kaur, K.; Thundat, T., Microfluidic cantilever detects bacteria and measures their susceptibility to antibiotics in small confined volumes. *Nat Commun* **2016,** 7, 12947.
82. Villalba, M. I.; Stupar, P.; Chomicki, W.; Bertacchi, M.; Dietler, G.; Arnal, L.; Vela, M. E.; Yantorno, O.; Kasas, S., Nanomotion Detection Method for Testing Antibiotic Resistance and Susceptibility of Slow-Growing Bacteria. *Small* **2018,** 14, (4).
83. Ertl, P.; Robello, E.; Battaglini, F.; Mikkelsen, S. R., Rapid antibiotic susceptibility testing via electrochemical measurement of ferricyanide reduction by Escherichia coli and Clostridium sporogenes. *Anal Chem* **2000,** 72, (20), 4957-64.
84. Mann, T. S.; Mikkelsen, S. R., Antibiotic susceptibility testing at a screen-printed carbon electrode array. *Anal Chem* **2008,** 80, (3), 843-8.
85. Chotinantakul, K.; Suginta, W.; Schulte, A., Advanced amperometric respiration assay for antimicrobial susceptibility testing. *Anal Chem* **2014,** 86, (20), 10315-22.
86. Besant, J. D.; Sargent, E. H.; Kelley, S. O., Rapid electrochemical phenotypic profiling of antibiotic-resistant bacteria. *Lab Chip* **2015,** 15, (13), 2799-807.
87. Safavieh, M.; Pandya, H. J.; Venkataraman, M.; Thirumalaraju, P.; Kanakasabapathy, M. K.; Singh, A.; Prabhakar, D.; Chug, M. K.; Shafiee, H., Rapid Real-Time Antimicrobial Susceptibility Testing with Electrical Sensing on Plastic Microchips with Printed Electrodes. *ACS Appl Mater Interfaces* **2017,** 9, (14), 12832-12840.
88. Pandey, R.; Ter Beek, A.; Vischer, N. O.; Smelt, J. P.; Brul, S.; Manders, E. M., Live cell imaging of germination and outgrowth of individual bacillus subtilis spores; the effect of heat stress quantitatively analyzed with SporeTracker. *PLoS One* **2013,** 8, (3), e58972.
89. de Jong, I. G.; Beilharz, K.; Kuipers, O. P.; Veening, J. W., Live Cell Imaging of Bacillus subtilis and Streptococcus pneumoniae using Automated Time-lapse Microscopy. *J Vis Exp* **2011**, (53).

90. Maeda, Y.; Dobashi, H.; Sugiyama, Y.; Saeki, T.; Lim, T. K.; Harada, M.; Matsunaga, T.; Yoshino, T.; Tanaka, T., Colony fingerprint for discrimination of microbial species based on lensless imaging of microcolonies. *PLoS One* **2017,** 12, (4), e0174723.
91. Hazan, R.; Que, Y.-A.; Maura, D.; Rahme, L. G., A method for high throughput determination of viable bacteria cell counts in 96-well plates. *BMC Microbiology* **2012,** 12, 259-259.
92. Austin, B., The value of cultures to modern microbiology. *Antonie Van Leeuwenhoek* **2017,** 110, (10), 1247-1256.
93. Messer, J. W.; Rice, E. W.; Johnson, C. H., Total viable counts. Spread plate technique. *Encyclopedia of Food Microbiology* **2000,** 3, 2159-2160.
94. Frost, H. R.; Tsoi, S. K.; Baker, C. A.; Laho, D.; Sanderson-Smith, M. L.; Steer, A. C.; Smeesters, P. R., Validation of an automated colony counting system for group A Streptococcus. *BMC Res Notes* **2016,** 9, 72.
95. Sutton, S., Accuracy of plate counts. *Journal of validation technology* **2011,** 17, (3), 42.
96. Wang, X.; Yamaguchi, N.; Someya, T.; Nasu, M., Rapid and automated enumeration of viable bacteria in compost using a micro-colony auto counting system. *J Microbiol Methods* **2007,** 71, (1), 1-6.
97. Jung, J. H.; Lee, J. E., Real-time bacterial microcolony counting using on-chip microscopy. *Sci Rep* **2016,** 6, 21473.
98. Frost, W. D., Improved Technic for the Micro or Little Plate Method of Counting Bacteria in Milk. *The Journal of Infectious Diseases* **1921,** 28, (2), 176-184.
99. Jiang, C.; Chen, P.; Shan, S., Total microcolony counting on the moving narrow culture band. *Journal of Microbiological Methods* **1995,** 23, (3), 297-300.
100. Preibisch, S.; Saalfeld, S.; Tomancak, P., Globally optimal stitching of tiled 3D microscopic image acquisitions. *Bioinformatics* **2009,** 25, (11), 1463-5.
101. Jaeger, P. A.; McElfresh, C.; Wong, L. R.; Ideker, T., Beyond Agar: Gel Substrates with Improved Optical Clarity and Drug Efficiency and Reduced Autofluorescence for Microbial Growth Experiments. *Appl Environ Microbiol* **2015,** 81, (16), 5639-49.
102. Chen, M. T.; Weiss, R., Artificial cell-cell communication in yeast Saccharomyces cerevisiae using signaling elements from Arabidopsis thaliana. *Nat Biotechnol* **2005,** 23, (12), 1551-5.
103. Gu, Y. H.; Ko, W. H., Water agarose medium for studying factors affecting germination of conidia of Ampelomyces quisqualis. *Mycological Research* **1997,** 101, (4), 422-424.
104. Choi, J.; Kang, J. S.; Hong, S. C.; Bae, G.-N.; Jung, J. H., A new method for the real-time quantification of airborne biological particles using a coupled inertial aerosol system with in situ fluorescence imaging. *Sensors and Actuators B: Chemical* **2017,** 244, 635-641.
105. Karanja, C. W.; Hong, W.; Younis, W.; Eldesouky, H. E.; Seleem, M. N.; Cheng, J. X., Stimulated Raman Imaging Reveals Aberrant Lipogenesis as a Metabolic Marker for Azole-Resistant Candida albicans. *Anal Chem* **2017,** 89, (18), 9822-9829.

106. Mitchell, A. J.; Wimpenny, J. W., The effects of agar concentration on the growth and morphology of submerged colonies of motile and non-motile bacteria. *J Appl Microbiol* **1997,** 83, (1), 76-84.
107. Su, P. T.; Liao, C. T.; Roan, J. R.; Wang, S. H.; Chiou, A.; Syu, W. J., Bacterial colony from two-dimensional division to three-dimensional development. *PLoS One* **2012,** 7, (11), e48098.
108. Jonkman, J.; Brown, C. M., Any Way You Slice It-A Comparison of Confocal Microscopy Techniques. *J Biomol Tech* **2015,** 26, (2), 54-65.
109. Singh, A.; Gopinathan, K., Confocal microscopy: A powerful technique for biological research. *Current Science* **1998,** 74, (10), 841-851.
110. Wright, S. J.; Centonze, V. E.; Stricker, S. A.; DeVries, P. J.; Paddock, S. W.; Schatten, G., Chapter 1 Introduction to Confocal Microscopy and Three-Dimensional Reconstruction. In *Methods in Cell Biology*, Matsumoto, B., Ed. Academic Press: 1993; Vol. 38, pp 1-45.
111. Shotton, D.; White, N., Confocal scanning microscopy: three-dimensional biological imaging. *Trends Biochem Sci* **1989,** 14, (11), 435-9.
112. Guo, K.; Liao, J.; Bian, Z.; Heng, X.; Zheng, G., InstantScope: a low-cost whole slide imaging system with instant focal plane detection. *Biomed Opt Express* **2015,** 6, (9), 3210-6.
113. Liao, J.; Wang, Z.; Zhang, Z.; Bian, Z.; Guo, K.; Nambiar, A.; Jiang, Y.; Jiang, S.; Zhong, J.; Choma, M.; Zheng, G., Dual light-emitting diode-based multichannel microscopy for whole-slide multiplane, multispectral and phase imaging. *J Biophotonics* **2018,** 11, (2).
114. Liao, J.; Jiang, S.; Zhang, Z.; Guo, K.; Bian, Z.; Jiang, Y.; Zhong, J.; Zheng, G., Terapixel hyperspectral whole-slide imaging via slit-array detection and projection. *J Biomed Opt* **2018,** 23, (6), 1-7.
115. Boucher, H. W.; Talbot, G. H.; Bradley, J. S.; Edwards, J. E.; Gilbert, D.; Rice, L. B.; Scheld, M.; Spellberg, B.; Bartlett, J., Bad bugs, no drugs: no ESKAPE! An update from the Infectious Diseases Society of America. *Clin Infect Dis* **2009,** 48, (1), 1-12.
116. Gajdacs, M., The Continuing Threat of Methicillin-Resistant Staphylococcus aureus. *Antibiotics (Basel)* **2019,** 8, (2).
117. Ahmed, M. O.; Baptiste, K. E., Vancomycin-Resistant Enterococci: A Review of Antimicrobial Resistance Mechanisms and Perspectives of Human and Animal Health. *Microb Drug Resist* **2018,** 24, (5), 590-606.
118. Paterson, D. L.; Bonomo, R. A., Extended-spectrum beta-lactamases: a clinical update. *Clin Microbiol Rev* **2005,** 18, (4), 657-86.
119. Jean, S. S.; Lee, N. Y.; Tang, H. J.; Lu, M. C.; Ko, W. C.; Hsueh, P. R., Carbapenem-Resistant Enterobacteriaceae Infections: Taiwan Aspects. *Front Microbiol* **2018,** 9, 2888.
120. Gajdacs, M., The Concept of an Ideal Antibiotic: Implications for Drug Design. *Molecules* **2019,** 24, (5).
121. Silver, L. L., Challenges of Antibacterial Discovery. *Clinical Microbiology Reviews* **2011,** 24, (1), 71.

122. Idelevich, E. A.; Silling, G.; Niederbracht, Y.; Penner, H.; Sauerland, M. C.; Tafelski, S.; Nachtigall, I.; Berdel, W. E.; Peters, G.; Becker, K.; Molecular Diagnostics of Sepsis Study, G., Impact of multiplex PCR on antimicrobial treatment in febrile neutropenia: a randomized controlled study. *Med Microbiol Immunol* **2015,** 204, (5), 585-92.
123. Kollef, M. H., Inadequate antimicrobial treatment: an important determinant of outcome for hospitalized patients. *Clin Infect Dis* **2000,** 31 Suppl 4, S131-8.
124. Kumar, A.; Roberts, D.; Wood, K. E.; Light, B.; Parrillo, J. E.; Sharma, S.; Suppes, R.; Feinstein, D.; Zanotti, S.; Taiberg, L.; Gurka, D.; Kumar, A.; Cheang, M., Duration of hypotension before initiation of effective antimicrobial therapy is the critical determinant of survival in human septic shock. *Crit Care Med* **2006,** 34, (6), 1589-96.
125. Vrioni, G.; Tsiamis, C.; Oikonomidis, G.; Theodoridou, K.; Kapsimali, V.; Tsakris, A., MALDI-TOF mass spectrometry technology for detecting biomarkers of antimicrobial resistance: current achievements and future perspectives. *Ann Transl Med* **2018,** 6, (12), 240.
126. Pulido, M. R.; Garcia-Quintanilla, M.; Martin-Pena, R.; Cisneros, J. M.; McConnell, M. J., Progress on the development of rapid methods for antimicrobial susceptibility testing. *J Antimicrob Chemother* **2013,** 68, (12), 2710-7.
127. Schoepp, N. G.; Khorosheva, E. M.; Schlappi, T. S.; Curtis, M. S.; Humphries, R. M.; Hindler, J. A.; Ismagilov, R. F., Digital Quantification of DNA Replication and Chromosome Segregation Enables Determination of Antimicrobial Susceptibility after only 15 Minutes of Antibiotic Exposure. *Angew Chem Int Ed Engl* **2016,** 55, (33), 9557-61.
128. Schoepp, N. G.; Schlappi, T. S.; Curtis, M. S.; Butkovich, S. S.; Miller, S.; Humphries, R. M.; Ismagilov, R. F., Rapid pathogen-specific phenotypic antibiotic susceptibility testing using digital LAMP quantification in clinical samples. *Sci Transl Med* **2017,** 9, (410).
129. Gajdacs, M.; Spengler, G.; Urban, E., Identification and Antimicrobial Susceptibility Testing of Anaerobic Bacteria: Rubik's Cube of Clinical Microbiology? *Antibiotics (Basel)* **2017,** 6, (4).
130. Hughes, D.; Andersson, D. I., Environmental and genetic modulation of the phenotypic expression of antibiotic resistance. *FEMS Microbiol Rev* **2017,** 41, (3), 374-391.
131. Grobner, S.; Dion, M.; Plante, M.; Kempf, V. A., Evaluation of the BD GeneOhm StaphSR assay for detection of methicillin-resistant and methicillin-susceptible Staphylococcus aureus isolates from spiked positive blood culture bottles. *J Clin Microbiol* **2009,** 47, (6), 1689-94.
132. Syal, K.; Mo, M.; Yu, H.; Iriya, R.; Jing, W.; Guodong, S.; Wang, S.; Grys, T. E.; Haydel, S. E.; Tao, N., Current and emerging techniques for antibiotic susceptibility tests. *Theranostics* **2017,** 7, (7), 1795-1805.
133. Salipante, S. J.; Sengupta, D. J.; Rosenthal, C.; Costa, G.; Spangler, J.; Sims, E. H.; Jacobs, M. A.; Miller, S. I.; Hoogestraat, D. R.; Cookson, B. T.; McCoy, C.; Matsen, F. A.; Shendure, J.; Lee, C. C.; Harkins, T. T.; Hoffman, N. G., Rapid 16S rRNA

next-generation sequencing of polymicrobial clinical samples for diagnosis of complex bacterial infections. *PLoS One* **2013,** 8, (5), e65226.
134. Cummings, L. A.; Kurosawa, K.; Hoogestraat, D. R.; SenGupta, D. J.; Candra, F.; Doyle, M.; Thielges, S.; Land, T. A.; Rosenthal, C. A.; Hoffman, N. G.; Salipante, S. J.; Cookson, B. T., Clinical Next Generation Sequencing Outperforms Standard Microbiological Culture for Characterizing Polymicrobial Samples. *Clin Chem* **2016,** 62, (11), 1465-1473.
135. Young, K. D., The selective value of bacterial shape. *Microbiol Mol Biol Rev* **2006,** 70, (3), 660-703.
136. Al-Janabi, S.; Huisman, A.; Van Diest, P. J., Digital pathology: current status and future perspectives. *Histopathology* **2012,** 61, (1), 1-9.
137. Abels, E.; Pantanowitz, L., Current State of the Regulatory Trajectory for Whole Slide Imaging Devices in the USA. *J Pathol Inform* **2017,** 8, 23.
138. Ghaznavi, F.; Evans, A.; Madabhushi, A.; Feldman, M., Digital imaging in pathology: whole-slide imaging and beyond. *Annu Rev Pathol* **2013,** 8, 331-59.
139. Song, D.; Liu, H.; Dong, Q.; Bian, Z.; Wu, H.; Lei, Y., Digital, Rapid, Accurate, and Label-Free Enumeration of Viable Microorganisms Enabled by Custom-Built On-Glass-Slide Culturing Device and Microscopic Scanning. *Sensors (Basel)* **2018,** 18, (11).
140. Liao, J.; Jiang, Y.; Bian, Z.; Mahrou, B.; Nambiar, A.; Magsam, A. W.; Guo, K.; Wang, S.; Cho, Y. K.; Zheng, G., Rapid focus map surveying for whole slide imaging with continuous sample motion. *Opt Lett* **2017,** 42, (17), 3379-3382.
141. Arendrup, M. C., Epidemiology of invasive candidiasis. *Curr Opin Crit Care* **2010,** 16, (5), 445-52.
142. Pfaller, M. A.; Diekema, D. J., Epidemiology of invasive candidiasis: a persistent public health problem. *Clin Microbiol Rev* **2007,** 20, (1), 133-63.
143. Bassetti, M.; Righi, E.; Ansaldi, F.; Merelli, M.; Trucchi, C.; De Pascale, G.; Diaz-Martin, A.; Luzzati, R.; Rosin, C.; Lagunes, L.; Trecarichi, E. M.; Sanguinetti, M.; Posteraro, B.; Garnacho-Montero, J.; Sartor, A.; Rello, J.; Rocca, G. D.; Antonelli, M.; Tumbarello, M., A multicenter study of septic shock due to candidemia: outcomes and predictors of mortality. *Intensive Care Med* **2014,** 40, (6), 839-45.
144. Kollef, M.; Micek, S.; Hampton, N.; Doherty, J. A.; Kumar, A., Septic shock attributed to Candida infection: importance of empiric therapy and source control. *Clin Infect Dis* **2012,** 54, (12), 1739-46.
145. Kanafani, Z. A.; Perfect, J. R., Antimicrobial resistance: resistance to antifungal agents: mechanisms and clinical impact. *Clin Infect Dis* **2008,** 46, (1), 120-8.
146. Oxman, D. A.; Chow, J. K.; Frendl, G.; Hadley, S.; Hershkovitz, S.; Ireland, P.; McDermott, L. A.; Tsai, K.; Marty, F. M.; Kontoyiannis, D. P.; Golan, Y., Candidaemia associated with decreased in vitro fluconazole susceptibility: is Candida speciation predictive of the susceptibility pattern? *J Antimicrob Chemother* **2010,** 65, (7), 1460-5.
147. Cortegiani, A.; Misseri, G.; Fasciana, T.; Giammanco, A.; Giarratano, A.; Chowdhary, A., Epidemiology, clinical characteristics, resistance, and treatment of infections by Candida auris. *J Intensive Care* **2018,** 6, 69.

148. Meis, J. F.; Chowdhary, A., Candida auris: a global fungal public health threat. *Lancet Infect Dis* **2018,** 18, (12), 1298-1299.
149. Forsberg, K.; Woodworth, K.; Walters, M.; Berkow, E. L.; Jackson, B.; Chiller, T.; Vallabhaneni, S., Candida auris: The recent emergence of a multidrug-resistant fungal pathogen. *Med Mycol* **2019,** 57, (1), 1-12.
150. Lockhart, S. R., Candida auris and multidrug resistance: Defining the new normal. *Fungal Genet Biol* **2019,** 131, 103243.
151. Pfaller, M.; Boyken, L.; Hollis, R.; Kroeger, J.; Messer, S.; Tendolkar, S.; Diekema, D., Comparison of the broth microdilution methods of the European Committee on Antimicrobial Susceptibility Testing and the Clinical and Laboratory Standards Institute for testing itraconazole, posaconazole, and voriconazole against Aspergillus isolates. *J Clin Microbiol* **2011,** 49, (3), 1110-2.
152. Arendrup, M. C.; Cuenca-Estrella, M.; Lass-Florl, C.; Hope, W.; Eucast, A., EUCAST technical note on the EUCAST definitive document EDef 7.2: method for the determination of broth dilution minimum inhibitory concentrations of antifungal agents for yeasts EDef 7.2 (EUCAST-AFST). *Clin Microbiol Infect* **2012,** 18, (7), E246-7.
153. Espinel-Ingroff, A., Standardized disk diffusion method for yeasts. *Clinical Microbiology Newsletter* **2007,** 29, (13), 97-100.
154. Cuenca-Estrella, M.; Gomez-Lopez, A.; Alastruey-Izquierdo, A.; Bernal-Martinez, L.; Cuesta, I.; Buitrago, M. J.; Rodriguez-Tudela, J. L., Comparison of the Vitek 2 antifungal susceptibility system with the Clinical and Laboratory Standards Institute (CLSI) and European Committee on Antimicrobial Susceptibility Testing (EUCAST) broth microdilution reference methods and with the Sensititre YeastOne and Etest techniques for in vitro detection of antifungal resistance in yeast isolates. *Journal of clinical microbiology* **2010,** 48, (5), 1782-1786.
155. Cantón, E.; Espinel-Ingroff, A.; Pemán, J., Trends in antifungal susceptibility testing using CLSI reference and commercial methods. *Expert Review of Anti-infective Therapy* **2009,** 7, (1), 107-119.
156. Sanguinetti, M.; Posteraro, B., New approaches for antifungal susceptibility testing. *Clin Microbiol Infect* **2017,** 23, (12), 931-934.
157. Pham, C. D.; Bolden, C. B.; Kuykendall, R. J.; Lockhart, S. R., Development of a Luminex-based multiplex assay for detection of mutations conferring resistance to Echinocandins in Candida glabrata. *J Clin Microbiol* **2014,** 52, (3), 790-5.
158. Dudiuk, C.; Gamarra, S.; Leonardeli, F.; Jimenez-Ortigosa, C.; Vitale, R. G.; Afeltra, J.; Perlin, D. S.; Garcia-Effron, G., Set of classical PCRs for detection of mutations in Candida glabrata FKS genes linked with echinocandin resistance. *J Clin Microbiol* **2014,** 52, (7), 2609-14.
159. Zhao, Y.; Nagasaki, Y.; Kordalewska, M.; Press, E. G.; Shields, R. K.; Nguyen, M. H.; Clancy, C. J.; Perlin, D. S., Rapid Detection of FKS-Associated Echinocandin Resistance in Candida glabrata. *Antimicrob Agents Chemother* **2016,** 60, (11), 6573-6577.
160. Marinach, C.; Alanio, A.; Palous, M.; Kwasek, S.; Fekkar, A.; Brossas, J. Y.; Brun, S.; Snounou, G.; Hennequin, C.; Sanglard, D.; Datry, A.; Golmard, J. L.; Mazier, D.,

MALDI-TOF MS-based drug susceptibility testing of pathogens: the example of Candida albicans and fluconazole. *Proteomics* **2009,** 9, (20), 4627-31.
161. De Carolis, E.; Vella, A.; Florio, A. R.; Posteraro, P.; Perlin, D. S.; Sanguinetti, M.; Posteraro, B., Use of matrix-assisted laser desorption ionization-time of flight mass spectrometry for caspofungin susceptibility testing of Candida and Aspergillus species. *J Clin Microbiol* **2012,** 50, (7), 2479-83.
162. Vella, A.; De Carolis, E.; Vaccaro, L.; Posteraro, P.; Perlin, D. S.; Kostrzewa, M.; Posteraro, B.; Sanguinetti, M., Rapid antifungal susceptibility testing by matrix-assisted laser desorption ionization-time of flight mass spectrometry analysis. *J Clin Microbiol* **2013,** 51, (9), 2964-9.
163. Vatanshenassan, M.; Boekhout, T.; Meis, J. F.; Berman, J.; Chowdhary, A.; Ben-Ami, R.; Sparbier, K.; Kostrzewa, M., Candida auris Identification and Rapid Antifungal Susceptibility Testing Against Echinocandins by MALDI-TOF MS. *Front Cell Infect Microbiol* **2019,** 9, 20.
164. Song, D.; Liu, H.; Ji, H.; Lei, Y., Whole Slide Imaging for High-Throughput Sensing Antibiotic Resistance at Single-Bacterium Level and Its Application to Rapid Antibiotic Susceptibility Testing. *Molecules* **2019,** 24, (13).
165. Zhang, Y.; Alexander, M.; Yang, S.; Bian, Y.; Botvinick, E.; Lakey, J. R. T.; Ozcan, A., High-Throughput Screening of Encapsulated Islets Using Wide-Field Lens-Free On-Chip Imaging. *ACS Photonics* **2018,** 5, (6), 2081-2086.
166. Koydemir, H. C.; Coulibaly, J. T.; Tseng, D.; Bogoch, II; Ozcan, A., Design and validation of a wide-field mobile phone microscope for the diagnosis of schistosomiasis. *Travel Med Infect Dis* **2019,** 30, 128-129.
167. Rivenson, Y.; Ceylan Koydemir, H.; Wang, H.; Wei, Z.; Ren, Z.; Günaydın, H.; Zhang, Y.; Göröcs, Z.; Liang, K.; Tseng, D.; Ozcan, A., Deep Learning Enhanced Mobile-Phone Microscopy. *ACS Photonics* **2018,** 5, (6), 2354-2364.
168. Rivenson, Y.; Göröcs, Z.; Günaydin, H.; Zhang, Y.; Wang, H.; Ozcan, A., Deep learning microscopy. *Optica* **2017,** 4, (11), 1437-1443.
169. Zielinski, B.; Plichta, A.; Misztal, K.; Spurek, P.; Brzychczy-Wloch, M.; Ochonska, D., Deep learning approach to bacterial colony classification. *PLoS One* **2017,** 12, (9), e0184554.
170. Qu, K.; Guo, F.; Liu, X.; Lin, Y.; Zou, Q., Application of Machine Learning in Microbiology. *Front Microbiol* **2019,** 10, 827.